INFORMATION TO USERS

This manuscript has been reproduced from the microfilm master. UMI films the text directly from the original or copy submitted. Thus, some thesis and dissertation copies are in typewriter face, while others may be from any type of computer printer.

The quality of this reproduction is dependent upon the quality of the copy submitted. Broken or indistinct print, colored or poor quality illustrations and photographs, print bleedthrough, substandard margins, and improper alignment can adversely affect reproduction.

In the unlikely event that the author did not send UMI a complete manuscript and there are missing pages, these will be noted. Also, if unauthorized copyright material had to be removed, a note will indicate the deletion.

Oversize materials (e.g., maps, drawings, charts) are reproduced by sectioning the original, beginning at the upper left-hand corner and continuing from left to right in equal sections with small overlaps. Each original is also photographed in one exposure and is included in reduced form at the back of the book.

Photographs included in the original manuscript have been reproduced xerographically in this copy. Higher quality 6" x 9" black and white photographic prints are available for any photographs or illustrations appearing in this copy for an additional charge. Contact UMI directly to order.

UMI

University Microfilms International
A Bell & Howell Information Company
300 North Zeeb Road, Ann Arbor, MI 48106-1346 USA
313/761-4700 800/521-0600

Order Number 9510907

Microstrip discontinuities and coplanar waveguide dispersions and discontinuities including anistropic substrates

Hsu, ChungJen, Ph.D.

Case Western Reserve University, 1994

U·M·I
300 N. Zeeb Rd.
Ann Arbor, MI 48106

MICROSTRIP DISCONTINUITIES AND COPLANAR WAVEGUIDE DISPERSIONS AND DISCONTINUITIES INCLUDING ANISTROPIC SUBSTRATES

by

CHUNGJEN HSU

Submitted in partial fulfillment of the requirements

for the degree of Doctor of Philosophy

Dissertation advisor: R.E. Collin

Department of Electrical Engineering and applied Physics

Department of Electrical Engineering and Applied Physics

CASE WESTERN RESERVE UNIVERSITY

August, 1994

CASE WESTERN RESERVE UNIVERSITY

GRADUATE STUDIES

We hereby approve the thesis of

ChungJen Hsu

candidate for the Ph.D

degree.*

(signed) _____
(chair)

Robert L. Brown

Don Hazony

Francis Merat

date July 7, 1994

*We also certify that written approval has been obtained for any proprietary material contained therein.

Abstract

by

CHUNGJEN HSU

This dissertation contains three main topics. The first one is the development of the dynamic source reversal method, based on potential theory with the help of the Tangent method, to characterize microstrip discontinuities. Detailed analysis of microstrip open-end and symmetrical and asymmetrical gap discontinuities, with anisotropic substrates, is carried out.

The second one is to develop an efficient and accurate method to solve coplanar waveguide dispersion. The method uses the conformal mapping technique to derive the general expressions, as seen for the first time in the literature, for the sources on the central strip and ground planes of coplanar waveguide. These expressions are also proved to be very useful and precise to treat microstrip propagation characteristics.

The third topic is to extend the dynamic source reversal method to characterize coplanar waveguide discontinuities with the help of the known propagation characteristics for no discontinuity obtained in the second topic. Detailed calculations for CPW open end discontinuities are accomplished in the transform domain.

All the problems studied for these three topics include anisotropic substrates. The results for the three topics show very good accuracy and excellent efficiency. Some comparisons with the results obtained by other methods proposed by authors are included.

Acknowledgments

I am very indebted to my mother and all the other members of my family for their true love and encouragement. Without these, this work would not have been accomplished.

Thanks also go to my advisor, professor Robert E. Collin, for providing partial financial aid and valuable discussions on my dissertation.

Table of contents

CHAPTER 1:

MICROSTRIP DISCONTINUITIES & COPLANAR WAVEGUIDE DISPERSIONS AND DISCONTINUITIES

Chapter 1

Microstrip discontinuities & coplanar waveguide dispersions and discontinuities

In this chapter, we review some of the analytical methods proposed by other authors for characterizing microstrip discontinuities. These include both quasi-static analysis and full-wave analysis. Experimental techniques for some microstrip discontinuities, such as resonator measurements, are mentioned. In order to more efficiently and precisely characterize microstrip discontinuities we study the dynamic source reversal technique, based on potential theory. Also we examine some of the methods used to treat coplanar waveguide propagation characteristics. This is followed by a few discussions of reported work on coplanar waveguide discontinuities along with experimental work. The last part of the chapter gives a short summary of the research carried out in this dissertation that develops the dynamic source reversal technique for some microstrip discontinuities, including anisotropic substrates, and applies the technique to coplanar waveguide discontinuities with the help of the method we develop to solve coplanar waveguide dispersion characteristics.

1.1 Introduction

Microstrip and coplanar waveguide discontinuities are respectively the basic constituent elements of microwave integrated circuits and monolithic microwave integrated circuits. In the design of microwave circuits and systems, it is preferable to represent the effects of the discontinuities in the microstrip and coplanar waveguide interconnections by equivalent lumped element networks since designers can then simulate the design in the software program with time-saving steps. Obviously, if the elements of the equivalent

circuit for a discontinuity can be expressed in terms of the microstrip width-to-height ratio or the coplanar waveguide width- and width-plus-slot-to-height ratio and the dielectric constant of the substrate, a designer needn't be involved in the electromagnetic boundary value problem and can determine the associated element values for the discontinuity and include its effects in the design with ease.

In early investigations, the techniques used to characterize microstrip discontinuities were based on quasi-static analyses which considered wave propagation on the line to be pure TEM and assumed only a perturbed charge distribution on the conductor near a discontinuity. The techniques yielded good results for frequencies only up to 1-2 GHz and gave poor outcomes for the higher frequencies.

To overcome this limitation many researchers developed sophisticated full-wave analyses which gave better results for characterizing microstrip discontinuities at high frequencies. Because of the increased complexity, the numerical calculation was much more demanding and required greater computer power for the efficient finding of the equivalent circuit parameters. Therefore, the usefulness of many of these techniques in microwave design is limited.

Collin and Toncich developed a new approach called the dynamic source reversal method for characterizing microstrip discontinuities with isotropic substrates, based on potential theory [1]. It was an extension of the line sources with charge reversal method presented by Silvester and Benedek [2]. The major features of it are that an accurate representation of the sources on the strips can be specified in terms of the dominant mode fields, only the perturbed current and charge near the discontinuity appear as the unknown quantities, and all three equivalent circuit parameters of a lossless two-port

junction for a gap discontinuity can be found by using a single matrix inversion. Some of the earlier methods developed to treat microstrip discontinuities require three matrix inversions to be carried out, in turn demanding more computational time.

A coplanar waveguide, consisting of a conductor centered between two ground planes with all on the same plane surface, permits easy shunt connection of external elements in hybrid and monolithic integrated circuits. Because of many advantages over microstrip, coplanar waveguides are popularly used as passive elements in microwave design. Hence, it naturally attracted many researchers to investigate the dispersion characteristics and discontinuities in coplanar waveguides.

Most investigations of coplanar waveguide propagation characteristics dealt with structures without any enclosure whereas in practice a shielding enclosure is normally used. Moreover, no accurate analytic expressions, at least in the mathematical sense, for the sources on the central strip and ground planes were found.

Although the parasitic effects which occur when the coplanar lines are conductor-backed and/or shielded have been discussed and evaluated from a quantitative point of view, the simple analytical formulas obtained for the coplanar waveguide propagation parameters with quasi-static analysis are still questionable for higher frequencies.

The full-wave numerical methods utilized to solve coplanar waveguide discontinuity problems are formulated in the spatial domain, the spectral domain, or the time domain. Although these techniques are rigorous and produce some good results, they require long computational time and often large memories in the computer.

In this dissertation, we develop the powerful dynamic source reversal method to solve microstrip discontinuity problems including anisotropic substrates, derive the general expressions for the sources to accurately treat coplanar waveguide dispersion characteristics, and apply the method to coplanar waveguide discontinuities with the help of the obtained propagation parameters.

1.2 Literature review of microstrip discontinuities

As the complexity and operating frequency range of microwave circuits and systems increase, microstrip technology offers the designers the features of small size, weight reduction, ease of component interconnection, and realization of integrated passive circuits which other forms of the waveguiding systems cannot provide.

Microstrip discontinuity effects at open ends, gaps, steps, bends, junctions, and crossings must be included when synthesizing the matching networks in microwave circuit design. If the dimensions of discontinuities are smaller than the wavelength of the propagating wave, their effects appear and may be characterized by lumped equivalent circuits whose element values are frequency-dependent. To improve the design, an accurate knowledge of the discontinuity equivalent circuits along with their frequency dependence becomes a necessity.

A microstrip line consists of a strip conductor over a ground plane separated by a dielectric slab which also provides the structural support for the line. Since the field lines between the conductor and the ground plane are not entirely confined within the dielectric material, a pure TEM wave can not propagate along the line. Instead, a quasi-TEM mode with longitudinal field components may travel on the stripline. Fig. 1.1 shows the typical microstrip geometry.

A discontinuity in microstrip is caused by abrupt change in the geometry of the strip conductors. Therefore, electric and magnetic fields are modified near the discontinuity. The change in electric field distribution gives rise to an equivalent capacitance and that in the magnetic field results in an equivalent inductance. However, most of the microstrip discontinuities are predominantly capacitive over the operating frequency range of interest and

inductive effects are normally high frequency corrections to the capacitive effects.

Some often encountered microsrtip discontinuities are shown in Fig. 1.2. In general, most techniques used theoretically to analyze microstrip discontinuities fall into two categories ; namely, quasi-static and full-wave analyses.

The quasi-static method which is a low frequency technique assumes the wave propagating on the line to be a pure TEM wave which can be characterized by the charge distribution on the conducting strip. The quasi-static methods have been used to find static capacitances and inductances and the element values of the equivalent circuits.

The full-wave method is a more rigorous approach to the analysis of discontinuities than the quasi-static method since it retains all the field components and solves Maxwell's equations. Therefore, it leads to a more complete characterization of microstrip discontinuities at higher frequencies.

Several representative techniques for each analysis method is briefly discussed in the next few sections, with an accompanying examination of their limitations in microwave applications.

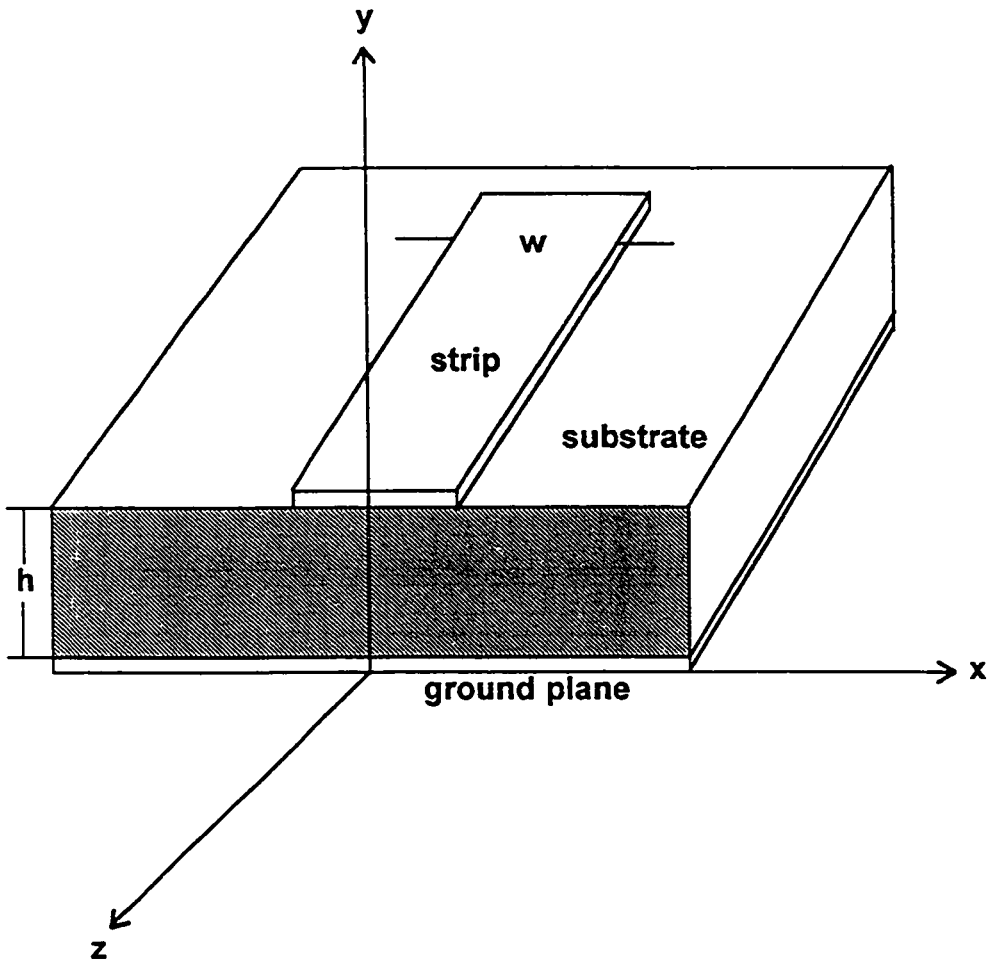

ε_r - effective dielectric constant of substrate

μ_r - effective permeability of substrate

h - substrate thickness

w - strip width

Fig. 1.1 Typical microstrip geometry

(a) Open end

(b) Gap

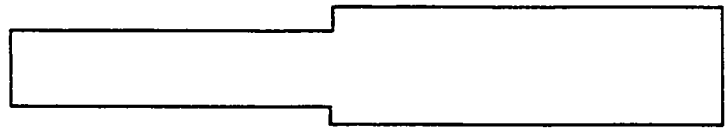

(c) Step

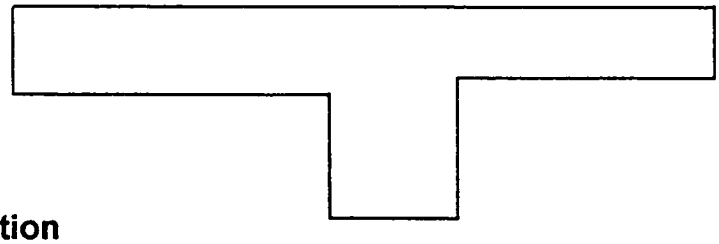

(d) T junction

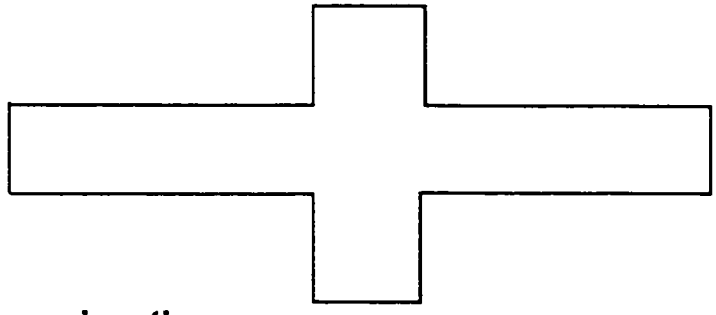

(e) Cross over junction

Fig. 1.2 Some discontinuities in microstrip line

1.3 Quasi-static analysis for microstrip discontinuities

Static capacitances associated with the discontinuity are able to be determined by finding the excess charge distribution near the discontinuity. Several techniques commonly used are :

(1)Moments method in the spatial domain [3].

(2)Variational expression [4].

(3)Galerkin's method in the spectral domain [5].

(4)Line charge reversal method [2], [6], [7].

Calculation of the static inductances for microstrip discontinuities can be treated by determining the excess current density in the vicinity of the discontinuity.

(5)Evaluating inductances by Galerkin's method in the spatial domain [8].

In [3], the potential at a point r(x,y,z) due to a charge distribution $\sigma(r')$ is given by the integral

$$\phi(r) = \int \sigma(r')G(r,r')dr' \qquad (1.1)$$

where G(r,r') is the Green's function which is the solution of Poison's equation for a point charge source. The solution must satisfy the appropriate boundary conditions and leads to an integral equation for the unknown charge distribution.

If the conductor is assumed to be infinitely thin and located at a height h above the ground plane, the volume integral becomes a surface integral. Once a suitable expression for the Green's function is found, the integral equation may be formulated and solved for the unknown charge distribution. This is done by converting it to a matrix equation and inverting the matrix equation numerically [3].

In this method, the charge density could be assumed to be constant over every subsection of the strip conductor. The matrix equation associated with Eq.(1.1) can be written as

$$[V] = [D][\sigma] \tag{1.2}$$

Because the conductor may be assumed to be at a known potential, such as 1.0 volt , Eq.(1.2) may be inverted to determine the unknown $[\sigma]$ in terms of $[D]$. Then, the capacitance C can be found by summing over all the σ_i. This technique was used to calculate the excess capacitances of open ends, gaps, and steps.

Since the equivalent capacitance of a discontinuity is due to the excess charge in the vicinity of the discontinuity, the TEM mode capacitance must be subtracted from the computed capacitance. This results in the subtraction of two nearly equal numbers which can yield significant errors. Another limitation of this method is the slow convergence of the Green's function series. As a result, large computer time is required to achieve good outcomes in the calculation. Also, as shown by Silvester and Benedek [9], and recently by Kobayashi [10], the source distribution on the conductor strip above a ground plane is not uniform as shown in Fig.1.3. In view of the singular behavior at the edges, smaller and smaller subsections at these areas are needed, thus increasing the computational time.

Relatively little numerical data has been presented in useful form for microwave design. Since this method is limited in accuracy, it has not been extensively used.

In [4], the technique relies on the fact that the capacitance can be calculated by a variational expression

$$\frac{1}{C} = \frac{\iint \sigma(r)G(r,r')\sigma(r')dV'dV}{\left[\int \sigma(r')dv'\right]^2} \tag{1.3}$$

where G(r,r') is the three dimensional Green's function. Since it is stationary with respect to arbitrary first order variation in the charge distribution on the strip, the exact nature of the distribution needn't be known in this technique. But a suitable choice of the charge distribution as a trial function is necessary to obtain the capacitance by minimizing the variational integral.

In a symmetric gap problem solved by this method, the three dimensional Green's functions for electric wall and magnetic wall cases must be determined first. These walls can be placed successively along the plane located midway between the gap. The calculated capacitances are related to the capacitances of the pi equivalent network through

$$C_g = \frac{1}{2}(C_e - C_m) \tag{1.4a}$$

$$C_p = C_m \tag{1.4b}$$

where C_p is the fringing capacitance, C_g is the coupling capacitance, C_m is the excess capacitance at the gap with a bisecting magnetic wall, and C_e is the excess capacitance with a electric wall. An open end discontinuity is then characterized by allowing the spacing between the gap to go to infinity. The major disadvantages of this technique are that the two Green's functions are slowly convergent series and the expression for the charge density must be suitably chosen ; otherwise, it affects the numerical accuracy.

In [5] which formulates the problem in the spectral domain, the potential at the interface between the conducting strip and the dielectric can be expressed as the product of the two dimensional Green's function at the interface and the charge density on the conducting strip. The equation can be

formed by solving Poison's equation along with the appropriate boundary conditions in the Fourier transform domain. Expanding the charge distribution by suitable basis functions and applying Galerkin's method, the unknown coefficients associated with the basis functions can be found in the spectral domain. From these coefficients, we can determine the total capacitance for the discontinuous strip. Then, the fringing capacitance at the open-ends can be found by the subtraction of two nearly equal capacitances. Also, this technique can be utilized to calculate the edge capacitances for the gaps.

The major advantage of this technique is that the Green's function has a closed form in the spectral domain. But, the procedure developed in this method is numerically time consuming and involves the subtraction of two nearly equal numbers. Moreover, the accuracy is dependent on the choice of basis functions used to expand the charge distribution.

It should be mentioned that Galerkin's method is a general technique applied to any linear operator equation and is not limited to the spectral domain. When used in the spatial domain, it is a special case of the method of moments.

In [6], the basic element common to all discontinuity analysis by the charge reversal method is a semi-infinite line charge. In this analysis, the residual potential near the discontinuity determines the excess charge which in turn is responsible for the capacitances of the equivalent circuit. In reality, the semi-infinite line charge can be considered as a superposition of two infinite lines having reversed charges, with respect to each other, on the extension intervals to form the infinite lines. The Green's functions for the even and odd charge distributions on the infinite lines are determined. Based on them, the residual potential in the vicinity of the discontinuity may be

found and used to find the excess charge from which the capacitances can be calculated.

To economize on the computational time, this technique took into consideration the essential charge edge singularities on the strip conductor when expansion functions were used to represent the charge distribution. This method was used to compute the excess capacitances existing in open ends, gaps, steps, bends, junctions, and crossings. Its major feature is that this technique avoids the use of the subtraction of two nearly equal numbers for the capacitances [6], [7].

In [8], the integro-differential skin effect equation relating the vector potential and the current density to the gradient of the scalar potential was used along with the excess current technique, which is similar to the charge reversal method proposed by Silvester and Benedeck, to find the quasi-static inductance of a discontinuity. By applying Galerkin's method in the spatial domain, we can calculate the excess currents in each region due to the perturbation from the uniform field condition. Therefore, the increase in inductance, associated with the discontinuity, can be found through the excess current.

However, in the absence of any rigorous time-dependent solution, the associated results for steps, bends, T junctions were estimated to be valid up to 5 GHz. In addition, the quasi-static inductance calculation described above was based on a separate inductance calculation which doesn't include the capacitive effects. Thus, it is an open question if the results obtained are physically meaningful.

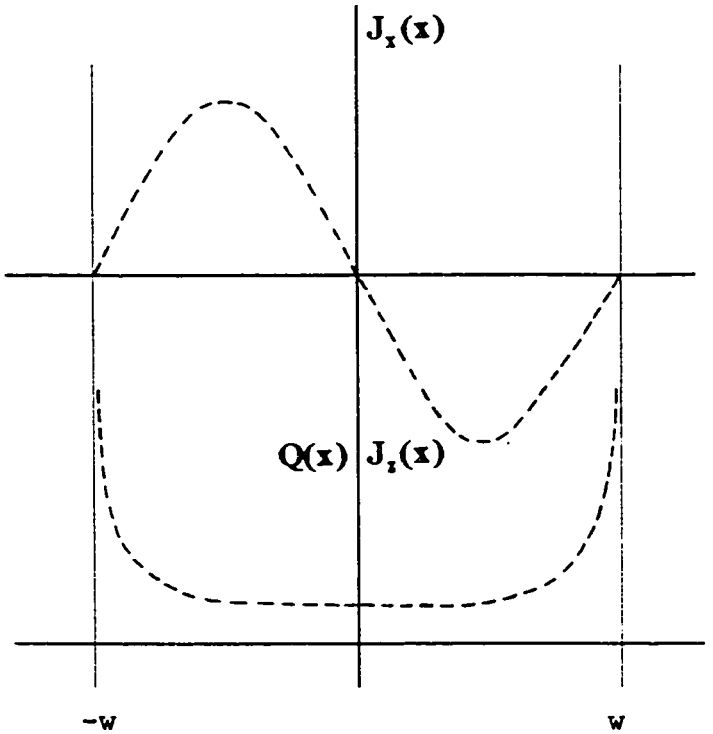

Fig. 1.3 Longitudinal and transverse current distribution on a microstrip line

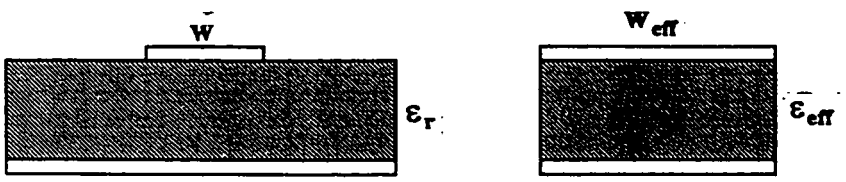

Fig. 1.4 Planar waveguide model

1.4 Experimental technique for microstrip discontinuities

In the papers reviewed above only theoretical results for the quasi-static capacitances and inductances of equivalent circuits for microstrip discontinuities have been given. However, useful data on single microstrip discontinuities need to be of high accuracy, so it was important to carry out measurements of the specific discontinuity. Therefore, some authors [11] developed experimental methods of determining microstrip discontinuity parameters which enabled a check on the validity of theoretical data and provided data where the theory was not yet fruitful.

Measurement procedures were devised to employ microstrip resonant configurations incorporating the discontinuity to be characterized. This approach has the advantage that only light coupling to the microstrip circuit is required to determine the resonant frequency, and errors attributable to the coaxial-to-microstrip transition by conventional measurement techniques can thus be much reduced. The technique was used to characterize several types of discontinuities such as right angle bends, T-junctions, and cross-over junctions. Although the measured data seem to agree with some of the quasi-static theoretical results, this experimental approach is limited in its repeatability and by the experimenters' laboratory experience. Also, the fabrication of test circuits used for measurements can vary in quality and thus yield non-repeatable data.

An accurate method for the measurements on microstrip open ends, which is an extension of the resonator technique, was presented by C. Gupta et. al. , [12]. In this technique, an electrically centered gap identical to a feed-line gap width was etched into the straight resonator. Since the original straight resonator had been laid down for the measurements and was subsequently etched to the other resonator configurations for further

measurements, the effects of the variations in the dielectric height, strip width, and relative dielectric constant was reduced. However, some of the drawbacks mentioned above along with etching precision problems still exist.

Although the quasi-static techniques were utilized extensively to characterize microstrip discontinuities, the microstrip, as pointed out in the literature, can not support a pure TEM mode. Therefore, the results for the microstrip discontinuities are only valid up to a few gigahertz when the quasi-static analysis is used. Moreover, the measuring techniques for the microstrip discontinuities have their special limitations ; for example, no capability to supply the bountiful results of interest and no assurance of the accuracy for the measured data. This led many researchers to develop other useful analytic methods. Since the hybrid modes present in the microstrip can not be described by the quasi-static method, one has to introduce the time varying electric and magnetic fields and solve the wave equation. Moreover, the charge density used in the electrostatic analyses becomes time varying and so we must include the current density for full-wave analysis.

1.5 Full-wave analysis for microstrip discontinuities

By full-wave analysis, we mean the process of rigorously solving the electro-magnetic boundary value problems by retaining all field components.

Many main techniques which were used to carry out the full-wave characterization of microstrip discontinuities are

(1)Fourier transform domain method [13].

(2)Planar waveguide model [14], [15].

(3)Cavity method [16], [17], [19], [20].

(4)Time domain finite difference method [21].

(5)Other methods [22], [23], [24].

In [13], Itoh used Galerkin's method in the spectral domain to calculate the excess capacitance of open ends, and gaps by analyzing a resonator enclosed in conducting walls with a cover plate. The fields in the resonator are assumed to be a superposition of TE and TM modes and are transformed into the Fourier transform domain. Along with the required boundary conditions, the wave equations are solved in the spectral domain. The feature of this method is that solutions are extracted from algebraic equations rather than from coupled integral equations of the convolution type. This simplifies the numerical calculation. By the application of Galerkin's method, the characteristic equation with unknown coefficients for the current density in the spectral domain can be obtained. Seeking the wave number of the resonator ; i.e. , the root of the resulting characteristic equation, one can set the determinant of the coefficient matrix equal to zero. Based on it, the effective increased length l for a microstrip resonator and herewith the discontinuity capacitance can be obtained.

The results track well with those found by quasi-static approaches ; however, the l computed by this method is smaller. Since very few

expansion functions were used for the current, it seems likely that this was the cause of the discrepancy. Accuracy and computational time are inversely related to the number of basis functions used and also depend on the choice of the functions.

In [14], the planar waveguide model for microstrip represents an intermediate stage of complexity between transmission line and waveguide models. In the planar waveguide approach, the microstrip line was modeled as an equivalent dielectric-filled waveguide with magnetic side walls, with an effective width and dielectric constant as shown in Fig.1.4. The effective dielectric constant of the filling and width of the guide are assumed to be frequency dependent and determined in such a way that the waveguide model and the actual microstrip line have the same propagation constant and characteristic impedance.

In this model, the fundamental TEM mode was assumed to propagate in the waveguide and higher order waveguide modes may be generated near microstrip discontinuities. The discontinuities may be characterized by matching the modes on both sides of the discontinuity for the electric and magnetic fields. From the matching coefficients, the scattering parameters can be obtained for the discontinuity. This mode-matching method is particularly suited for the characterization of symmetric discontinuities such as steps and T-junctions.

However, this model is not correct and doesn't give accurate results for the phase angles of the scattering matrix elements. This results from those realities that it didn't take into account the radiation effects and surface wave generation, and that the actual modes which are excited in microstrip discontinuities are not the same as those used in the model.

Jansen et. al. , [16], [17] employed a three dimensional spectral domain resonator approach to treat the asymmetrical series gap and step discontinuities. The resonance condition is formulated in terms of strip lengths for a fixed given operating frequency. This approach is a rigorous hybrid-mode method, in conjunction with the use of a modification of the Tangent method [18], originally developed as an experimental technique to characterize the discontinuities by the equivalent circuits containing three parameters. The complex wave amplitudes on the stubs can be derived for each of the experiments and these amplitudes may be used to determine the scattering parameters. However, in this technique, the scattering matrix of a strip discontinuity is derived from resonance experiments which are not performed in reality but are simulated on a computer. Since this approach doesn't include radiation effects, it can't be applied for the systems where the radiation loss mechanism is appreciable.

Katehi et. al. , [19] started with Pocklington's integral equation which expresses the radiated electric field in terms of the unknown current distribution on the transmission-line sections for the discontinuities. By applying Galerkin's method and using proper impressed source mechanism, the unknown coefficients for the current were found. This technique was used to characterize open ends, gaps, and coupled resonators by lumped parameters of the equivalent circuits, for the various discontinuities, which can be derived by determining the equivalent guide wavelength and the characteristic impedance of the line. This model accounts for the surface-wave effects, strip finite thickness, and radiation losses.

In [20], Dunleavy and Katehi used the reciprocity theorem to obtain the integral equation which relates the fields caused by a test current to a frill current and the excited conduction current on the strip inside a cavity. The

longitudinal conduction current is expanded into overlapping sinusoidal basis functions, along with the built-in edge condition for the transverse variation of the current. By choosing the proper expression for the frill current and applying the method of moments to deal with the integral equation, the current distribution was found through the matrix inversion. In the paper, they worked a lot to discuss the convergences of impedance matrix, the excitation vector elements, and network parameters for an open-end discontinuity to prove the numerical accuracy of the technique.

In the above mentioned investigations, the full-wave analyses were done in the frequency domain ; that is, the data for the whole frequency range are calculated one frequency at a time. This led Zhang and Mei to seek an alternative way of calculating the data for a wide range of frequencies [21].

Since a pulse response contains all the information of a system for the whole frequency range, it is a natural approach to use a pulse in the time domain to excite a microstrip structure. From the time domain pulse response one can extract the frequency-domain characteristics of the system via the Fourier transform. This method directly solved Maxwell's equations using the finite difference approach in the time domain with the initial conditions specified for the electric and magnetic fields, along with the boundary conditions and Sommerfeld's radiation condition.

In the algorithm, the placement of the electric and magnetic field nodes are spaced by half a space step. Also, the time instants at which the electric or magnetic fields are calculated are spaced by half a time step. The excitation pulse used at the front surface in this investigation was chosen to be Gaussian in shape.

In order not to accumulate the numerical error generated in one step of the calculation, the stability criterion called the Courant condition must be

obeyed. From the scattering parameters defined in terms of the associated voltages transformed in the spectral domain, we can extract the element values of the equivalent circuits for the discontinuities. This method was used to calculate the scattering parameter data for open ends, gaps, steps, and T-junctions. However, except for the open ends, only the magnitudes for the scattering parameters were shown.

The major disadvantage of this technique is that the Fourier transform of the time domain results is very sensitive to numerical error. The absorbing boundary conditions used to truncate the numerical components must be accurately treated ; otherwise, even though the time domain results are reasonably accurate, the frequency domain outcomes obtained from their Fourier transforms may not be acceptable as useful data.

Uzunoglu et. al. [22] employed a mode matching technique to analyze the frequency-dependent characteristics of a step discontinuity in width enclosed in a waveguide structure. The fields on both sides of the discontinuity are expanded in terms of the hybrid modes. By applying the boundary condition that the continuity of the transversal field components must be met at the location of the step, these modes are matched to find the unknown coefficients associated with the hybrid modes by which scattering parameters are determined for the step.

Jackson and Pozar [23] formulated the integral equations for open-end and gap discontinuities in terms of the grounded dielectric slab and four different types of expansion modes for the electric surface current density, including the piecewise sinusoidal modes to model the nonuniform current near the discontinuities. Obviously, the accuracy of this method relies on the number of unknown coefficients associated with piecewise modes used to represent the excess current. It is questionable that they used a sufficient

number of expansion functions to obtain accurate characterizations of the discontinuities. However, with the formulation, surface wave excitation and space wave radiation can be included to determine the amount of radiation from the open end.

In [24], finite element expansion currents are used to formulate a full-wave analysis of stubs, bent stubs, and steps in width, including radiation, surface wave effect and coupling between closely spaced junctions. This method modeled microstrip junctions on an open substrate by using rooftop functions and sinusoidal pre-computed expansion currents for input and output microstrip lines. This setup achieved a substantial improvement in accuracy and numerical efficiency and measurements were presented to verify stub calculations. The technique used has a natural limitation to the strip dimensions that are multiples of the element size.

1.6 Dynamic source reversal method based on potential theory [1]

The technique developed in Toncich's thesis for solving microstrip discontinuity problems is based on using the dynamic source reversal method formulated in terms of the vector and scalar potentials.

The discontinuous microstrip structure analyzed is enclosed in a dielectric loaded waveguide as shown in Fig.1.5. It has dimensions chosen such that at the frequency of operation for the dominant mode, all waveguide modes are nonpropagating. The substrate with zero-thickness strip conductor is assumed to be lossless, non-magnetic and isotropic. No radiation loss is accounted for since the structure is completely enclosed by the waveguide.

Inside the waveguide, let G_x, G_z, and G be scalar Green's functions corresponding to the components of A_{oxr} and A_{ozr}, the vector potentials, and that of ϕ_o, the scalar potential respectively. Define J_{oxr}, J_{ozr}, and ρ_o as the relative currents and the charge for a propagating dominant mode on the infinite microstrip line.

The potentials are then related to the dominant mode sources by

$$A_{oxr} = \mu_0 \int_{-\infty}^{\infty} \int_{-w}^{w} G_x(x,z;x',z') J_{oxr}(x') e^{-j\beta z'} dx' dz' \tag{1.5a}$$

$$A_{ozr} = \mu_0 \int_{-\infty}^{\infty} \int_{-w}^{w} G_z(x,z;x',z') J_{ozr}(x') e^{-j\beta z'} dx' dz' \tag{1.5b}$$

$$\phi_o = \varepsilon_0^{-1} \int_{-\infty}^{\infty} \int_{-w}^{w} G(x,z;x',z') \rho_o(x') e^{-j\beta z'} dx' dz' \tag{1.5c}$$

where the prime coordinates are the source points and the unprimed coordinates are field points.

Expressions for the Green's functions in Eq.(1.5) can be obtained by a Fourier transform method in which they are properly chosen to ensure that the corresponding boundary conditions are satisfied.

Precise expressions with the edge conditions built in for the dominant propagating charge and longitudinal current on the infinite strip are given in [1] and can readily be derived through conformal mapping techniques. There is no dominant mode transverse current J_{ox} assumed on the strip since its effect is negligible for a wide range of useful geometries. For some discontinuities like asymmetrical gap problems, this current is included as a fading dominant term plus a perturbation term which are localized near the discontinuity.

From Eq.1.5b and 1.5c, an iteration technique was developed by Kretch and Collin [25] to determine the coefficients associated with the source expressions and to find the effective dielectric constant for a given waveguide geometry without a top cover.

In this approach, $\varepsilon_0\phi_o$ is set equal to 1 on the strip, and A_{ozr}/μ_0 is also set equal to 1 on the strip where ϕ_o is an absolute value for the scalar potential, and A_{ozr} is the reference value for the vector potential caused by the relative current J_{ozr} which is related to the true current by $J_{oz} = (\beta c / k_0)J_{ozr}$.

Applying Galerkin's method, one can reduce the above two integrals to a system of linear equations. Then, using a trial value of β in the matrix, the iteration is repeated , if the new value of the effective dielectric constant, ε_e, differs from the old value of ε_e by more than 1% ; otherwise, the iteration is terminated after the condition is satisfied.

Now assume that instead of an infinite line, the line is terminated at some point in a discontinuity. The presence of a discontinuity causes a reflected dominant mode charge and current to appear on the line along with a perturbation in the sources localized in the vicinity of the discontinuity. For the gap problem, the total charge and relative current expressions on the coupling line can be also found. We can form the equations for the vector and

scalar potentials for the discontinuity due to the total source distributions including the perturbations on the line or lines. Actually, we can make the dominant mode sources extend over the other semi-infinite interval to form an infinite line, and then subtract the effects of these sources in the extension interval, in the mathematical sense.

When the tangential components of the electric field, E_x and E_z, are calculated by the potentials through $\vec{E} = -j\omega\vec{A} - \nabla\phi$, the contributions from the dominant mode sources on the infinite line already satisfy the boundary conditions so that these terms can be dropped. The terms involving integrals from the extension interval may be considered as the source reversed terms and produce the impressed field on the original semi-infinite line.

Since these source reversal terms are given in terms of the solved dominant mode amplitudes of charge and current for the infinite line, they now make up a known forcing function. This is the basis of the dynamic source reversal technique presented in [1].

Applying the moment method, and using suitable testing functions to enforce the boundary conditions that the tangential components of the electric field, E_x and E_z, vanish on the conducting strip, one can construct a set of linear equations. Then, by inverting the matrix, the unknown perturbed charge and current along with the unknown input susceptance can be determined.

After finding the input susceptance, one can extract the element values of the equivalent circuits for the discontinuities. The equivalent circuit of an open end discontinuity is represented by an excess capacitance. It can be computed immediately by a very simple equation. However, that of a gap is a two port network and must be represented by a three-element equivalent circuit, such as the capacitive pi network. For this problem, one can use the Tangent method [18] to find the equivalent element values.

The Tangent method was developed as an experimental technique to characterize the discontinuity by an equivalent circuit with three parameters as shown in Fig.1.6.a. The measurement should be made at reference planes located sufficiently far away from the discontinuity so that only dominant modes are present on the line. A plot of the null positions ϕ_1 as a function of the short circuit position ϕ_2 yields a curve as shown in Fig.1.6.b. An analysis of the equivalent circuit gives expressions for the equivalent circuit parameters θ_1 , θ_2 , and n:1 in terms of the curve parameters ϕ_1 vs. ϕ_2.

With reference to these Figures, a bilinear relationship between electrical null positions ϕ_1 and ϕ_2 may be expressed as

$$\tan(\phi_1) = \frac{A + B\tan(\phi_2)}{C + D\tan(\phi_2)} \tag{1.6}$$

where ϕ_1 is the location of an electric field null on the input side of the discontinuity with a given short circuit position ϕ_2 on the output side. In the dynamic source reversal method the coefficients A, B, C, and D can be obtained from a single matrix inversion of the equations that determine the perturbed currents and charges. A similar bilinear equation can be derived for any lossless two-port network with A, B, C, and D being functions of the equivalent circuit parameters that are used. A comparison of two sets of coefficients enables the equivalent circuit parameters to be found.

The above is the dynamic source reversal technique presented in Toncich's thesis and used to find the excess capacitances of microstrip open ends and gaps with isotropic substrates.

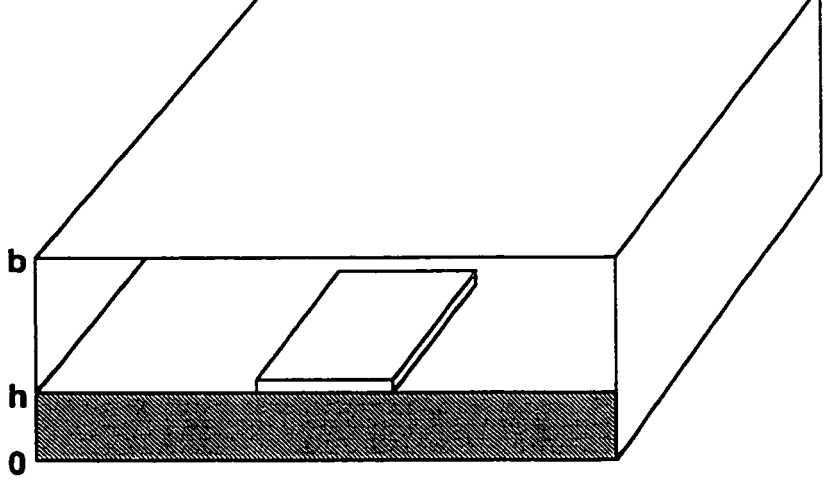

(a) Front view

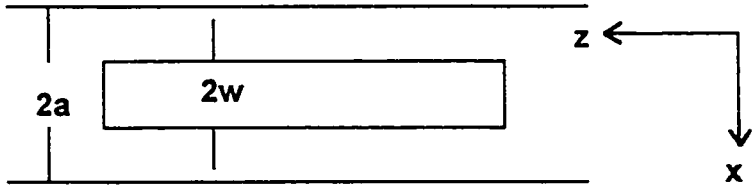

(b) Top view

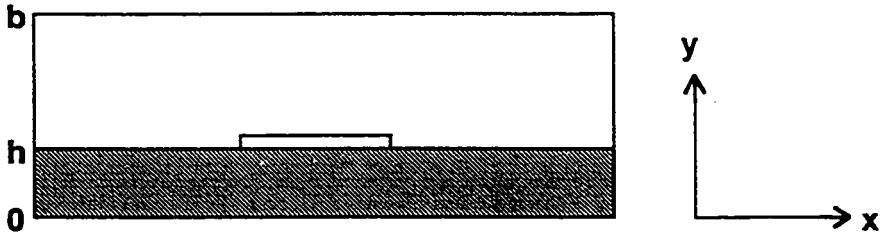

(c) End view

Fig. 1.5 Shielded microstrip geometry

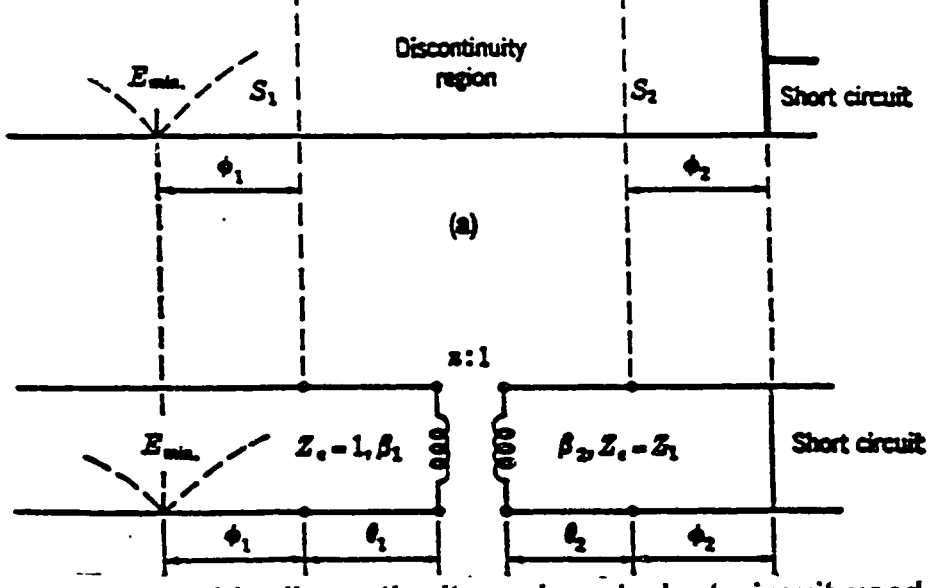

Fig. 1.6.a Waveguide discontinuity and equivalent circuit used in Tangent method

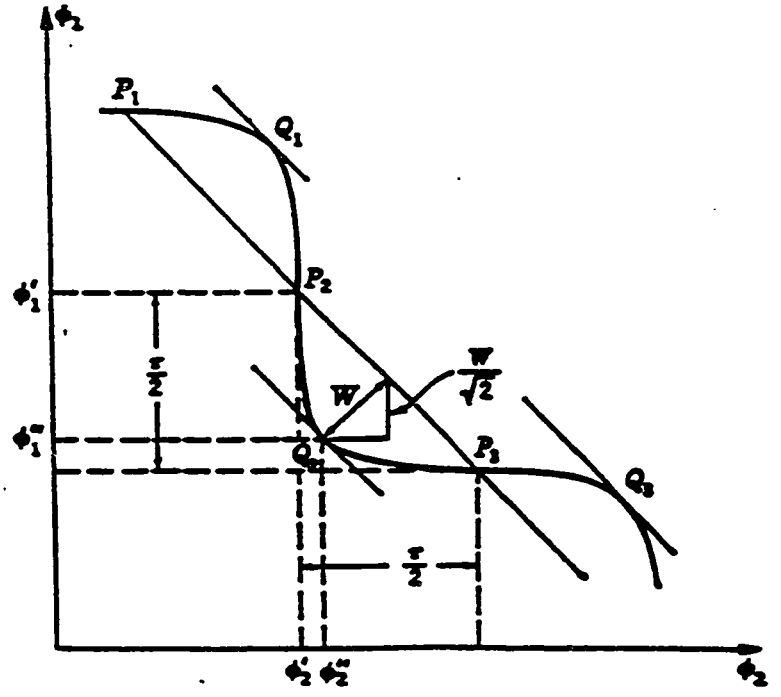

Fig. 1.6.b Plot of ϕ_1 vs. ϕ_2 as determined by Tangent method

1.7 Literature review of coplanar waveguide dispersion

A coplanar waveguide (CPW) whose configuration is shown in Fig.1.7 consists of a conductor centered between two ground planes, all on the same plane surface. This structure permits easy shunt connection of external elements in hybrid and monolithic microwave integrated circuits (MMIC). Coplanar Waveguides have the advantage over microstrip of not requiring substrate vias. Also, coplanar waveguide losses can be less than those of microstrip.

Because of the built-in elliptically polarized magnetic field which is easily accessible in the slots at the air-dielectric interface, CPW lends itself to non-reciprocal gyromagnetic device applications. In addition, low loss substrates with high dielectric constant may be used to reduce the longitudinal dimension of the integrated circuits due to the fact that the characteristic impedance of coplanar waveguide is relatively independent of the substrate thickness.

An early paper on coplanar waveguide propagation characteristics was presented by Wen who used a zero-order quasi-static approximation and conformal mapping [26]. This paper calculated some propagation and characteristic impedance data and demonstrated that it is a natural structure to incorporate in nonreciprocal gyromagnetic devices, such as resonator isolators and differential phase shifters. However, his method assumed a non-shielded configuration and the infinite ground planes and substrate thickness, to derive simple formulas for the CPW characteristics. The dispersion characteristics are, to some extent, influenced by these parameters and are a function of frequency.

In [27], the analysis of coplanar waveguide dispersion characteristics was developed in the spectral domain. All hybrid-field components can be

obtained from a superposition of TE and TM modes expressed in terms of two scalar potential functions. By applying Fourier transforms to these functions and the boundary conditions of the fields at the interfaces separating three regions, one can form a matrix relating the current density to the electric field components. By choosing the appropriate basis functions for the electric-field components and applying Galerkin's method to the matrix, the authors solved the generated set of homogeneous linear equations to find the propagation constant by an iteration scheme. The first-order approximation, which is the assumption that $E_z = 0$, was utilized to achieve greater computational efficiency. Also, the even and odd mode characteristic impedances were calculated by using the power-voltage definition for characteristic impedance.

Although this work involved the extensive manipulation of the equations to reduce the calculation time the simplified structure under investigation and choice of a one-term basis function caused inaccuracy so the results have limited accuracy.

Naldi et. al. , considered several possible configurations of coplanar waveguide which are shielded or/and conductor-backed in their paper [28]. The influence of the finite extent of lateral ground planes on the impedance level of the line was dealt with, also. The equations they derived by conformal mapping techniques have very simple closed forms and are user handy. However, all analytical formulas were obtained by quasi-static analysis which produces inaccurate results at the higher frequencies where most applications are found for coplanar waveguide.

In [29], a full-wave analysis of coplanar waveguide using the time-domain finite-difference method was proposed. Mei et. al. , treated the open structure coplanar waveguide so artificial boundaries must be employed to

truncate the mesh. Due to its smoothness in time and the easy adjustment of the specific pulse width, a retarded Gaussian pulse was used as an excitation in the time domain calculations.

After setting up the simulation area and subsequent pulse excitation, they evaluated the field distributions produced by the given Gaussian pulse over the whole computation region. With the field distributions in the time domain, the frequency-domain parameters, such as the effective dielectric constant and the complex characteristic impedance, were found by the Fourier transform inversion of the time domain data.

In this approach, since Fourier transforms are very sensitive to errors caused by reflected waves from the artificial boundaries, the reflection from these walls must be minimized. Unlike the microstrip case where one may apply exact Dirichlet or Neumann boundary conditions to the bottom plane, the structure of the coplanar waveguide under their investigation didn't allow any simple way to enforce these boundary conditions.

Chang et. al. [30] presented a rigorous full wave analysis of coplanar waveguide dispersion characteristics, based on reaction theory. It is the combination of variational method and a modification of Wen's conformal mapping technique to facilitate a finite solution. The mapping function transforms the infinite original domain into finite image domain and also overcomes the difficulty of field singularities near the conductor edge. In this paper, particular attention is paid to the electric field distributions over the air-dielectric interface of slots and the current distributions on the conducting strip varying with frequency. The authors also showed that the calculated results for characteristic impedance are different from each other with the various definitions. However, this method needs very long computational time

and the data for characteristic impedance shows that there is something wrong at the higher frequency range.

Kitazawa and Itoh [31] analyzed the propagation characteristics of coplanar waveguide with lossy media. The analysis used in the paper is founded on the hybrid-mode formulation by using both the spectral-domain method and the perturbation method. The unknown aperture fields are expanded in terms of the appropriate basis functions for which they proposed two sets of expansion functions with the different edge conditions built-in. One set is expressed by Chebyshev polynomials and the other is given by Gegenbauer polynomials to account for the conductor loss calculated by the perturbation scheme. This special choice of basis functions with Gegenbauer polynomials for the thick conductor model prevents the integrals , which are used for the calculation of the conductor losses, from becoming singular when evaluated at the conductor edge. Numerical results show that these special functions chosen but not derived in the mathematical sense result in convergence rates as fast as those for the zero-thickness cases.

In [32], a scattering-type formulation of the transverse resonance technique was applied to treat a variety of currently practically used (M)MIC configurations. By introducing transverse boundary conditions in terms of reflection coefficient matrices, the transverse resonance procedure can easily be adapted to include open, conductor-backed, and shielded configurations while the resonance condition itself remains unchanged. Also this method preserves numerical stability by allowing the number of expansion terms in different subregions to be individually selected. Although the author claimed that the FORTRAN software code is operational on 386-type personal computers, the CPU time required to calculate the effective dielectric

constant and characteristic impedance per frequency sample varies from five to twenty minutes.

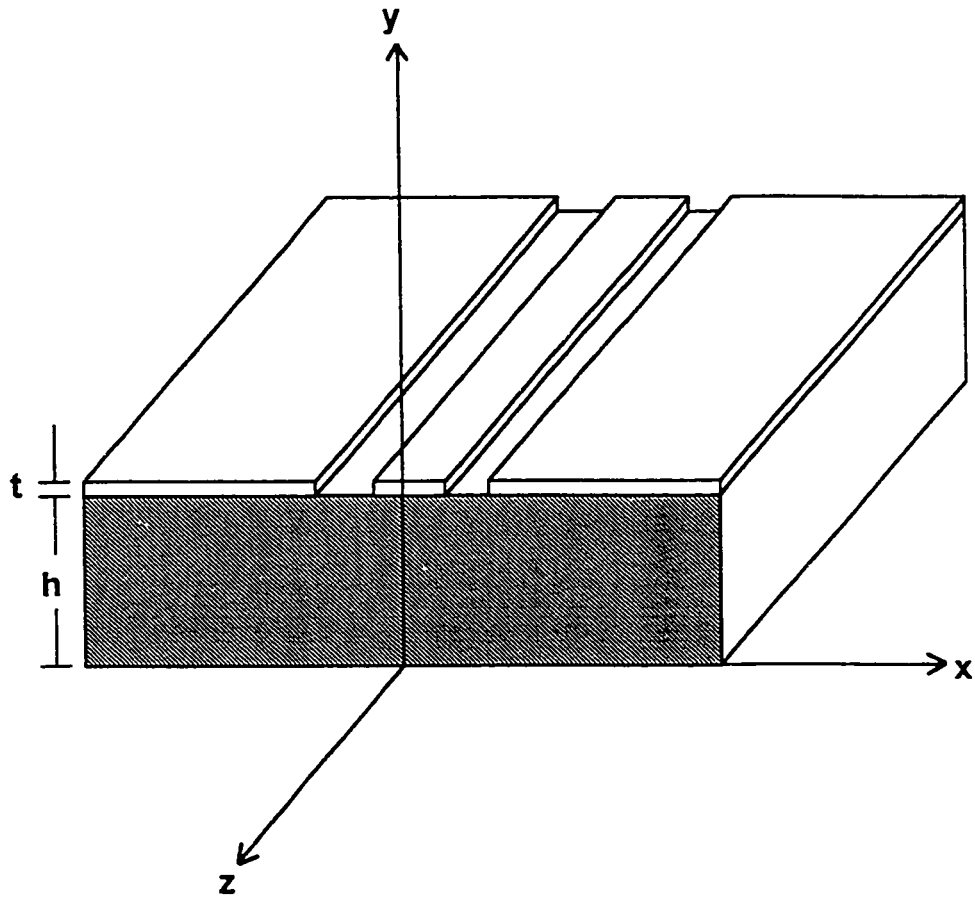

Fig. 1.7 Coplanar waveguide geometry

1.8 Literature review of coplanar waveguide discontinuities

Since coplanar waveguide is popularly used as passive elements in the design of monolithic microwave integrated circuits, CPW discontinuities are often encountered. In this section, we review the following techniques to characterize the discontinuities including quasi-static analysis and full-wave analysis

(1)Three dimensional finite difference method [33].

(2)Mode conversion method [34].

(3)Moments method in the spatial domain [35].

(4)Mode matching method [36].

(5)An extension of the spectral domain method [37].

(6)Three dimensional time domain finite difference method [38].

Ingo Wolff et. al. , used a three dimensional finite difference approach to treat coplanar waveguide discontinuity problems [33]. This is a quasi-static analysis and is a modified version of the well-known finite difference method. The planar structure containing a discontinuity and the semi-infinite transmission lines was surrounded by the electric and magnetic shielding walls. The two magnetic walls were defined at suitable distances away from the discontinuity where the input and output ports were formed such that perturbations due to the discontinuity can be neglected at these ports.

Using Laplace's equation, the electrical potential at any point inside the box can be written in finite difference form as a linear combination of the neighboring potentials at the grid points. The relaxation method, where the relaxation constant has the optimal value, determines the speed of convergence, and was used for the solution of the resulting system of equations.

Because of the small dispersion of coplanar lines, the good agreement between the calculated data and the measurements up to 25 GHz was found. However, for other dispersive lines the validity of this method is not guaranteed.

In [34], for the coplanar waveguide embedded in a waveguide, it was found that the structure supports modes which can be categorized into three groups ; namely, the modes guided by the CPW slots, the parallel plate modes guided between the CPW plane and lower conducting plane, and the parallel plate modes guided by the cover. The third group of modes is relatively less important than the first two groups. The second microstrip-like lowest mode is usually present and can serve as a vehicle for energy leakage from the CPW. The leakage occurs when the velocity of the parasitic mode is slower than the phase velocity of the fundamental mode. To confine the propagating energy at the desired frequencies, the mode degeneracies or interactions between the CPW mode and the waveguide or microstrip-like mode which depends on the sidewall conditions must be avoided.

For the configuration with magnetic side walls, there are overmoding problems the same as those of an overmoded rectangular waveguide. In [34], the energy coupling from one mode to the other for the open end and shorted end discontinuities was calculated. In this structure, there are three significant modes which are coplanar waveguide mode (CPW), coplanar microstrip mode (CPM), and microstrip mode (MS). Actually, part of the incident CPW wave is reflected back as a CPW wave, part is reflected back as a CPM wave traveling on the same line, and part is transmitted beyond the discontinuities as an MS mode. This conversion is important since the CPM or MS modes do not couple to active devices on the CPW surface. It may result in resonances and power suck-outs which could render a circuit inoperable.

Using a finite element technique, which is rigorous in the moments method sense, Jackson concluded from the theoretical results that a smaller structure for the center conductor converts less power, and the power converted at a shorted end is much less than at a gap end. However, the measurement of the transmission for an open end indicates that the calculated results are somewhat greater than the measured ones by about 1 dB, but no meaningful data for the shorted end were reported.

In [35], the method used to study CPW discontinuities is based on a space domain integral equation (SDIE) which was solved by the method of moments. Thus, in the SDIE approach, the Fourier transforms of the basis functions which are used in the spectral domain are not needed. This makes it simpler to handle complicated geometries.

By introducing an equivalent magnetic current on the slot aperture and applying the continuity of the tangential components of magnetic field on the surface of the slot aperture, we can form a space-domain integral equation as shown in Eq.1.8. The unknown magnetic current is then expressed as a finite double summation with a family of rooftop functions where the subdomain basis functions for each current components have piecewise-sinusoidal variation along the longitudinal direction and constant variation along the transverse direction. The required integral equation is

$$\bar{a}_y \times \int_{S_s} \int \left[\overline{G}_0 + \overline{G}_1\right] \cdot \bar{M}(\bar{r}) dS' = \bar{J}_s \tag{1.8}$$

where S_S is the surface of the slot aperture, $\overline{G}_{0,1}$ is the dyadic Green's functions in the two waveguide regions, $\bar{M}(\bar{r})$ is the unknown equivalent magnetic surface current density, and $\bar{J}_s$ vanishes everywhere on the plane of

the slot apertures except at the position of the electric current sources exciting the CPW.

By this method, theoretical results for the scattering parameters of two CPW discontinuities ; that is, open ends and shorted ends , were computed. From the scattering parameters, the lumped element equivalent circuits have been derived and used to model the discontinuities by closed-form equations, as functions of the stub length. The agreement between the theoretical results and the experimental data in both magnitudes and phase angles for the scattering matrix elements is very good for the frequency range 5 to 25 GHz

In [36], Itoh et. al. , presented the mode matching method to analyze the shielded junction discontinuities in coplanar waveguide including the finite metal thickness effect since neglecting this effect in MMIC design may result in substantial inaccuracy, especially when the dimensions of the circuits are comparable to the wavelength and the thickness becomes significant. Electromagnetic fields for coplanar waveguide with no discontinuity in each region can be formulated in terms of the mode voltages and currents which were derived by applying conventional circuit theory to the equivalent circuit in the y direction. After some mathematical manipulations, the mode voltages and currents can be expressed as the Fourier transforms of the unknown aperture electric fields. Using the boundary conditions that the magnetic fields are continuous at the interfaces of the conducting lines and the dielectric or the air, one can obtain a system of equations relating these Fourier transforms to the surface current distribution on the top and bottom surfaces of the metallization.

For the numerical calculation, the unknown aperture electric fields were expanded by appropriate basis functions with the edge condition. Then, applying Galerkin's method to the system of equations, the propagation

constant was found. With this, electromagnetic fields on both sides of the discontinuity are expressed as the eigenmodes of the individual transmission lines. Since the tangential components of the fields are continuous across the plane the discontinuity is located at, the set of mode-matching equations on both sides was obtained. Utilizing the inner product where the electric field equations were taken from the waveguide having the smaller aperture and the magnetic field equations were used for the larger aperture, the unknown coefficients associated with the eigenmodes were solved and from them the scattering parameters are found.

The calculated magnitudes and phases of the scattering parameters for coplanar waveguide step discontinuity with different metallization thickness were shown in this paper which notes that throughout the frequency range of interest, the finite metallization thickness effects the reflection coefficient significantly only at the high frequency range.

Ingo Wolff and Thomas Becks [37] used an extension of the spectral domain method to analyze various types of air-bridges within CPW bends and T-junctions. This method starts with the introduction of magnetic surface currents to restore the slot electric fields at the apertures. Then, in the following, the derivation of the integral equation, application of image theory in connection with superposition principle, and the technique to extract generalized S-parameters are described briefly. In order to check the accuracy of the algorithm, four coplanar T-junctions on a GaAs substrate, containing three standard modified air-bridges, were built and measured. For the even mode scattering parameters, a very good agreement over the whole frequency range was obtained when compared with the calculated results. Various data for the conversion from the even-mode to the odd mode within these structure is also given.

Visan et. al. [38] presented a rigorous and efficient full-wave analysis for characterizing air bridges and via holes, based on a 3D finite difference time domain method. To obtain the discrete formulations to approximate Maxwell's curl equations, the centered difference approximation is used in the first order partial derivative with respect to both time and space. This method can be used to accurately determine the structure field solution in a very broad frequency band, by simulating the propagation of a gaussian pulse through each studied structure. Then, by the Fourier transform of the transient results, the parameters in the frequency domain can be calculated over the whole required frequency range. In this paper, they analyzed an air bridge and two via holes which can be used to suppress the coupled slotline-like mode in MMIC conductor-backed coplanar waveguides. It can be seen from the data shown in the article that the via hole solution gives better transmission property than the air bridge one although the via hole can complicate the fabrication of the structure.

1.9 Experimental techniques for coplanar waveguide discontinuities

Since little information is available in the literature on discontinuity models for coplanar waveguide, it has limited the application of CPW in microwave circuit design. In [39], the discontinuities characterized are an open end, a series gap in the center conductor, and a symmetric step in the center strip as shown in Fig. 1.8. The element values of the corresponding equivalent circuit are de-embedded from the measured scattering parameters of the discontinuities through a two-tier de-embedding technique which consists of calibrating the automatic network analyzer (ANA) using precision coaxial standards and then making use of the calibrated ANA to characterize the test fixture.

A CPW open circuit is formed by terminating the center conductor away from the slot ends by a short distance. The open circuit capacitance is a parallel combination of the capacitance due to the fringing fields across the gap and those across the slot. It is known that the gap-dependent capacitance changes proportionally as the inverse of the short distance while the slot-dependent capacitance is relatively constant.

A series gap is still modeled as a lumped pi network, consisting of one coupling capacitance and two fringing ones. The coupling capacitance decreases proportionally as the inverse of the distance between the gap.

The step discontinuity perturbs the normal CPW electric and magnetic fields which give rise to additional reactances. The modeling experiments show that the reactances can be modeled as a shunt capacitance located in the plane of discontinuity. The influence of this capacitance is to effectively lengthen the lower impedance CPW line towards the higher impedance CPW line.

All the above-mentioned capacitances of the equivalent circuits for the discontinuities have the same feature that the capacitances are larger for the line with wider center conductor if two CPW lines with identical aspect ratio on the same substrate are compared.

However, there are three basic sources of error for the equivalent circuit element values ; i.e. , modeling errors, RF measurement errors, and geometrical errors. Therefore, some modifications and optimization routines must be used to reduce errors.

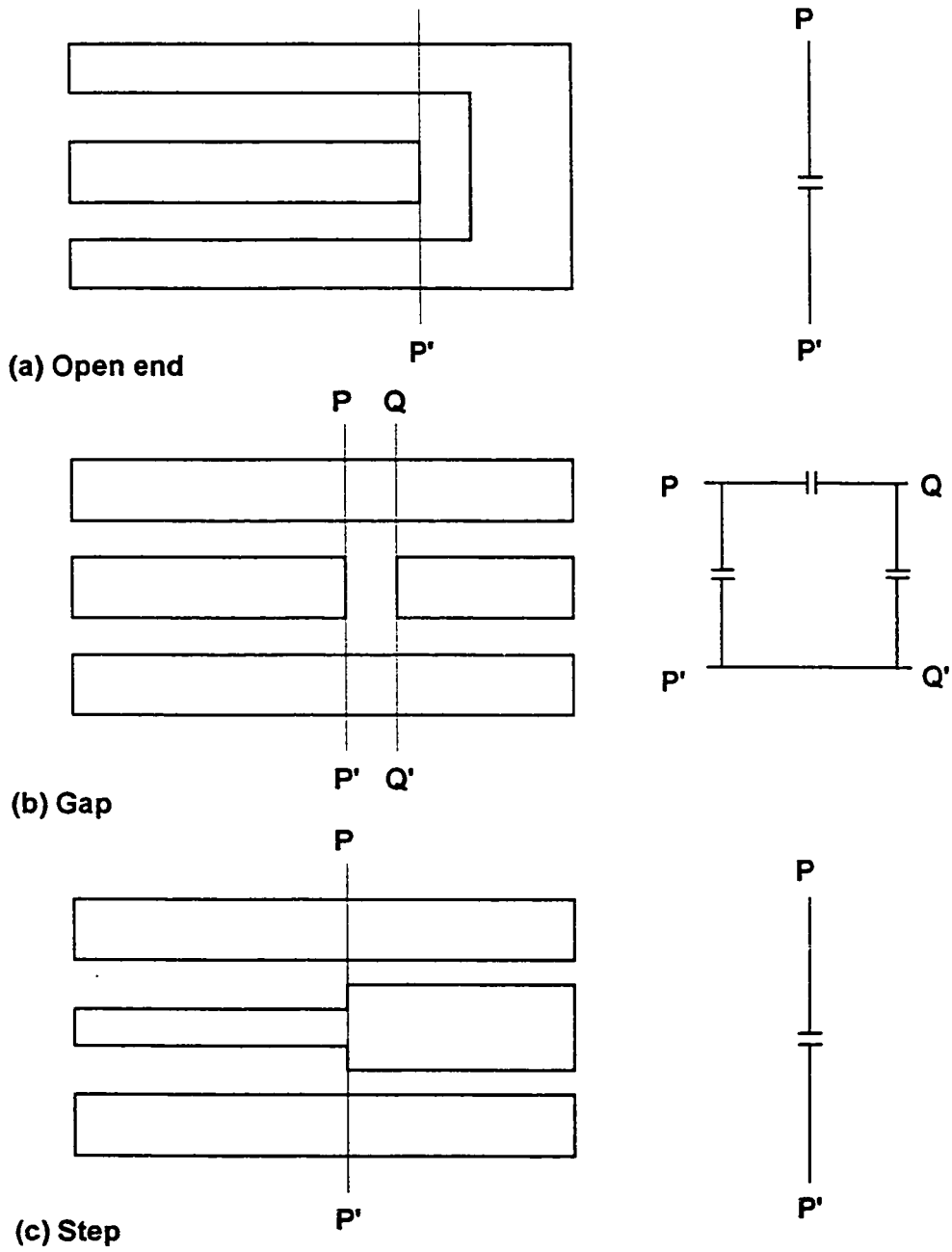

Fig. 1.8 Some discontinuities in coplanar waveguide

1.10 Overview of dissertation research

The research work in this dissertation involves the following topics

(1)Applications of the dynamic source reversal method to microstrip open end and gap discontinuities in which anisotropic substrate materials, frequently encountered in practice, are used in analytical computation.

(2)Treatment of the propagation characteristics for coplanar waveguides containing anisotropic substrates.

(3)Development of the dynamic source reversal method to analyze some coplanar waveguide discontinuities including anisotropic substrates.

Basically, the concepts used to extend the dynamic source reversal technique are the same as those used in Toncich's work. The major differences are that

(a)We develop this powerful dynamic source reversal method to characterize microstrip discontinuities including anisotropic substrates which are often encountered in reality.

(b)We utilize two pairs of expansion functions for the perturbed charge and current. One is called TP representation , the same as that used by Toncich, which uses triangle functions to expand the perturbed current and bipolar functions for the perturbed charge. The other is denoted QT representation that uses a quadratic approximation for the current and triangle functions for the charge expansion. This leads us to take advantage of two different testing functions, offset and nonoffset.

(c)We maintain the source vector terms when the transverse current is considered in the gap problem. These source vector terms were originally assumed as a zero vector in Toncich's thesis. As it is a time-saving approach, we attack the gap problem directly, and then allow the gap spacing to go to infinity to solve the open-end problem.

(d)Also, we use another testing technique in the x direction for E_x, different from Toncich's, when the transverse current is included. We find that his testing approach in this problem causes some troubles, which make the terms summed over the index n not accurate unless a very large number of terms are used, especially when the line width is narrow.

The dynamic source reversal method developed to treat microstrip discontinuities can be applied to coplanar waveguide discontinuities, with some techniques modified. The discontinuous coplanar waveguide to be characterized is similar to that in Fig.1.5, but containing two ground planes on each side of the central strip. Obviously, the expressions for the Green's functions have the same forms as those obtained for microstrip lines.

As a first step, we develop an efficient way to find the dominant mode charge and current expressions on the central strip and ground planes for a coplanar waveguide without any discontinuities. This method uses the conformal mapping to establish the exact low frequency charge and current distributions in a shielded coplanar waveguide. This new expression is sufficiently general to cover the shielded microstrip line as well by letting the ground planes have a vanishing width.

The general expressions for the sources, derived for the first time in the literature, are applicable to both coplanar waveguide and microstrip line. Also, included are expressions for the charge and current on the ground planes, with the same form relative to those on the central strip in the transform domain.

The iteration technique used for microstrip line is revised to find the effective dielectric constant for an enclosed coplanar waveguide structure with a top cover. Then, having the dominant mode charge and current

coefficients, we can obtain the characteristic impedance, which is defined as the ratio of the voltage across the slot to the total current in the central strip.

The analysis that we develop for discontinuities in coplanar waveguide is an extension of the dynamic source reversal method used in microstrip, except for the consideration of also requiring the dominant mode and perturbations in charge and current on the ground planes. Since the method presented to describe the source distributions is an excellent and accurate first step static approximation, we can obtain very efficient numerical calculation of those parameter values of the equivalent circuits for coplanar waveguide discontinuities. Detailed evaluations are accomplished for the open-end.

Chapter 2

Formulation of integral equations

In this chapter, we derive the Green's functions which are necessary to develop the dynamic source reversal method with the satisfaction of the boundary conditions for a dielectric loaded waveguide including anisotropic substrates. The expressions for the sources, the charges and currents existing on the microstrip line, are given. Then, integrating the product of the Green's functions and the sources over the width of the line yields the scalar and vector potentials, from which we can determine the electric fields existing inside the enclosure.

2.1 Derivation of Green's functions

Considering Fig.1.5 with anisotropic substrates, we can express the dielectric constant as

$$\bar{\kappa} = \kappa\bar{I} + [\kappa_y(y) - \kappa(y)]\bar{a}_y\bar{a}_y \tag{2.1}$$

where $\bar{I}$ is the unit dyadic function, $\kappa_y(y)$ is the dielectric constant in the y direction of the substrate and $\kappa(y)$ is the dielectric constant in both the x and z direction. In this configuration it is assumed that the microstrip line with negligible thickness is located at a height just above the slab. The sources on the strip are defined as the transverse and longitudinal sources which are both x and z dependent. First of all, we start with Maxwell's equations to derive the equations for the potentials $\vec{A}$ and ϕ, in terms of the sources $\vec{J}$ and ρ on the strip with all source and field quantities having a time dependence $e^{j\omega t}$.

$$\nabla \cdot \vec{D} = \rho \tag{2.2a}$$

$$\nabla \cdot \vec{B} = 0 \tag{2.2b}$$

$$\nabla \times \vec{E} = -j\omega\vec{B} \tag{2.2c}$$

$$\nabla \times \vec{B} = \mu_0\vec{J} + j\omega\mu_0\varepsilon_0\vec{\kappa}\cdot\vec{E} \tag{2.2d}$$

Since the magnetic flux density vector $\vec{B}$ is always solenoidal, it may be given in terms of the curl of a vector potential function

$$\vec{B} = \nabla \times \vec{A} \tag{2.3}$$

When Eq.(2.3) is substituted into Eq.(2.2c), it yields

$$\nabla \times (\vec{E} + j\omega\vec{A}) = 0 \tag{2.4}$$

and, in turn, the vector in the parenthesis can be expressed as the gradient of a scalar potential function by

$$\vec{E} = -j\omega\vec{A} - \nabla\phi \tag{2.5}$$

Starting with Eq.(2.2d) into which Eq.'s(2.3) and (2.4) are substituted, we have, after some arrangement of terms,

$$\nabla(\nabla\cdot\vec{A}) - \nabla^2\vec{A} = \mu_0\vec{J} + k_0^2\kappa\vec{A} - j\omega\mu_0\varepsilon_0\nabla(\kappa\phi) + j\omega\mu_0\varepsilon_0\phi\frac{\partial\kappa}{\partial y}\vec{a}_y + j\omega\mu_0$$
$$\varepsilon_0(\kappa_y - \kappa)\frac{\partial\phi}{\partial y}\vec{a}_y + k_0^2(\kappa_y - \kappa)A_y\vec{a}_y \tag{2.6}$$

By using Lorentz condition, $\nabla\cdot\vec{A} = -j\omega\mu_0\varepsilon_0\kappa\phi$, and separating each equation utilizing the fact that $\vec{J} = J_x\vec{a}_x + J_z\vec{a}_z$, three scalar equations are produced

$$\nabla^2 A_x + \kappa k_0^2 A_x = -\mu_0 J_x \tag{2.7a}$$

$$\nabla^2 A_z + \kappa k_0^2 A_z = -\mu_0 J_z \tag{2.7b}$$

$$\nabla^2 A_y + \kappa k_0^2 A_y = j\omega\mu_0\varepsilon_0\left[(\kappa_y - \kappa)\frac{\partial\phi}{\partial y} + (\kappa - 1)\phi(h)\delta(y - h)\right] \tag{2.7c}$$

where $\frac{\partial \kappa}{\partial y} = (1-\kappa)\delta(y-h)$ is used

Now tackling Eq.(2.2a) by noting that $\vec{D} = \bar{\kappa} \cdot \vec{E}$ and using Eq.(2.5), we obtain

$$\kappa\left[\frac{\partial \phi}{\partial x^2} + \frac{\partial \phi}{\partial y^2}\right] + \frac{\partial}{\partial y}\left(\kappa_y \frac{\partial \phi}{\partial y}\right) + k_0^2 \kappa^2 \phi = -\frac{\rho}{\varepsilon_0} + j\omega(\kappa_y - 1)A_y(h)\delta(y-h) - j\omega(\kappa_y - \kappa)\frac{\partial A_y}{\partial y} \qquad (2.8)$$

A dielectric loaded waveguide can support longitudinal section electric (LSE) and longitudinal section magnetic (LSM) modes. An LSE mode has no component of $\vec{E}$ normal to the air-dielectric interface, while an LSM mode has no $\vec{H}$ component normal to the interface. Consequently, H_y may be given in terms of LSE modes, while E_y requires LSM modes. It can be understood from Eq.(2.5) that ϕ which contributes to all three components of $\vec{E}$ must be represented by both LSE and LSM modes.

The Green's functions G_x, G_z, and G respectively associated with A_x, A_z, and ϕ can be determined in such a way to satisfy the appropriate boundary conditions which are listed below

$$(1) A_z = \begin{cases} 0 & \text{at } x=\pm a \\ 0 & \text{at } y=0,b \end{cases} \qquad (2.9a)$$

$$(2) \frac{\partial A_x}{\partial x} = 0 \quad \text{at } x = \pm a\,,\ A_x = 0 \quad \text{at } y = 0, b \qquad (2.9b)$$

$$(3) A_y = 0 \quad \text{at } x = \pm a\,,\ \frac{\partial A_y}{\partial y} = 0 \quad \text{at } y = 0, b \qquad (2.9c)$$

$$(4) \phi = \begin{cases} 0 & \text{at } x=\pm a \\ 0 & \text{at } y=0,b \end{cases} \qquad (2.9d)$$

Besides these, all of the above components are continuous at y=h and the first derivatives of them with respect to y are discontinuous at y=h.

Expressions for the Green's functions can be obtained by a Fourier transform method. Since G_x and G_z are similar, the expression for G_z is derived first from

$$(\nabla^2 + \kappa k_0^2)G_z = -\delta(x - x')\delta(y - h)\delta(z - z') \tag{2.10}$$

Assume a general solution for G_z to have the form

$$G_z = \frac{1}{2\pi}\sum_{n=1,3}^{\infty}\int_{-\infty}^{\infty}\cos(u_n x)f_n(y)e^{-j\omega z}d\omega \tag{2.11}$$

where $u_n = \frac{n\pi}{2a}$, n=1,3,5 $\cdots$.The x dependence for G_z has been chosen as a Fourier series expansion in terms of $\cos(u_n x)$, ensuring that the boundary conditions are satisfied at $x = \pm a$.

After substituting Eq.(2.11) into (2.10), taking the Fourier transform of it, multiplying both sides by $\cos(u_n x)$, and integrating it between $\pm a$, we obtain

$$a\left(\frac{\partial}{\partial y^2} + \kappa k_0^2 - u_n^2 - \omega^2\right)f_n(y) = -\cos(u_n x')\delta(y - h)e^{j\omega z'} \tag{2.12}$$

In order to satisfy continuity conditions for G_z, it is assumed that

$$f_n(y) = \begin{cases} A_n \sin(ly)\sin(pc) & 0 \le y < h \\ A_n \sin(lh)\sin[p(b-y)] & h \le y < b \end{cases} \tag{2.13}$$

where $l^2 = \kappa k_0^2 - u_n^2 - \omega^2$ and $p^2 = k_0^2 - u_n^2 - \omega^2$.

Integrating (2.12) over an infinitesimal interval in y centered at y=h results in the other required condition

$$a\frac{\partial}{\partial y}f_n(y)\Big|_{h^-}^{h^+} = -\cos(u_n x')e^{j\omega z'} \tag{2.14}$$

from which we find, after substituting Eq.(2.13),

$$A_n = \frac{\cos(u_n x')e^{j\omega z'}}{a[p\sin(lh)\cos(pc) + l\cos(lh)\sin(pc)]} \tag{2.15}$$

Therefore, the desired expression for G_z is

$$G_z(x,z;x',z') = \frac{1}{2\pi a}\sum_{n=1,3}^{\infty}\int_{-\infty}^{\infty}\cos(u_n x)\cos(u_n x')\sin(lh)\sin(pc)\frac{1}{D_{ln}}e^{-j\omega(z-z')}d\omega \tag{2.16}$$

where $D_{ln} = p\sin(lh)\cos(pc) + l\cos(lh)\sin(pc)$.

Similarly we have, with $\sin(u_n x)$ in place of $\cos(u_n x)$, the expression for G_x as follows

$$G_x(x,z;x',z') = \frac{1}{2\pi a}\sum_{n=1,3}^{\infty}\int_{-\infty}^{\infty}\sin(u_n x)\sin(u_n x')\sin(lh)\sin(pc)\frac{1}{D_{ln}}e^{-j\omega(z-z')}d\omega \tag{2.17}$$

To solve the Green's function for the scalar potential, we need to consider both G and G_y because Eq.'s (2.7.c) and (2.8) are coupled. Let us assume

$$G_y = \frac{1}{2\pi}\sum_{n=1,3}^{\infty}\int_{-\infty}^{\infty}\cos(u_n x)g_n(y)e^{-j\omega z}d\omega \tag{2.18a}$$

$$G = \frac{1}{2\pi}\sum_{n=1,3}^{\infty}\int_{-\infty}^{\infty}\cos(u_n x)h_n(y)e^{-j\omega z}d\omega \tag{2.18b}$$

With the same procedures as used in deriving G_z, we obtain

$$\left(\frac{\partial}{\partial y^2} + \kappa k_0^2 - u_n^2 - \omega^2\right)g_n(y) = j\omega\mu_0\varepsilon_0\left[(\kappa_y - \kappa)\frac{\partial h_n(y)}{\partial y} + (\kappa - 1)h_n(y)\delta(y-h)\right]$$

(2.19a)

$$\left(\frac{\partial}{\partial y}\kappa_y\frac{\partial}{\partial y}+\kappa^2k_0^2-\kappa u_n^2-\kappa\omega^2\right)h_n(y)=j\omega\left[-(\kappa_y-\kappa)\frac{\partial g_n(y)}{\partial y}+(\kappa_y-1)g_n(h)\right.$$
$$\left.\delta(y-h)-\frac{\delta(y-h)}{aj\omega\varepsilon_0}\cos(u_nx')e^{j\omega z'}\right]$$

(2.19b)

The functions of y may be chosen as

$$g_n(y)=\begin{cases}B_{1n}\cos(qy)+B_{2n}\cos(ly) & 0\le y<h\\ B_{3n}\cos[p(b-y)] & h\le y<b\end{cases} \quad (2.20a)$$

$$h_n(y)=\begin{cases}C_{1n}\sin(qy)+C_{2n}\sin(ly) & 0\le y<h\\ C_{3n}\sin[p(b-y)] & h\le y<b\end{cases} \quad (2.20b)$$

where $q^2=\frac{\kappa}{\kappa_y}(\kappa_yk_0^2-u_n^2-\omega^2)$.

The first derivatives of $g_n(y)$ and $h_n(y)$ with respect to y satisfy the conditions

$$\frac{\partial}{\partial y}g_n(y)\Big|_{h^-}^{h^+}=j\omega\mu_0\varepsilon_0(\kappa-1)h_n(h) \quad (2.21a)$$

$$a\kappa_y\frac{\partial}{\partial y}h_n(y)\Big|_{h^-}^{h^+}=-\frac{1}{\varepsilon_0}\cos(u_nx')e^{j\omega z'}+aj\omega(\kappa_y-1)g_n(h) \quad (2.21b)$$

After solving for the unknown coefficients corresponding to $g_n(y)$ and $h_n(y)$, we get the expression for G, which is

$$G(x,z;x',z')=\frac{1}{2\pi a}\sum_{n=1,3}^{\infty}\int_{-\infty}^{\infty}\cos(u_nx)\cos(u_nx')\frac{N_n}{(\kappa k_0^2-l^2)D_{1n}D_{2n}}e^{-j\omega(z-z')}d\omega \quad (2.22)$$

where $N_n=\{\kappa k_0^2[p\cos(qh)\sin(pc)+q\sin(qh)\cos(pc)]\sin(lh)-lq[p\cos(lh)\sin(pc)+l\sin(lh)\cos(pc)]\sin(qh)\}\sin(pc)$ and $D_{2n}=\kappa p\cos(qh)\sin(pc)+q\sin(qh)\cos(pc)$.

The integrals over ω can be evaluated by the method of residues, which states that $\oint f(z)dz = 2\pi j \cdot \sum \text{residues}$. To achieve this we must use the following partial fraction expansion

$$\frac{N_n}{(\kappa k_0^2 - l^2)D_{1n}D_{2n}} = \frac{k_0^2 \sin(lh)\sin(pc)}{(\kappa k_0^2 - l^2)D_{1n}} - \frac{qp\sin(qh)\sin(pc)}{(k_0^2 - p^2)D_{2n}} \tag{2.23}$$

Let γ_{nm} be the roots of D_{1n} and $\bar{\gamma}_{nm}$ be the roots of D_{2n}. Then, the residues of Eq.(2.23) at γ_{nm} are R_{nm} and those at $\bar{\gamma}_{nm}$ are $\bar{R}_{nm}$ as shown in the following

$$R_{nm} = \left[\frac{k_0^2 \sin(lh)\sin(pc)}{\kappa k_0^2 - l^2} \frac{1}{\frac{\partial D_{1n}}{\partial \omega}} \right]_{\omega = \pm\gamma_{nm}} \tag{2.24a}$$

$$\bar{R}_{nm} = \left[\frac{\bar{q}\bar{p}\sin(\bar{q}h)\sin(\bar{p}c)}{k_0^2 - \bar{p}^2} \frac{1}{\frac{\partial D_{2n}}{\partial \omega}} \right]_{\omega = \pm\bar{\gamma}_{nm}} \tag{2.24b}$$

where $\gamma_{nm} = (l_m^2 - \kappa k_0^2 + u_n^2)^{\frac{1}{2}}$ and $\bar{\gamma}_{nm} = (\frac{\kappa_y}{\kappa}\bar{q}_m^2 - \kappa_y k_0^2 + u_n^2)^{\frac{1}{2}}$. Note that the zeros of D_{1n} correpond to LSE mode eigenvalues while those of D_{2n} are the LSM ones. Note that the residues at the poles $l = \pm\sqrt{\kappa}k_0$ or $\bar{p} = \pm k_0$ for each term are canceled respectively.

Since the integral range is in $\pm\infty$, the contour can be closed at infinity in the upper half plane if $z<z'$, or in the lower half plane if $z> z'$. Considering the case $z'>z$, we obtain, after a lot of manipulations,

$$R_{nm} = \frac{k_0^2}{\kappa k_0^2 - l_m^2} \frac{p_m^2 l_m \sin(l_m h)\sin(p_m c)}{j\gamma_{nm} DR_{1nm}} \tag{2.25a}$$

$$\overline{R}_{nm} = \frac{\overline{q}_m^2 \overline{p}_m^3 \kappa_y}{k_0^2 - \overline{p}_m^2} \frac{\sin(\overline{q}_m h)\sin(\overline{p}_m c)}{j\overline{\gamma}_{nm} DR_{2nm}} \tag{2.25b}$$

where $DR_{1nm} = (\kappa - 1)k_0^2 \cos(l_m h)\sin(p_m c) + b p_m^2 l_m \sin(l_m h)\sin(p_m c) - p_m($ $p_m^2 h + l_m^2 c)\cos(l_m h)\cos(p_m c)$ and $DR_{2nm} = \kappa k_0^2(\kappa_y - 1)\sin(\overline{q}_m h)\cos(\overline{p}_m c) +$ $\overline{p}_m(\kappa^2 \overline{p}_m^2 h + \kappa_y \overline{q}_m^2 c)\sin(\overline{q}_m h)\sin(\overline{p}_m c) - \kappa \overline{p}_m^2 \overline{q}_m(\kappa_y c + h)\cos(\overline{q}_m h)\cos(\overline{p}_m c)$. Note that p_m, l_m, $\overline{p}_m$, $\overline{q}_m$ can be found from the following transcendental equations

$$l_m^2 - p_m^2 = (\kappa - 1)k_0^2$$
$$p_m \sin(l_m h)\cos(p_m c) + l_m \cos(l_m h)\sin(p_m c) = 0 \tag{2.26a}$$
$$\frac{\kappa_y}{\kappa}\overline{q}_m^2 - \overline{p}_m^2 = (\kappa_y - 1)k_0^2$$
$$\kappa \overline{p}_m \cos(\overline{q}_m h)\sin(\overline{p}_m c) + \overline{q}_m \sin(\overline{q}_m h)\cos(\overline{p}_m c) = 0 \tag{2.26b}$$

The expression for G, evaluated at y=h, can now be written as

$$G(x,z;x',z') = \frac{1}{a}\sum_{n=1,3}^{\infty}\sum_{m=1,2}^{\infty} \cos(u_n x)\cos(u_n x')\left[\frac{k_0^2}{\kappa k_0^2 - l_m^2}\frac{p_m^2 l_m \sin(l_m h)\sin(p_m c)}{\gamma_{nm}}\right.$$
$$\left.\frac{e^{-\gamma_{nm}|z-z'|}}{DR_{1nm}} - \frac{\kappa_y}{k_0^2 - \overline{p}_m^2}\frac{\overline{q}_m^2 \overline{p}_m^3 \sin(\overline{q}_m h)\sin(\overline{p}_m c)e^{-\overline{\gamma}_{nm}|z-z'|}}{\overline{\gamma}_{nm} DR_{2nm}}\right] \tag{2.27}$$

It is useful to define the new quantities F_m, H_m, and $\overline{H}_m$ as

$$F_m = \frac{p_m^2 l_m \sin(l_m h)\sin(p_m c)}{DR_{1nm}} \tag{2.28a}$$
$$H_m = \frac{k_0^2 F_m}{\kappa k_0^2 - l_m^2} \tag{2.28b}$$
$$\overline{H}_m = -\frac{\kappa_y}{k_0^2 - \overline{p}_m^2}\frac{\overline{q}_m^2 \overline{p}_m^3 \sin(\overline{q}_m h)\sin(\overline{p}_m c)}{DR_{2nm}} \tag{2.28c}$$

, then the expressions for G_z, G_x, G can be finally expressed as

$$G_z(x,z;x',z') = \frac{1}{a}\sum\sum \cos(u_n x)\cos(u_n x')\frac{I_m}{\gamma}e^{-\gamma|z-z'|} \tag{2.29a}$$

$$G_x(x,z;x',z') = \frac{1}{a}\sum\sum \sin(u_n x)\sin(u_n x')\frac{F_m}{\gamma}e^{-\gamma|z-z'|} \tag{2.29b}$$

$$G(x,z;x',z') = \frac{1}{a}\sum\sum \cos(u_n x)\cos(u_n x')\left[\frac{H_m}{\gamma}e^{-\gamma|z-z'|} + \frac{\overline{H}_m}{\bar{\gamma}}e^{-\bar{\gamma}|z-z'|}\right] \tag{2.29c}$$

where we simplify the notation by dropping the subscripts on the γ's and $\bar{\gamma}$'s. These are the required Green's functions for the dielectric-loaded waveguide.

2.2 Expressions for the source representations

In a microstrip or coplanar waveguide discontinuity, both the dominant mode and perturbed sources exist where the former can be derived and the latter are chosen to have the same forms accordingly. In microstrip, an accurate expression for the x dependence of the dominant propagating mode charge and current on the infinite strip is given by

$$\rho_o(x') = \left[Q_0 - Q_1 T_2(x'/w) + Q_2 T_4(x'/w)\right]\left[1-(x'/w)^2\right]^{-\frac{1}{2}} \qquad (2.29a)$$

$$J_{ozr}(x') = \left[I_0 - I_1 T_2(x'/w) + I_2 T_4(x'/w)\right]\left[1-(x'/w)^2\right]^{-\frac{1}{2}} \qquad (2.29b)$$

where $T_n(x'/w)$ is the n'th Chebyshev polynomial and Q_i and I_i, i=0・・・2 , are the unknown amplitudes respectively for the dominant mode charge and the dominant mode relative current, which is related to the true current by $J_{oz} = (\beta c / k_0) J_{ozr}$. Note that the edge conditions are already built into these expressions.

In a later chapter, we derive new general expressions for the dominant mode sources applicable for both microstrip and coplanar waveguides. For the microstrip line, it is assumed that there is no dominant mode transverse current J_{ox} on the strip since its effect is negligible for a wide range of useful geometries. When a component of J_{ox} is required, such as for the case of an asymmetrical gap and a step, it is included as a fading dominant term plus a perturbation term, localized near the discontinuity.

The sources given in Eq.(2.29) can be transformed, with $x' = \sin(\theta')$, into

$$\rho_o(\theta') = \sum_{i=0}^{2} Q_i \frac{\cos(2i\theta')}{\cos(\theta')} \qquad (2.30a)$$

$$J_{ozr}(\theta') = \sum_{i=0}^{2} I_i \frac{\cos(2i\theta')}{\cos(\theta')} \tag{2.30b}$$

These sources can also be expressed by a Fourier series expansion as

$$\rho_o(x') = \sum_{n=1,3}^{\infty} \rho_n \cos(u_n x') \tag{2.31a}$$

$$J_{ozr}(x') = \sum_{n=1,3}^{\infty} J_{zrn} \cos(u_n x') \tag{2.31b}$$

where the coefficients in both sets of equations are respectively related to each other by

$$\rho_n = \frac{2w}{a} \sum_i Q_i \int_0^{\frac{\pi}{2}} \cos(2i\theta') \cos[u_n w \sin(\theta')] d\theta' \tag{2.32a}$$

$$J_{zrn} = \frac{2w}{a} \sum_i I_i \int_0^{\frac{\pi}{2}} \cos(2i\theta') \cos[u_n w \sin(\theta')] d\theta' \tag{2.32b}$$

Since the integral in Eq.(2.32) is used many times hereafter, it is computed once and stored as

$$p_{ni} = 2 \int_0^{\frac{\pi}{2}} \cos(2i\theta') \cos[u_n w \sin(\theta')] d\theta' \tag{2.33}$$

This integral is given by $p_{ni} = \pi J_{2i}(n\pi w / 2a)$, where J_{2i} is the Bessel function of order 2i. The backward recursion method is used to find $J_{2i}(x)$, then, in turn, p_{ni} for each particular value of x.

2.3 Formulation of potential equations

With the proper Green's functions and the accurate expressions for the dominant mode sources we can find the potentials, for the microstrip with an infinite line enclosed in the structure with a top cover, by using

$$A_{ozr} = \mu_0 \int_{z'} \int_{x'} G_z(x,z;x',z') J_{ozr}(x',z') dx' dz' \tag{2.34a}$$

$$A_{oxr} = \mu_0 \int_{z'} \int_{x'} G_x(x,z;x',z') J_{oxr}(x',z') dx' dz' \tag{2.34b}$$

$$\phi_o = \varepsilon_0^{-1} \int_{z'} \int_{x'} G(x,z;x',z') \rho_o(x',z') dx' dz' \tag{2.34c}$$

From Eq.(2.34a) and (2.34c), an iteration technique is developed to determine the coefficients, Q_i and I_i, and to find the effective dielectric constant for a given waveguide geometry.

In this approach [25], $\varepsilon_0\phi_o$ is set equal to 1 on the strip, and A_{ozr}/μ_0 is also set equal to 1 on the strip where ϕ_o is an absolute value for the scalar potential, and A_{ozr} is the reference value for the vector potential caused by the relative current J_{ozr}. Carrying out the integration over the source points in Eq.'s (2.34a) and (2.34c) and applying Galerkin's method to them, we can reduce the two integral equations to a system of linear equations as shown below

$$\frac{w}{a} \sum_i I_i \sum_n \sum_m \frac{F_m}{\gamma^2 + \beta^2} p_{ni} p_{nj} = \delta_{0j} \frac{\pi}{2} \tag{2.35a}$$

$$\frac{w}{a} \sum_i Q_i \sum_n \sum_m \left[\frac{H_m}{\gamma^2 + \beta^2} + \frac{\bar{H}_m}{\bar{\gamma}^2 + \beta^2} \right] p_{ni} p_{nj} = \delta_{0j} \frac{\pi}{2} \tag{2.35b}$$

where δ_{0j}=1 for j=0 and 0 for j>0. Note that the double sums over n and m, involving the terms like $p_{ni}p_{nj}/(\gamma^2+\beta^2)$, are slowly convergent. The asymptotic values of $\sum_m \frac{F_m}{\gamma^2+\beta^2}$ and $\sum_m \left[\frac{H_m}{\gamma^2+\beta^2} + \frac{\bar{H}_m}{\bar{\gamma}^2+\beta^2} \right]$ decay as 1/n

where $\sum_n \frac{\cos(u_n x)\cos(u_n x')}{n}$ represents the dominant part of G and G_z, arising when the field and source points coincide, and can be expressed as

$$\sum_{n=1,3}^{\infty} \frac{\cos(u_n x)\cos(u_n x')}{n} = -\frac{1}{4}\ln|\tan[\pi(x-x')/4a]\tan[\pi(x+x')/4a]| \tag{2.36}$$

Note that we see the singularity of the Green's functions in this equation. Fortunately, as described in Appendix 1, the integral involving this term can be efficiently calculated.

By using a trial value for β, the unknowns for Q_i and I_i are found from this matrix. Then the total charge and relative current on the strip are given by $I_{Tm} = \pi I_0$ and $Q_{Tm} = \pi Q_0$. To satisfy $E_z = 0$ we set $\omega A_{ozr} = \beta\phi_o$ on the strip. Next we use $\nabla_s \cdot \vec{J} = -j\omega\rho$, giving $\beta I^m_{TOT} = \omega Q^m$ when integrated across the strip, to obtain a new estimate of the propagation constant

$$\beta = \sqrt{\varepsilon_{em}}k_0 \tag{2.37}$$

where I^m_{TOT} is the total z-direction current and Q^m is the total charge per unit length on the strip, and $\varepsilon_{em} = Q_{Tm}/I_{Tm} = Q_0/I_0$ is the effective dielectric constant.

If the new value of ε_{em} differs from the old value of ε_{em} by less than 1%, the iteration is terminated ; otherwise, the iteration is repeated. The latest values of β, Q_i, and I_i are used as the new entries in the matrix for each successive iteration until the condition is satisfied. The iteration converges very fast, and typically 1, 2, or 3 iterations are all that is required.

After a convergent value of ε_{em} is found, the characteristic impedance of the microstrip is calculated. It is defined as the ratio of the voltage between

the center of the conducting strip and the ground plane to the total current flowing along the strip which is reduced to that equation in [10] if we assume there is no top cover. Since A_{oy} can also be expressed in terms of a Fourier series we have

$$Z_c^m = \frac{1}{I_{TOT}^c}\int_0^h -E_y dy = \frac{1}{I_{TOT}^c}\int_0^h \left(\frac{\partial\phi}{\partial y} + j\omega A_{oy}\right)_{x=0} dy = \frac{120}{\sqrt{I_0 Q_0}}\left\{1 + \sum_{n=1,3}^{\infty} \frac{\rho_n k_0^2}{\beta^2 + u_n^2}\left[\kappa\frac{\zeta_n}{\zeta_{2n}}\frac{\sinh(\zeta_n c)\sinh(\zeta_{2n}h)}{\left[\zeta_{2n}\cosh(\zeta_n c)\sinh(\zeta_{2n}h) + \kappa\zeta_n\sinh(\zeta_n c)\cosh(\zeta_{2n}h)\right]} - \frac{\sinh(\zeta_n c)\sinh(\zeta_{1n}h)}{\left[\zeta_{1n}\sinh(\zeta_n c)\cosh(\zeta_{1n}h) + \zeta_n\cosh(\zeta_n c)\sinh(\zeta_{1n}h)\right]}\right]\right\} \quad (2.38)$$

where the integral of E_y is carried out at $x = 0$ and $\zeta_n = (\beta^2 - k_0^2 + u_n^2)^{\frac{1}{2}}$, $\zeta_{1n} = (\beta^2 - \kappa k_0^2 + u_n^2)^{\frac{1}{2}}$, and $\zeta_{2n} = (\kappa / \kappa_y)^{\frac{1}{2}}(\beta^2 - \kappa_y k_0^2 + u_n^2)^{\frac{1}{2}}$.

This completes the determination of the dominant mode charge and relative current, the propagation constant, and the characteristic impedance for the enclosed microstrip with anisotropic substrates. The dominant mode charge and current distributions, as well as knowledge of the propagation constant and characteristic impedance, are required in order to analyze microstrip discontinuities.

Chapter 3

Microstrip open-end and gap discontinuities

In this chapter, we discuss the choices for the expansion functions for the perturbed mode sources and formulate the potential integral equations for the microstrip gap discontinuity, which are also applicable to the open end discontinuity. In addition we point out the importance of selecting the testing functions which are used to generate as many equations as there are unknowns. Then, we consider the effects of the transverse current in the asymmetric gap problem. In the last section we show how the connection of the matrix of the set of linear equations to the Tangent method is obtained.

3.1 Expansion functions for perturbed sources

In a discontinuity the perturbed mode charge and current exist and must be added to the dominant mode sources to account for the total source distributions near the discontinuity. Since the line is terminated arbitrarily at some point in a discontinuity we can assume that it is located at z'=0. Taking the reflection into account, we express the dominant mode sources as follows

$$\rho_{o1}(x_1', z_1') = \rho_{o1}(x_1')(e^{-j\beta_1 z_i} + Re^{j\beta_1 z_i})$$
$$= \rho_{o1}(x_1')(1+R)[B_{in}\sin(\beta_1 z_1') + \cos(\beta_1 z_1')] \qquad (3.1a)$$
$$J_{ozr1}(x_1', z_1') = J_{ozr1}(x_1')(e^{-j\beta_1 z_i} - Re^{j\beta_1 z_i})$$
$$= J_{ozr1}(x_1')j(1+R)[B_{in}\cos(\beta_1 z_1') - \sin(\beta_1 z_1')] \qquad (3.1b)$$

where $B_{in} = -j(1-R)/(1+R)$ is the normalized input susceptance and R is the reflection coefficient. Note that since the amplitude of the incident mode is arbitrary, (1+R) can be chosen as its amplitude and set equal to 1.

For this reason, the perturbed sources can be expressed as follows

$$J_{pzr}(\theta',z') = -j\sum_{i=0}^{2}\sum_{s=0}^{N} C_k U_{si} \frac{\cos(2i\theta')}{\cos(\theta')} d_s(z') \quad (3.2a)$$

$$\rho_p(\theta',z') = \sum_{i=0}^{2}\sum_{s=0}^{N} C_k H_{si} \frac{\cos(2i\theta')}{\cos(\theta')} e_s(z') \quad (3.2b)$$

where s is the expansion function number beginning with 0, i is the mode number, k is the line number, $C_k U_{si}$ and $C_k H_{si}$ are the unknown amplitudes, and $d_s(z')$ and $e_s(z')$ are functions of z' which must be chosen so as to give an accurate representation of the dependence of the sources on z'.

In our research work we use two kinds of representations for the functions in Eq.(3.1) that satisfy the continuity equation, $\nabla \cdot \bar{J} = -j\omega\rho$, when no transverse current is considered. One set is denoted the TP representation where triangle functions are chosen for the perturbed current and bipolar rectangle functions are chosen for expanding the perturbed charge ; that is to say,

$$d_s(z') = T_s(z') \quad \text{and} \quad e_s(z') = P_s(z') \quad (3.3)$$

as shown in Fig.3.1. Unipolar pulses are used in the calculations because of their simplicity and then bipolar pulses are formed from them.

The other set is called the QT representation where the quadratic approximations are used for the current and the triangle functions are used for the charge expansion ; namely,

$$e_s(z') = T_s(z') \text{ and } \sum_{s=0} C_k U_{si}\, d_s(z') = \frac{k_0^2}{\beta}\int_{-(N+1)\Delta}^{z'} \sum_{s=0} C_k H_{si}\, e_s(z')dz' \quad (3.4)$$

where $J_z[\theta', -(N+1)\Delta] = 0$ is assumed.

Therefore, the total charge and relative current distributions on the input line may be written as

$$\rho_1(x_1',z_1') = \rho_{o1}(x_1',z_1') + \rho_{p1}(x_1',z_1') \tag{3.5a}$$

$$J_{zr1}(x_1',z_1') = J_{ozr1}(x_1',z_1') + J_{pzr1}(x_1',z_1') \tag{3.5b}$$

where the subscript 1 stands for line 1, the input line.

For the gap discontinuity the total charge and relative current on the terminated output line can be chosen in the forms

$$\rho_2(x_2',z_2') = \tau\rho_{o2}(x_2')\sin[\beta_2(z_2'-l)] + \rho_{p2}(x_2',z_2') \tag{3.6a}$$

$$J_{zr2}(x_2',z_2') = j\tau J_{ozr2}(x_2')\cos[\beta_2(z_2'-l)] + J_{pzr2}(x_2',z_2') \tag{3.6b}$$

where τ is the unknown transmission coefficient and the output line has been assumed to be terminated in a short circuit at $z_2' = l$ where l is a long distance away from the discontinuity.

With these total source expressions and the corresponding Green's functions derived, we can formulate the equations, for the vector and scalar potentials on the discontinuous lines. From these the electric fields existing on the strip are generated. The boundary condition which forces the total tangential electric field on the strips to vanish is used to formulate the required integral equations that determine the unknown quantities.

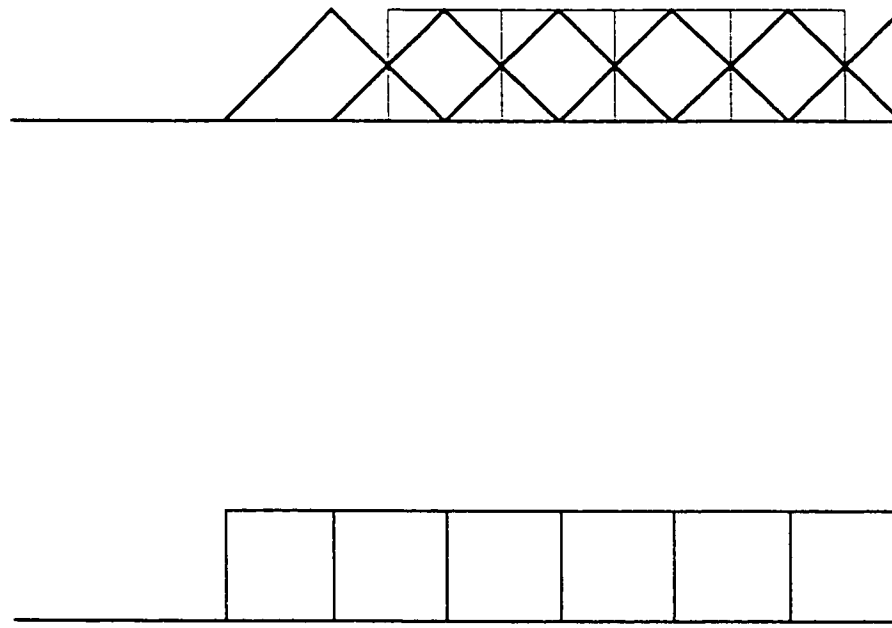

Fig. 3.1 Testing pulses used for the expansion pulses. Half pulses are shown for the charge pulses for the sake of clarity

3.2 Open-end and gap discontinuities

We treat the gap problem first. We then let the gap spacing be theoretically infinite, actually $e^{-\gamma\delta}$ and $e^{-\bar{\gamma}\delta}$ equal to zeros in the software programs so that we can kill out the coupling effects, to obtain the excess capacitance for the open-end discontinuity where δ is the gap spacing. The electric field can be given in terms of the potentials through the expression, $\bar{E} = -j\omega\bar{A} - \nabla\phi$. On the conducting striplines the tangential components of the electric field must vanish. Applying the boundary condition $E_z = -(j\omega\beta c / k_0)A_{zr} - \partial\phi / \partial z = 0$ to each line, we have, for line 1,

$$
\begin{aligned}
&j\beta_1 \int_{-\infty}^{0}\int_{-w_1}^{w_1} G_z J_{pzr1} dx_1' dz_1' + \frac{\partial}{\partial z}\int_{-\infty}^{0}\int_{-w_1}^{w_1} G\rho_{p1} dx_1' dz_1' \\
&+j\beta_2 \int_{\delta}^{\infty}\int_{-w_2}^{w_2} G_z J_{pzr2} dx_2' dz_2' + \frac{\partial}{\partial z}\int_{\delta}^{\infty}\int_{-w_2}^{w_2} G\rho_{p2} dx_2' dz_2' \\
&-j\beta_1 \int_{0}^{\infty}\int_{-w_1}^{w_1} G_z j J_{ozr1}[B_{in}\cos(\beta_1 z_1') - \sin(\beta_1 z_1')] dx_1' dz_1' \\
&-\frac{\partial}{\partial z}\int_{0}^{\infty}\int_{-w_1}^{w_1} G\rho_{o1}[B_{in}\sin(\beta_1 z_1') + \cos(\beta_1 z_1')] dx_1' dz_1' \\
&+j\beta_2 \int_{\delta}^{\infty}\int_{-w_2}^{w_2} G_z j\tau J_{ozr2}\cos[(\beta_2(z_2' - l)] dx_2' dz_2' \\
&+\frac{\partial}{\partial z}\int_{\delta}^{\infty}\int_{-w_2}^{w_2} G\tau\rho_{o2}\sin[\beta_2(z_2' - l)] dx_2' dz_2' = 0
\end{aligned}
\tag{3.7}
$$

where the dynamic source reversal technique is used. These source reversed terms are given in terms of the known dominant mode amplitudes of charge and current, thus making up a forcing function in the equation.

For line 2,

$$
\begin{aligned}
&j\beta_1\int_{-\infty}^{0}\int_{-w_1}^{w_1} G_z J_{pzr1}\,dx_1'\,dz_1' + \frac{\partial}{\partial z}\int_{-\infty}^{0}\int_{-w_1}^{w_1} G\rho_{p1}\,dx_1'\,dz_1' \\
&+j\beta_2\int_{\delta}^{\infty}\int_{-w_2}^{w_2} G_z J_{pzr2}\,dx_2'\,dz_2' + \frac{\partial}{\partial z}\int_{\delta}^{\infty}\int_{-w_2}^{w_2} G\rho_{p2}\,dx_2'\,dz_2' \\
&+j\beta_1\int_{-\infty}^{0}\int_{-w_1}^{w_1} G_z jJ_{ozr1}[B_{in}\cos(\beta_1 z_1') - \sin(\beta_1 z_1')]dx_1'\,dz_1' \\
&+\frac{\partial}{\partial z}\int_{-\infty}^{0}\int_{-w_1}^{w_1} G\rho_{o1}[B_{in}\sin(\beta_1 z_1') + \cos(\beta_1 z_1')]dx_1'\,dz_1' \\
&-j\beta_2\int_{-\infty}^{\delta}\int_{-w_2}^{w_2} G_z j\tau J_{ozr2}\cos[(\beta_2(z_2'-l)]dx_2'\,dz_2' \\
&-\frac{\partial}{\partial z}\int_{-\infty}^{\delta}\int_{-w_2}^{w_2} G\tau\rho_{o2}\sin[\beta_2(z_2'-l)]dx_2'\,dz_2' = 0
\end{aligned}
\tag{3.8}
$$

Substituting the source and Green's function expressions gives

$$
\beta_1\sum_{i=0}^{2}\sum_{s=0}^{n} C_1^z U_{si}\sum_{n}\sum_{m}\frac{F_m}{\gamma}p_{ni1}zp_{nj1}\int_{-\infty}^{0} d_s(z_1')e^{-\gamma|z-z_1'|}dz_1' + \sum_{i=0}^{2}\sum_{s=0}^{n} C_1 H_{si}\sum_{n}\sum_{m}
$$

$$
p_{ni1}zp_{nj1}\frac{\partial}{\partial z}\left[\frac{H_m}{\gamma}\int_{-\infty}^{0} e_s(z_1')e^{-\gamma|z-z_1'|}dz_1' + \frac{\overline{H}_m}{\bar{\gamma}}\int_{-\infty}^{0} e_s(z_1')e^{-\bar{\gamma}|z-z_1'|}dz_1'\right] +
$$

$$
\beta_2\sum_{i=0}^{2}\sum_{s=0}^{n} C_2^z U_{si}\sum_{n}\sum_{m}\frac{F_m}{\gamma}p_{ni2}p_{nj1}\int_{\delta}^{\infty} d_s(z_2')e^{-\gamma|z-z_2'|}dz_2' + \sum_{i=0}^{2}\sum_{s=0}^{n} C_2 H_{si}\sum_{n}\sum_{m}
$$

$$
p_{ni2}zp_{nj1}\frac{\partial}{\partial z}\left[\frac{H_m}{\gamma}\int_{-\infty}^{0} e_s(z_2')e^{-\gamma|z-z_2'|}dz_2' + \frac{\overline{H}_m}{\bar{\gamma}}\int_{-\infty}^{0} e_s(z_2')e^{-\bar{\gamma}|z-z_2'|}dz_2'\right] + B_{in}
$$

$$
\beta_1\sum_{i=0}^{2}\left\{I_{1i}\sum_{n}\sum_{m}p_{ni1}zp_{nj1}\frac{F_m e^{\gamma z}}{\gamma^2+\beta_1^2} - Q_{1i}\sum_{n}\sum_{m}p_{ni1}zp_{nj1}\left[\frac{H_m e^{\gamma z}}{\gamma^2+\beta_1^2} + \frac{\overline{H}_m e^{\bar{\gamma} z}}{\bar{\gamma}^2+\beta_1^2}\right]\right\} - \tau
$$

$$
\sum_{i=0}^{2}\left\{\beta_2 I_{2i}\sum_{n}\sum_{m}p_{ni2}zp_{nj1}\frac{F_m e^{\gamma(z-\delta)}}{\gamma(\gamma^2+\beta_2^2)}[\gamma\cos(\vartheta) - \beta_2\sin(\vartheta)] - Q_{2i}\sum_{n}\sum_{m}p_{ni2}zp_{nj1}\right.
$$

$$
\left.\left[\frac{H_m e^{\gamma(z-\delta)}}{(\gamma^2+\beta_2^2)}[\beta_2\cos(\vartheta) + \gamma\sin(\vartheta)] + \frac{\overline{H}_m e^{\bar{\gamma}(z-\delta)}}{(\bar{\gamma}^2+\beta_2^2)}[\beta_2\cos(\vartheta) + \bar{\gamma}\sin(\vartheta)]\right]\right\} = \sum_{i=0}^{2}
$$

$$
\left\{\beta_1^2 I_{1i}\sum_{n}\sum_{m}p_{ni1}zp_{nj1}\frac{F_m e^{\gamma z}}{\gamma(\gamma^2+\beta_1^2)} + Q_{1i}\sum_{n}\sum_{m}p_{ni1}zp_{nj1}\left[\frac{\gamma H_m e^{\gamma z}}{(\gamma^2+\beta_1^2)} + \frac{\bar{\gamma}\overline{H}_m e^{\bar{\gamma} z}}{(\bar{\gamma}^2+\beta_1^2)}\right]\right\}
$$

(3.9)

where $z<0$ for line 1 and

$$\beta_1\sum_{i=0}^{2}\sum_{s=0}^{n}C_1^z U_{si}\sum_n\sum_m\frac{F_m}{\gamma}p_{ni1}zp_{nj2}\int_{-\infty}^{0}d_s(z_1')e^{-\gamma|z-z_1'|}dz_1'+\sum_{i=0}^{2}\sum_{s=0}^{n}C_1H_{si}\sum_n\sum_m$$

$$p_{ni1}zp_{nj2}\frac{\partial}{\partial z}\left[\frac{H_m}{\gamma}\int_{-\infty}^{0}e_s(z_1')e^{-\gamma|z-z_1'|}dz_1'+\frac{\overline{H}_m}{\overline{\gamma}}\int_{-\infty}^{0}e_s(z_1')e^{-\overline{\gamma}|z-z_1'|}dz_1'\right]+$$

$$\beta_2\sum_{i=0}^{2}\sum_{s=0}^{n}C_2^z U_{si}\sum_n\sum_m\frac{F_m}{\gamma}p_{ni2}zp_{nj2}\int_{\delta}^{\infty}d_s(z_2')e^{-\gamma|z-z_2'|}dz_2'+\sum_{i=0}^{2}\sum_{s=0}^{n}C_2H_{si}\sum_n\sum_m$$

$$p_{ni2}zp_{nj2}\frac{\partial}{\partial z}\left[\frac{H_m}{\gamma}\int_{-\infty}^{0}e_s(z_2')e^{-\gamma|z-z_2'|}dz_2'+\frac{\overline{H}_m}{\overline{\gamma}}\int_{-\infty}^{0}e_s(z_2')e^{-\overline{\gamma}|z-z_2'|}dz_2'\right]-B_{in}$$

$$\beta_1\sum_{i=0}^{2}\left\{I_{1i}\sum_n\sum_m p_{ni1}zp_{nj2}\frac{F_m e^{-\gamma z}}{\gamma^2+\beta_1^2}-Q_{1i}\sum_n\sum_m p_{ni1}zp_{nj2}\left[\frac{H_m e^{-\gamma z}}{\gamma^2+\beta_1^2}+\frac{\overline{H}_m e^{-\overline{\gamma}z}}{\overline{\gamma}^2+\beta_1^2}\right]\right\}-\tau$$

$$\sum_{i=0}^{2}\left\{\beta_2 I_{2i}\sum_n\sum_m p_{ni2}zp_{nj2}\frac{F_m e^{-\gamma(z-\delta)}}{\gamma(\gamma^2+\beta_2^2)}[\gamma\cos(\vartheta)+\beta_2\sin(\vartheta)]-Q_{2i}\sum_n\sum_m p_{ni2}zp_{nj2}\right.$$

$$\left.\left[\frac{H_m e^{-\gamma(z-\delta)}}{(\gamma^2+\beta_2^2)}[\beta_2\cos(\vartheta)-\gamma\sin(\vartheta)]+\frac{\overline{H}_m e^{-\overline{\gamma}(z-\delta)}}{(\overline{\gamma}^2+\beta_2^2)}[\beta_2\cos(\vartheta)-\overline{\gamma}\sin(\vartheta)]\right]\right\}=\sum_{i=0}^{2}$$

$$\left\{\beta_1^2 I_{1i}\sum_n\sum_m p_{ni1}zp_{nj2}\frac{F_m e^{-\gamma z}}{\gamma(\gamma^2+\beta_1^2)}+Q_{1i}\sum_n\sum_m p_{ni1}zp_{nj2}\left[\frac{\gamma H_m e^{-\gamma z}}{(\gamma^2+\beta_1^2)}+\frac{\overline{\gamma}\overline{H}_m e^{-\overline{\gamma}z}}{(\overline{\gamma}^2+\beta_1^2)}\right]\right\}$$

(3.10)

where $z>\delta$ for line 2.

The integrals over z' in the above integral equations can be carried out analytically, leaving the expressions in terms of the field points. By choosing suitable testing functions these integral equations are reduced to a set of algebraic linear equations.

For the testing in x the unweighted Chebyshev polynomials are used since testing with the edge condition places a greater emphasis on the field

near the edge of the strip but de-emphasizes the rest. As a result the complete integrals to be evaluated are given by

$$zp_{nj} = 2w\int_0^{\frac{\pi}{2}} \cos[u_n w \sin(\theta)]\cos(2j\theta)\cos(\theta)d\theta \qquad (3.11)$$

where j=0,1,2.

For the TP pair, the testing rectangle pulses in the z direction are offset by a $\Delta/2$ since the field E_z arising from a bipolar charge pulse is even-symmetric about its center as shown in Fig.3.1. This kind of testing procedure which tests near a field maximum in one expansion of bipolar pulses for the charge produces the largest contributions to the diagonal elements of the coefficient matrix. If the testing pulses were not offset by any amount, the result would be almost zero.

On the contrary, in the QT pair, the z-direction testing pulses are not shifted and begin with the terminated ends for each line. Since it is proved that this sort of testing is successful in our research, we are sure that the conclusion made in [40] is not necessarily correct.

For gaps that are not too narrow the charge density varies like $1/\sqrt{|z|}$ near the open ends. For very narrow gaps the charge density varies more like 1/|z| near the end. Because of the singular behavior of the charge density near the gap narrow pulse widths must be used for expanding the charge distribution in the region close to the gap. Further away from the gap wider pulse widths can be used. In the computer program three or five pulses were combined to form wider pulses in regions remote from the gap. This has the advantage of reducing the number of unknowns and thus the size of the matrix that must be inverted.

When there is no transverse current J_x on the line the perturbed charge and current coefficients for the TP pair are related by

$$C_k H_{si} = \frac{\beta_l}{\Delta k_0^2} C_k U_{si} \tag{3.12}$$

and for the TQ pair the current at each node position of triangles is related to the charge by

$$J_{pzr}(\theta', -s\Delta) = \frac{k_0^2 \Delta}{\beta} \sum_{i=0}^{2} \frac{\cos(2i\theta')}{\cos(\theta')} (C_k H_{ni} + C_k H_{n-1,i} + .. + \frac{1}{2} C_k H_{si}) \tag{3.13a}$$

At in-between points, for $-s\Delta \le z \le -(s+1)\Delta$,

$$J_{pzr}(\theta', z') = J_{pzr}(\theta', -s\Delta) + \frac{k_0^2}{\beta} \sum_{i=0}^{2} \frac{\cos(2i\theta')}{\cos(\theta')} \left[C_k H_{si} + \frac{C_k H_{si} - C_k H_{s+1,i}}{2\Delta} (z' + s\Delta) \right] (z' + s\Delta) \tag{3.13b}$$

Moreover, the perturbed current must cancel the dominant mode current at each terminated end, so as to assure that the total current at each end is zero. This gives

$$C_1^z U_{0i} = I_{1i} B_{in} \qquad \text{and} \qquad C_2^z U_{0i} = I_{2i} \tau \cos(\beta_2 l) \tag{3.14}$$

With these relations the number of the unknowns ; namely, the size of the coefficient matrix and, in turn, the number of testing functions is diminished.

Among the testing results in z, most terms have an exponential decay because the expansions of the fields inside the waveguide is carried out in terms of its evanescent modes. But those terms caused by the coincidence of the source and field points have no exponential decay and can be efficiently summed into closed forms like those in Eq.(2.34) except that $\beta^2 = 0$ and instead of a p_{nj}, there is a zp_{nj}.

3.3 Consideration of transverse current

When the transverse current is included its mode expressions are related to the charge and the longitudinal current by

$$\frac{\partial J_{xr1}}{\partial x_1'} = -j\frac{k_0^2}{\beta_1}\rho_1 - \frac{\partial J_{zr1}}{\partial z_1'} = -j\frac{k_0^2}{\beta_1}\rho_{o1} - \frac{\partial J_{ozr1}}{\partial z_1'} - j\frac{k_0^2}{\beta_1}\rho_{p1} - \frac{\partial J_{pzr1}}{\partial z_1'}$$

$$= j\sum_i \frac{1}{\beta_1}(\beta_1^2 I_{1i} - k_0^2 Q_{1i})\frac{\cos(2i\theta')}{\cos(\theta')}[B_{in}\sin(\beta_1 z_1') + \cos(\beta_1 z_1')] - j\sum_i\sum_s$$

$$\left(-\frac{C_1^z U_{si}}{\Delta} + \frac{k_0^2}{\beta_1}C_1 H_{si}\right)\frac{\cos(2i\theta')}{\cos(\theta')}e_s(z_1') \qquad (3.15)$$

for line 1 with a similar form for line 2, except that the quantity in the brackets is replaced by $\tau\sin[\beta_2(z_2'-l)]$ and the subscript 1 in all quantities is changed to 2.

By using the boundary condition, $E_x = -(j\omega\beta c/k_0)A_{xr} - \partial\phi/\partial x = 0$ for each line we have, for line 1,

$$j\beta_1\int_{-\infty}^{0}\int_{-w_1}^{w_1} G_x J_{pxr1}dx_1'dz_1' + \frac{\partial}{\partial x}\int_{-\infty}^{0}\int_{-w_1}^{w_1} G\rho_{p1}dx_1'dz_1'$$

$$+j\beta_2\int_{\delta}^{\infty}\int_{-w_2}^{w_2} G_x J_{pxr2}dx_2'dz_2' + \frac{\partial}{\partial x}\int_{\delta}^{\infty}\int_{-w_2}^{w_2} G\rho_{p2}dx_2'dz_2'$$

$$-j\beta_1\int_{0}^{\infty}\int_{-w_1}^{w_1} G_x jJ_{oxr1}[B_{in}\cos(\beta_1 z_1') - \sin(\beta_1 z_1')]dx_1'dz_1'$$

$$-\frac{\partial}{\partial x}\int_{0}^{\infty}\int_{-w_1}^{w_1} G\rho_{o1}[B_{in}\sin(\beta_1 z_1') + \cos(\beta_1 z_1')]dx_1'dz_1'$$

$$+j\beta_2\int_{\delta}^{\infty}\int_{-w_2}^{w_2} G_x j\tau J_{oxr2}\cos[(\beta_2(z_2'-l)]dx_2'dz_2'$$

$$+\frac{\partial}{\partial x}\int_{\delta}^{\infty}\int_{-w_2}^{w_2} G\tau\rho_{o2}\sin[\beta_2(z_2'-l)]dx_2'dz_2' = 0 \qquad (3.16)$$

and for line 2,

$$
\begin{aligned}
&j\beta_1\int_{-\infty}^{0}\int_{-w_1}^{w_1} G_x J_{pxr1}dx_1'dz_1' + \frac{\partial}{\partial x}\int_{-\infty}^{0}\int_{-w_1}^{w_1} G\rho_{p1}dx_1'dz_1' \\
&+j\beta_2\int_{\delta}^{\infty}\int_{-w_2}^{w_2} G_x J_{pxr2}dx_2'dz_2' + \frac{\partial}{\partial x}\int_{\delta}^{\infty}\int_{-w_2}^{w_2} G\rho_{p2}dx_2'dz_2' \\
&+j\beta_1\int_{-\infty}^{0}\int_{-w_1}^{w_1} G_x jJ_{oxr1}[B_{in}\cos(\beta_1 z_1') - \sin(\beta_1 z_1')]dx_1'dz_1' \\
&+\frac{\partial}{\partial x}\int_{-\infty}^{0}\int_{-w_1}^{w_1} G\rho_{o1}[B_{in}\sin(\beta_1 z_1') + \cos(\beta_1 z_1')]dx_1'dz_1' \\
&-j\beta_2\int_{-\infty}^{\delta}\int_{-w_2}^{w_2} G_x j\tau J_{oxr2}\cos[(\beta_2(z_2'-l)]dx_2'dz_2' \\
&-\frac{\partial}{\partial x}\int_{-\infty}^{\delta}\int_{-w_2}^{w_2} G\tau\rho_{o2}\sin[\beta_2(z_2'-l)]dx_2'dz_2' = 0
\end{aligned}
\tag{3.17}
$$

where the x component, A_{xr}, of the vector potential, like A_{zr}, is a relative value and related to the absolute value by $A_x = (\beta c / k_0)A_{xr}$.

To make use of Eq.(3.15) but not deal directly with the integration containing $J_{xr}(x',z')$ over x', we convert these integrals to those involving $\frac{\partial J_{xr}(x',z')}{\partial x'}$ explicitly, with the help of an integration by parts,

$$
\begin{aligned}
\int_{-w}^{w} G_x(x,z;x',z')J_{xr}(x',z')dx' = \Big[J_{xr}(x',z')\int^{x'} G_x(x,z;x',z')dx'\Big|_{-w}^{w} - \int_{-w}^{w}\Big[\int^{x'} \\
G_x(x,z;x',z')\Big]\frac{\partial J_{xr}(x',z')}{\partial x'}dx'\Big]
\end{aligned}
\tag{3.18}
$$

The first term vanishes since $J_{xr}(x',z') = 0$ for x'=0 and w, while the second term gives

$$
\frac{1}{u_n}\int_{-w}^{w}\cos(u_n x')\frac{\partial J_{xr}(x',z')}{\partial x'}dx' \tag{3.19}
$$

where J_{xr}, the relative transverse current, is related to the true current by $J_x = (\beta c / k_0)J_{xr}$.

In both Eq.'s (3.16) and (3.17), we retain the source vectors which were assumed to be zero in [1]. Actually, we consider that maintaining the source terms in this problem is necessary since the contributions come mostly from the charge term which may be significant, unlike the fading term.

Setting $C_l^x U_{si} = -\frac{C_l^z U_{si}}{\Delta} + \frac{k_0^2}{\beta_l} C_l H_{si}$ where l=1,2, substituting the source and Green's function expressions, and testing in the x direction with the proper testing functions produces

$$\beta_1 \sum_{i=0}^{2}\sum_{s=0}^{n} C_1^x U_{si} \sum_n \sum_m \frac{F_m}{u_n^2 \gamma} p_{ni1} zp_{nj1} \int_{-\infty}^{0} e_s(z_1') e^{-\gamma|z-z_1'|} dz_1' - \sum_{i=0}^{2}\sum_{s=0}^{n} C_1 H_{si} \sum_n \sum_m$$

$$p_{ni1} zp_{nj1} \frac{\partial}{\partial x}\left[\frac{H_m}{\gamma}\int_{-\infty}^{0} e_s(z_1') e^{-\gamma|z-z_1'|} dz_1' + \frac{\overline{H}_m}{\bar{\gamma}}\int_{-\infty}^{0} e_s(z_1') e^{-\bar{\gamma}|z-z_1'|} dz_1'\right] +$$

$$\beta_2 \sum_{i=0}^{2}\sum_{s=0}^{n} C_2^x U_{si} \sum_n \sum_m \frac{F_m}{u_n^2 \gamma} p_{ni2} zp_{nj1} \int_{\delta}^{\infty} e_s(z_2') e^{-\gamma|z-z_2'|} dz_2' - \sum_{i=0}^{2}\sum_{s=0}^{n} C_2 H_{si} \sum_n \sum_m$$

$$p_{ni2} zp_{nj1} \frac{\partial}{\partial x}\left[\frac{H_m}{\gamma}\int_{-\infty}^{0} e_s(z_2') e^{-\gamma|z-z_2'|} dz_2' + \frac{\overline{H}_m}{\bar{\gamma}}\int_{-\infty}^{0} e_s(z_2') e^{-\bar{\gamma}|z-z_2'|} dz_2'\right] + B_{in}$$

$$\sum_{i=0}^{2}\left\{\sum_n \sum_m \frac{S_{1i}}{u_n^2} p_{ni1} zp_{nj1} \frac{F_m e^{\gamma z}}{\gamma^2+\beta_1^2} - Q_{1i} \sum_n \sum_m p_{ni1} zp_{nj1}\left[\frac{H_m e^{\gamma z}}{\gamma^2+\beta_1^2} + \frac{\overline{H}_m e^{\bar{\gamma} z}}{\bar{\gamma}^2+\beta_1^2}\right]\right\} - \tau$$

$$\sum_{i=0}^{2}\left\{\sum_n \sum_m \frac{S_{2i}}{u_n^2} p_{ni2} zp_{nj1} \frac{F_m e^{\gamma(z-\delta)}}{\gamma(\gamma^2+\beta_2^2)}[\beta_2 \cos(\vartheta) + \gamma \sin(\vartheta)] + Q_{2i} \sum_n \sum_m p_{ni2} zp_{nj1}\right.$$

$$\left.\left[\frac{H_m e^{\gamma(z-\delta)}}{(\gamma^2+\beta_2^2)}[\beta_2 \cos(\vartheta) + \gamma \sin(\vartheta)] + \frac{\overline{H}_m e^{\bar{\gamma}(z-\delta)}}{(\bar{\gamma}^2+\beta_2^2)}[\beta_2 \cos(\vartheta) + \bar{\gamma} \sin(\vartheta)]\right]\right\} = \sum_{i=0}^{2} -$$

$$\left\{\sum_n \sum_m \frac{S_{1i}}{u_n^2} p_{ni1} zp_{nj1} \frac{F_m e^{\gamma z}}{\gamma(\gamma^2+\beta_1^2)} + Q_{1i} \sum_n \sum_m p_{ni1} zp_{nj1}\left[\frac{\gamma H_m e^{\gamma z}}{(\gamma^2+\beta_1^2)} + \frac{\bar{\gamma}\overline{H}_m e^{\bar{\gamma} z}}{(\bar{\gamma}^2+\beta_1^2)}\right]\right\}$$

(3.20)

where z<0 for line 1 and

$$\beta_1 \sum_{i=0}^{2}\sum_{s=0}^{n} C_1^x U_{si} \sum_n \sum_m \frac{F_m}{u_n^2 \gamma} p_{ni1} zp_{nj2} \int_{-\infty}^{0} e_s(z_1') e^{-\gamma|z-z_1'|} dz_1' - \sum_{i=0}^{2}\sum_{s=0}^{n} C_1 H_{si} \sum_n \sum_m$$

$$p_{ni1} zp_{nj2} \frac{\partial}{\partial x}\left[\frac{H_m}{\gamma} \int_{-\infty}^{0} e_s(z_1') e^{-\gamma|z-z_1'|} dz_1' + \frac{\overline{H}_m}{\overline{\gamma}} \int_{-\infty}^{0} e_s(z_1') e^{-\overline{\gamma}|z-z_1'|} dz_1' \right] +$$

$$\beta_2 \sum_{i=0}^{2}\sum_{s=0}^{n} C_2^x U_{si} \sum_n \sum_m \frac{F_m}{u_n^2 \gamma} p_{ni2} zp_{nj2} \int_{\delta}^{\infty} e_s(z_2') e^{-\gamma|z-z_2'|} dz_2' - \sum_{i=0}^{2}\sum_{s=0}^{n} C_2 H_{si} \sum_n \sum_m$$

$$p_{ni2} zp_{nj2} \frac{\partial}{\partial x}\left[\frac{H_m}{\gamma} \int_{-\infty}^{0} e_s(z_2') e^{-\gamma|z-z_2'|} dz_2' + \frac{\overline{H}_m}{\overline{\gamma}} \int_{-\infty}^{0} e_s(z_2') e^{-\overline{\gamma}|z-z_2'|} dz_2' \right] + B_{in}$$

$$\sum_{i=0}^{2} \left\{ \sum_n \sum_m \frac{S_{1i}}{u_n^2} p_{ni1} zp_{nj2} \frac{F_m e^{-\gamma z}}{\gamma^2 + \beta_1^2} + Q_{1i} \sum_n \sum_m p_{ni1} zp_{nj2} \left[\frac{H_m e^{-\gamma z}}{\gamma^2 + \beta_1^2} + \frac{\overline{H}_m e^{-\overline{\gamma} z}}{\overline{\gamma}^2 + \beta_1^2} \right] \right\} - \tau$$

$$\sum_{i=0}^{2} \left\{ \sum_n \sum_m \frac{S_{2i}}{u_n^2} p_{ni2} zp_{nj2} \frac{F_m e^{-\gamma(z-\delta)}}{\gamma(\gamma^2 + \beta_2^2)} [\beta_2 \cos(\vartheta) - \gamma \sin(\vartheta)] - Q_{2i} \sum_n \sum_m p_{ni2} zp_{nj2} \right.$$

$$\left. \left[\frac{H_m e^{-\gamma(z-\delta)}}{(\gamma^2 + \beta_2^2)} [\beta_2 \cos(\vartheta) - \gamma \sin(\vartheta)] + \frac{\overline{H}_m e^{-\overline{\gamma}(z-\delta)}}{(\overline{\gamma}^2 + \beta_2^2)} [\beta_2 \cos(\vartheta) - \overline{\gamma} \sin(\vartheta)] \right] \right\} = \sum_{i=0}^{2}$$

$$\left\{ \sum_n \sum_m \frac{S_{1i}}{u_n^2} p_{ni1} zp_{nj2} \frac{F_m e^{-\gamma z}}{\gamma(\gamma^2 + \beta_1^2)} + Q_{1i} \sum_n \sum_m p_{ni1} zp_{nj2} \left[\frac{\gamma H_m e^{-\gamma z}}{(\gamma^2 + \beta_1^2)} + \frac{\overline{\gamma} \overline{H}_m e^{-\overline{\gamma} z}}{(\overline{\gamma}^2 + \beta_1^2)} \right] \right\}$$

(3.21)

where $z > \delta$ for line 2. Note that the source difference terms in both of the above equations are $S_{1i} = (\beta_1^2 I_{1i} - k_0^2 Q_{1i})$. Note that for the testing in the x direction, we first evaluate the indefinite integration of Eq.s'(3.18) and (3.19) with respect to x so that we can use the existing testing results Eq.(3.11). If only one J_x mode is used in the expansion, then j=1. If two modes are used, then j=1,2.

For simplicity we just consider the TP pair for the perturbed source expansions when the transverse current is included. In this problem, the testing pulses in the z direction are not shifted and begin with the terminated ends for each line because the field E_x arising from a bipolar pulse is odd-symmetric about its center contrary to the case for E_z.

3.4 Tangent method

A gap is a two port network, so it must be represented by a three element equivalent circuit, such as the capacitive pi network as shown in Fig.3.2. To obtain three unknowns we would have to solve the above set of equations three times by using three different positions of the short circuit plane terminating line 2. Fortunately, a more efficient way to extract equivalent circuit values is to use the Tangent or Weissfloch method [18], mentioned in Chap. 1.

In the equations (3.9), (3.10), (3.20), and (3.21), it is clear that the transmission coefficient τ is affiliated with a function of $\cos(\vartheta)$ or $\sin(\vartheta)$. Now we define $T = \tau\cos(\vartheta)$, then the τ column contains the terms with the forms $T \cdot$constant and $T\tan(\vartheta) \cdot$constants.

After $T\tan(\vartheta)$ is brought over to the right hand sides of the equations and viewed as a second source term, the matrix can be written as

$$[A]\begin{bmatrix} B_{in} \\ x_i \\ T \\ \hat{x}_i \end{bmatrix} = [y_i] + T \cdot \tan(\vartheta)[u_i] \tag{3.23}$$

where $[A]$ is the coefficient matrix, $[y_i]$ is the original source vector, and $[u_i]$ associated with $T \cdot \tan(\vartheta)$ is the second source vector.

Assume that T is in row k and $[A]^{-1} = [c_{ij}]$, then inverting the matrix gives

$$B_{in} = \sum_i c_{1i} y_i + T \cdot \tan(\vartheta) \sum_i c_{1i} u_i \tag{3.24a}$$

$$T = \sum_i c_{ki} y_i + T \cdot \tan(\vartheta) \sum_i c_{ki} u_i \tag{3.24b}$$

and after arrangement of these equations we obtain

$$B_{in} = \frac{\sum_i c_{1i}y_i + \left[\sum_i c_{1i}u_i \sum_i c_{ki}y_i - \sum_i c_{ki}u_i \sum_i c_{1i}y_i\right]\tan(\vartheta)}{1 - \sum_i c_{ki}u_i \tan(\vartheta)}$$

$$= \frac{A + B\tan(\vartheta)}{C + D\tan(\vartheta)} \qquad (3.25)$$

where the coefficients $A = \sum_i c_{1i}y_i$, $B = \sum_i c_{1i}u_i \sum_i c_{ki}y_i - \sum_i c_{ki}u_i \sum_i c_{1i}y_i$, $C = 1$, $D = -\sum_i c_{ki}u_i$, and $\tan(\vartheta) = \tan[\beta_2(\delta - 1)] = -\tan(\beta_2 d)$.

For the circuit shown in Fig.3.2, B_{in} can be expressed as

$$B_{in} = \frac{(B1 + B2) - (B1 \cdot B2 + B2 \cdot B3 + B3 \cdot B1)\tan(\beta_2 d)/\overline{Y}_{c2}^m}{1 - (B2 + B3)\tan(\beta_2 d)/\overline{Y}_{c2}^m} \qquad (3.26)$$

Comparing Eq.(3.25) with (3.26) gives

$$B1 = A - (-B \cdot \overline{Y}_{c2}^m + A \cdot D \cdot \overline{Y}_{c2}^m)^{-\frac{1}{2}} \qquad (3.27a)$$

$$B2 = (-B \cdot \overline{Y}_{c2}^m + A \cdot D \cdot \overline{Y}_{c2}^m)^{-\frac{1}{2}} \qquad (3.27b)$$

$$B3 = \overline{Y}_{c2}^m \cdot D - (-B \cdot \overline{Y}_{c2}^m + A \cdot D \cdot \overline{Y}_{c2}^m)^{-\frac{1}{2}} \qquad (3.27c)$$

Since B1, B2, and B3 are normalized admittances relative to the characteristic impedance of the input line, the capacitances can be related to them by

$$C1 = \frac{B1}{\omega Z_{c1}^m}, \quad C2 = \frac{B2}{\omega Z_{c1}^m}, \quad \text{and} \quad C3 = \frac{B3}{\omega Z_{c1}^m} = C1 \qquad (3.28)$$

where Z_{c1}^m is the characteristic impedance of the input line, $\overline{Y}_{c2}^m$ is the nomalized admittance of the output line with respect to $\frac{1}{Z_{c1}^m}$, and $C3 = C1$.

Note that C1 and C3 have different expressions and thus provides one way to investigate if our software program is written correctly.

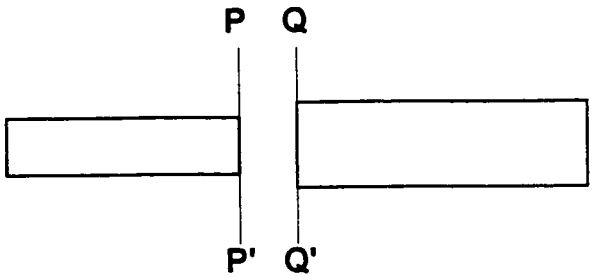

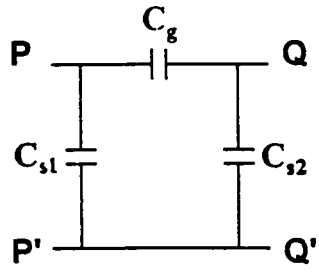

Fig. 3.2 Top view of MS gap **Equivalent circuit of gap**

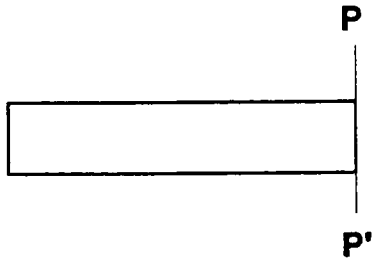

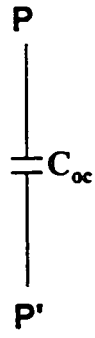

Fig. 3.3 Top view of MS open end **Equivalent circuit of open end**

Chapter 4

Coplanar waveguide dispersions

In this chapter, we develop an efficient way in the conformally mapped domain to find the charge and current distribution on a coplanar waveguide without discontinuities. By using the modified iteration technique and the same Green's functions as in microstrip, we obtain the dispersion characteristics.

4.1 Derivation of source expressions

An enclosed coplanar waveguide (CPW) to be characterized is similar to that in Fig.1.5, but containing two ground planes on each side of the central strip as shown in Fig.4.1a. Obviously, the expressions for the Green's functions have the same forms as those obtained for microstrip lines. In order to derive accurate expressions for the sources, we develop a method based on a conformal transformation that gives a numerically convenient representation for the singularity of the sources at the conductor edges.

Let us consider the geometries shown in Fig.4.1b and 4.1c and assume that the coordinates in the Z plane are transformed to those in the ξ plane by

$$Z = \int \frac{D_0 \, d\xi}{\sqrt{1-\xi^2}} = D_0 \sin^{-1}\xi + D_1 \tag{4.1}$$

where $D_0 = \frac{2a}{\pi}$ and $D_1 = 0$. Note that the point w in the Z plane is converted to $\sigma_1 = \sin(\pi w / 2a)$ in the ξ plane, (w+s) to $\sigma_2 = \sin[\pi(w+s)/2a]$, and a to 1.

Now consider the following conformal mapping by which Fig.4.1c is transformed to Fig.4.1d

$$W = \int \frac{\sigma_2 \, d\xi}{\sqrt{\sigma_1^2 - \xi^2}\sqrt{\sigma_2^2 - \xi^2}} = \int \frac{d\lambda}{\sqrt{1-\lambda^2}\sqrt{1-k^2\lambda^2}} \tag{4.2}$$

where $\lambda = \frac{\xi}{\sigma_1} = \frac{\sin(\pi z/2a)}{\sin(\pi w/2a)}$ and $k^2 = \frac{\sigma_1^2}{\sigma_2^2} = \frac{\sin^2(\pi w/2a)}{\sin^2[\pi(w+s)/2a]}$. Note that the point σ_1 in the ξ plane is transformed to K in the W plane and σ_2 to K+jK' where K and K' are the first kind of complete elliptic integrals with the modules k and k' respectively as calculated by

$$K = \int_0^1 \frac{d\lambda}{\sqrt{1-\lambda^2}\sqrt{1-k^2\lambda^2}} \tag{4.3a}$$

$$K' = \int_0^1 \frac{d\lambda}{\sqrt{1-\lambda^2}\sqrt{1-k'^2\lambda^2}} \tag{4.3b}$$

where $k' = (1-k^2)^{\frac{1}{2}}$.

Since there is a singular component existing in the Green's functions when the source and field points are coincident as shown in Eq.(2.36), it is necessary to extract this first and formulate the dominant part of the integral equations in closed form. Assume that the Green's function for Fig.4.1a is G_1 and that for Fig.4.1c is G_2 where one is derived in the original domain and the other is in the transform domain. From the geometry, the Green's function G_1 satisfies

$$\left(\frac{\partial^2}{\partial x^2} + \frac{\partial^2}{\partial y^2}\right) G_1 = -\delta(x-x')\delta(y-y') \tag{4.4}$$

with the boundary conditions $G_1 = 0$ at $x = \pm a$, $\frac{\partial G_1}{\partial y} = 0$ at $y = 0$, and $G_1 = 0$ at $y = \infty$.

A reasonable choice of the form for G_1 is

$$G_1 = \sum_{n=1,3}^{\infty} a_n(y)\cos(u_n x)$$

where u_n is defined as before. Following the same steps as those in chap. 2, we have

$$\left(\frac{\partial^2}{\partial y^2} + u_n^2\right) a_n(y) = -\cos(u_n x')\delta(y - y') \tag{4.5}$$

where $a_n(y) = \begin{cases} A_n \cosh(u_n y) & y \le y' \\ B_n e^{-u_n(y-y')} & y > y' \end{cases}$.

By applying the continuity of $a_n(y)$ and the discontinuity of its first derivative with respect to y, both at $y = h$, and solving for the unknowns we obtain

$$G_1(x,0;x',0) = \sum_{n=1,3}^{\infty} \frac{2}{n\pi}\cos(u_n x)\cos(u_n x') \tag{4.6}$$

where this G_1 has been evaluated at $y = y' = 0$.

In the transform domain, we must work out the Green's function for G_2 by solving

$$\left(\frac{\partial^2}{\partial u^2} + \frac{\partial^2}{\partial v^2}\right) G_2 = -\delta(u - u')\delta(v - v') \tag{4.7}$$

along with the boundary conditions $\frac{\partial G_2}{\partial u} = 0$ at $u = \pm K$, $\frac{\partial G_2}{\partial v} = 0$ at $v = 0$, and $G_2 = 0$ at $v = K'$. With similar procedures to that used above, we obtain, as evaluated at $v = v' = 0$,

$$G_2(u,0;u',0) = \frac{K'}{K} + \sum_{n=1,2}^{\infty} \frac{1}{n\pi}\cos(\alpha_n u)\cos(\alpha_n u')\tanh(\alpha_n K') \tag{4.8}$$

where $\alpha_n = \frac{n\pi}{K}$.

Although one may note that we selected different boundary conditions for the two Green's functions, our choice is based on the theory as follows

$$\phi = \oiint \left[\phi \frac{\partial G}{\partial n} - G \frac{\partial \phi}{\partial n} \right] dS_0 \tag{4.9}$$

which for this problem gives

$$\phi = \frac{1}{\varepsilon_0} \left[\oiint G_1 \rho_{oc1} \, dS_0 + \oiint G_1 \rho_{og1} \, dS_0 \right] = \frac{1}{\varepsilon_0} \oiint G_2 \rho_{oc2} \, dS_0 \tag{4.10}$$

where c denotes the source on the central strip and g stands for the ground planes.

Therefore, the above transformation gives the static approximation for the current on the central strip, after we formulate the equation for the scalar potential in the transform domain and set it equal to a constant Q' ; namely,

$$\int_{-K}^{K} G_2 \rho_{oc}[x'(u')] \frac{dx'}{du'} du' = Q' \tag{4.11}$$

To ensure that the integration over the range [-K,K] is a constant, we must have $\rho_{oc}[x'(u')]\frac{dx'}{du'}$ = a constant or $\rho_{oc}(x') = \frac{2}{K'} Q' \frac{du'}{dx'} = \frac{2}{K'} Q' \frac{dW}{dZ}$.

Therefore, we have

$$\rho_{oc}(x') = \frac{Q'\pi}{K'a} \frac{\sin\left[\frac{\pi(w+s)}{2a}\right] \sqrt{1 - \sin^2\left(\frac{\pi x'}{2a}\right)}}{\sqrt{\sin^2\left[\frac{\pi(w+s)}{2a}\right] - \sin^2\left(\frac{\pi x'}{2a}\right)} \sqrt{\sin^2\left(\frac{\pi w}{2a}\right) - \sin^2\left(\frac{\pi x'}{2a}\right)}} \tag{4.12}$$

Note that the current expression is chosen accordingly and that when we set (w+s) equal to a, the structure becomes a microstrip line and Eq.(4.12) is

reduced to the first term in Eq.(2.29b) for microstrip if we make the further assumption, a >> w. This is the reason why we called it the quasi-static expressions for the sources, which are very good first approximations to the source distributions at higher frequencies.

Therefore, if a is not much larger than w in microstrip, it is suggested that the reduced form of Eq.(4.12) with the Chebyshev polynomials in the numerator instead of Eq.(2.29) should be used to achieve greater accuracy.

Since we have to include more terms to account for the high frequency effects, we attach some complete functions, like Chebyshev polynomials in microstrip, to the form of Eq.(4.2). Here we choose the Fourier series in the transform domain as follows

$$\tilde{\rho}_{oc}(u') = \rho_{oc}[x'(u')]\frac{dx'}{du'} = \rho_{oc}(u')\frac{dx'}{du'} = \sum_{i=0}^{3} Q_{ci}\cos(\alpha_i u') \qquad (4.13)$$

where the subscript denotes the central strip and $\alpha_i = \frac{i\pi}{K}$.

These general expressions, given for the first time in the literature, are applicable to both coplanar waveguide and microstrip line. Actually, we use them to obtain the dispersion characteristics for microstrip, too. Besides, included are the expressions for the charge and current on the ground planes, with the same form relative to those on the central strip in the transform domain except that the subscript c is replaced by g.

Although all expressions for the charge and current are obtained in the conformally transformed domain, it is not hard to transform them back to the original domain and work out the problem in this domain. This is practically and successfully proved in our software program. However, it is more convenient to solve the problem in the transform domain.

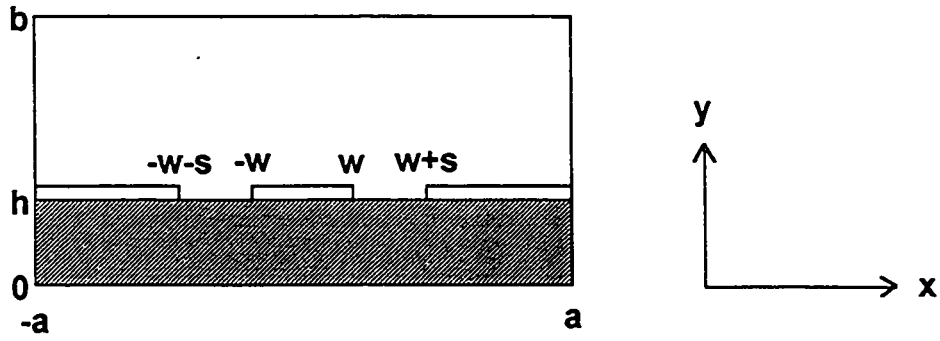

Fig. 4.1a. Shielded coplanar waveguide geometry

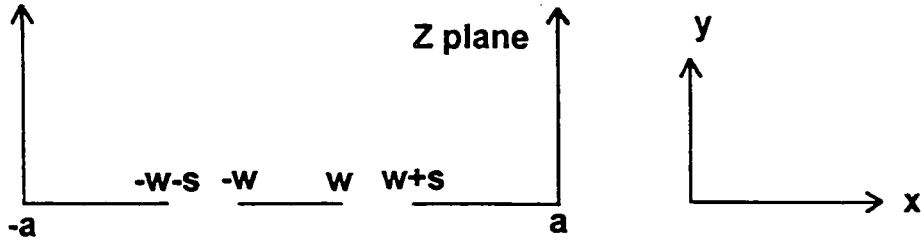

Fig. 4.1b. Simplified CPW structure outline

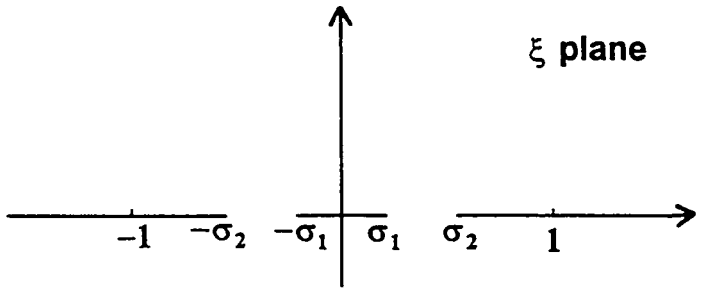

Fig. 4.1c. The transformation of Fig. 4.1b. by Eq. (4.1)

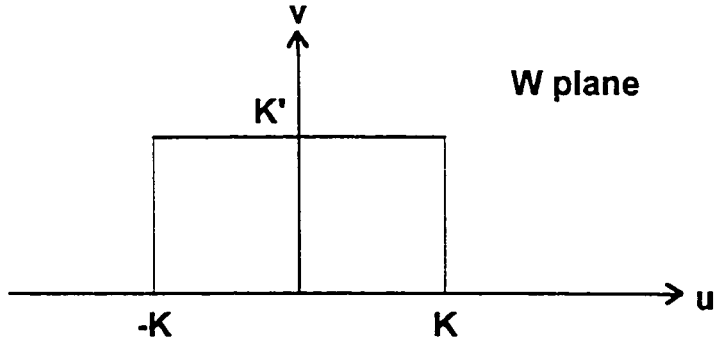

Fig. 4.1d. The transformation of Fig. 4.1c. by Eq. (4.2)

4.2 Calculation of the integrals for potentials

Since the ground planes must be always taken into consideration for coplanar waveguides, the transverse current is included and expressed in terms of the longitudinal current and the charge by the continuity equation. With the source expressions we can formulate the potential equations in both the original domain and the transform domain as follows

$$\begin{aligned} A_{oxr} &= \mu_0\Big[\int_{-\infty}^{\infty}\int_{-w}^{w} G_x(x,z;x',z')J_{oxcr}(x')e^{-j\beta z'}dx'dz' + \int_{-\infty}^{\infty}\int_{w+s}^{a} G_x(x,z;x',z') \\ &\quad J_{oxgr}(x')e^{-j\beta z'}dx'dz' + \int_{-\infty}^{\infty}\int_{-a}^{-(w+s)} G_x(x,z;x',z')J_{oxgr}(x')e^{-j\beta z'}dx'dz'\Big] \\ &= \mu_0\Big[\int_{-\infty}^{\infty}\int_{-K}^{K} G_x(x,z;x_c',z')\tilde{J}_{oxcr}(u')e^{-j\beta z'}du'dz' - \int_{-\infty}^{\infty}\int_{K_s}^{K} G_x(x,z;x_g',z') \\ &\quad \tilde{J}_{oxgr}(u')e^{-j\beta z'}du'dz' - \int_{-\infty}^{\infty}\int_{-K}^{-K_s} G_x(x,z;x_g',z')\tilde{J}_{oxgr}(u')e^{-j\beta z'}du'dz'\Big] \end{aligned} \tag{4.14a}$$

$$\begin{aligned} A_{ozr} &= \mu_0\Big[\int_{-\infty}^{\infty}\int_{-w}^{w} G_z(x,z;x',z')J_{ozcr}(x')e^{-j\beta z'}dx'dz' + \int_{-\infty}^{\infty}\int_{w+s}^{a} G_z(x,z;x',z') \\ &\quad J_{ozgr}(x')e^{-j\beta z'}dx'dz' + \int_{-\infty}^{\infty}\int_{-a}^{-(w+s)} G_z(x,z;x',z')J_{ozgr}(x')e^{-j\beta z'}dx'dz'\Big] \\ &= \mu_0\Big[\int_{-\infty}^{\infty}\int_{-K}^{K} G_z(x,z;x_c',z')\tilde{J}_{ozcr}(u')e^{-j\beta z'}du'dz' - \int_{-\infty}^{\infty}\int_{K_s}^{K} G_z(x,z;x_g',z') \\ &\quad \tilde{J}_{ozgr}(u')e^{-j\beta z'}du'dz' - \int_{-\infty}^{\infty}\int_{-K}^{-K_s} G_z(x,z;x_g',z')\tilde{J}_{ozgr}(u')e^{-j\beta z'}du'dz'\Big] \end{aligned} \tag{4.14b}$$

$$\phi_o = \frac{1}{\varepsilon_0}\left[\int_{-\infty}^{\infty}\int_{-w}^{w} G(x,z;x',z')\rho_{oc}(x')e^{-j\beta z'}dx'dz' + \int_{-\infty}^{\infty}\int_{w+s}^{a} G(x,z;x',z')\right.$$

$$\left.\rho_{og}(x')e^{-j\beta z'}dx'dz' + \int_{-\infty}^{\infty}\int_{-a}^{-(w+s)} G_z(x,z;x',z')\rho_{og}(x')e^{-j\beta z'}dx'dz'\right]$$

$$= \frac{1}{\varepsilon_0}\left[\int_{-\infty}^{\infty}\int_{-K}^{K} G_z(x,z;x_c',z')\tilde{\rho}_{oc}(u')e^{-j\beta z'}du'dz' - \int_{-\infty}^{\infty}\int_{K_a}^{K} G(x,z;x_g',z')\right.$$

$$\left.\tilde{\rho}_{og}(u')e^{-j\beta z'}du'dz' - \int_{-\infty}^{\infty}\int_{-K}^{-K_a} G(x,z;x_g',z')\tilde{\rho}_{og}(u')e^{-j\beta z'}du'dz'\right] \qquad (4.14c)$$

In the above integrals, K_a and the evaluations of x_c' and x_g' in terms of u' are respectively given by

$$K_a = K - \int_{\frac{1}{k}}^{\frac{1}{\sigma_1}} \frac{d\lambda}{\sqrt{\lambda^2-1}\sqrt{k^2\lambda^2-1}} \qquad (4.15a)$$

$$x_c' = \frac{2a}{\pi}\sin^{-1}\left[\sin\left(\frac{\pi w}{2a}\right)sn(u',k)\right] \qquad (4.15b)$$

$$x_g' = \frac{2a}{\pi}\sin^{-1}\left[\sin\left(\frac{\pi w}{2a}\right)sn(u'+jK',k)\right] \qquad (4.15c)$$

where $sn(u') = \sin.am(u')$ is one of the Elliptic functions.

As we mentioned in Chap. 2, there is a singularity in the Green's function, which accounts for the dominant part. Therefore, we can compute the integrals of these Green's functions first with respect to z' to extract this term, as also shown in Appendix 1,

$$\hat{G}_z(x,z;x_c') = \int_{-\infty}^{\infty} G_z(x,z;x_c',z')e^{-j\beta z'}dz' = \left\{\frac{2}{a}\sum_{n=1,3}^{\infty}[TF(n)-AF(n)]\cos(u_n x)\right.$$

$$\left.\cos(u_n x_c') + \frac{1}{\pi}\sum_{n=1,3}^{\infty}\frac{1}{n}\cos(u_n x)\cos(u_n x_c')\right\}e^{-j\beta z} \qquad (4.16a)$$

$$\hat{G}(x,z;x_c') = \int_{-\infty}^{\infty} G(x,z;x_c',z')e^{-j\beta z'}dz' = \left\{\frac{2}{a}\sum_{n=1,3}^{\infty}[TG(n)-AG(n)]\cos(u_n x)\right.$$

$$\left.\cos(u_n x_c') + \kappa_r \frac{2}{\pi}\sum_{n=1,3}^{\infty}\frac{1}{n}\cos(u_n x)\cos(u_n x_c')\right\}e^{-j\beta z} \qquad (4.16b)$$

and similarly for the ground planes by replacing x_c' by x_g' in the equations where the parameter x can be x_c or x_g and TF(n), AF(n), TG(n), AG(n), and κ_r are defined the same as in Appendix 1.

By calculating the remaining integrals in the transform domain over u' after substituting (4.13) into (4.14) shows that we have these results for the correction terms

$$t_{ni} = 2\int_0^K \cos(u_n x_c')\cos(\alpha_i u')du' \qquad (4.17a)$$

$$s_{ni} = 2\int_{K_a}^K \cos(u_n x_g')\cos(\alpha_i u')du' \qquad (4.17b)$$

Note that these expressions are also the testing results when we apply the testing functions, $\sum_{i=0}^{3}\cos(\alpha_i u)$, to the central strip and the ground planes.

For the dominant terms the summation over n is manipulated into the same form as Eq.(2.36). Then we have, after testing over u,

$$t_{ji} = -\int_0^K\int_0^K \ln\left|\tan\left[\frac{\pi(x_c - x_c')}{4a}\right]\tan\left[\frac{\pi(x_c + x_c')}{4a}\right]\right|\cos(\alpha_i u')\cos(\alpha_j u)du'du \qquad (4.18a)$$

$$s_{ji} = -\int_{K_a}^K\int_{K_a}^K \ln\left|\tan\left[\frac{\pi(x_g - x_g')}{4a}\right]\tan\left[\frac{\pi(x_g + x_g')}{4a}\right]\right|\cos(\alpha_i u')\cos(\alpha_j u)du'du \qquad (4.18b)$$

$$c_{ji} = \int_0^K\int_{K_a}^K \ln\left|\tan\left[\frac{\pi(x_c - x_g')}{4a}\right]\tan\left[\frac{\pi(x_c + x_g')}{4a}\right]\right|\cos(\alpha_i u')\cos(\alpha_j u)du'du$$

(4.18c)

$$d_{ji} = \int_{K_a}^{K} \int_{0}^{K} \ln\left|\tan\left[\frac{\pi(x_g - x_c')}{4a}\right]\tan\left[\frac{\pi(x_g + x_c')}{4a}\right]\right|\cos(\alpha_i u')\cos(\alpha_j u)\,du'du$$

(4.18d)

where we note that $t_{ji} = t_{ij}$ and $s_{ji} = s_{ij}$ are the self-testing results and $c_{ji} = d_{ij}$ are the cross-testing results.

For the self-testing results, only part of the terms need calculating numerically while all terms for either of the cross-testing results must be computed. Since there are singularities in each ln function for self-testing, special treatment is taken when we perform the integration by a numerical method.

4.3 Modified iteration technique

In microstrip lines we assumed there is no dominant mode transverse current J_{oxr} on the strip since its effect is negligible for a wide range of useful geometries. But, this is not true for coplanar waveguides especially since the ground planes must always be taken into consideration.

Therefore, unlike microstrip lines where $A_{ozr} / \mu_0 = 1$ and $\varepsilon_0 \phi_o = 1$ are assumed to execute the iteration method, we have to use the boundary conditions that the tangential components of the electric fields must vanish on both the central strip and the ground planes.

By using the conditions that $E_z = -j(\beta c / k_0) A_{ozr} - \partial\phi / \partial z = 0$ and $E_x = -j(\beta c / k_0) A_{oxr} - \partial\phi / \partial x = 0$ and applying the moment method, we generate a system of linear equations. Note that in evaluating A_{oxr} the techniques such as those used in Eq.s'(3.17) and (3.18) are again taken advantage of, and we utilize $J_{xcr}(w, z) = 0$ and $J_{xgr}(w + s, z) = 0$ which are proved mathematically.

Since there is $\sin(u_n x)$ in E_x instead of $\cos(u_n x)$, we perform the indefinite integration of E_x over x first to facilitate the use of the existing testing results ; namely, Eq.(4.17). Note that it is also adopted in our software programs for the microstrip gap discontinuity for the computational time-saving purpose and improved accuracy.

Similarly, using a trial value of β, the unknowns $Q_{c,gi}$ and $I_{c,gi}$ are found from this matrix. Now, the total charge and relative current on the central strip are given by $I_{Tc} = 2KI_{c0}$ and $Q_{Tc} = 2KQ_{c0}$.

A new estimate of the propagation constant can be calculated from Eq.(2.37) except that ε_{em} is replaced by $\varepsilon_{ec} = Q_{Tc} / I_{Tc} = Q_{c0} / I_{c0}$ defined as the effective dielectric constant for coplanar waveguide. If the new value of ε_{ec} differs from the old value of ε_{ec} by less than 1%, the iteration is

terminated ; otherwise, the iteration is repeated with the latest values of β, $Q_{c,gi}$, and $I_{c,gi}$ used as the new entries in the matrix for each successive iteration until the condition is satisfied. By this way, the iteration also converges very fast for coplanar waveguide dispersion problems.

After a convergent value of ε_{ec} is found, the characteristic impedance of coplanar waveguide is computed. It is defined as the ratio of the voltage between the center of the central strip and the ground planes to the total current flowing along the central strip. Since A_{ox} can also be expressed in terms of Fourier series we have

$$Z_c^c = \frac{1}{I_{TOT}^c}\int_{(w+s)}^{0} -E_x dx = \frac{1}{I_{TOT}^c}\int_{(w+s)}^{0}\left(\frac{\partial\phi}{\partial x} + j\omega A_{ox}\right)_{y=h} dx = \frac{60\pi}{K\sqrt{I_{c0}Q_{c0}}}$$

$$\left[1 + k_0^2 \sum_{n=1,3}^{\infty} \frac{\tilde{\rho}_{cn} - \varepsilon_{ec}\tilde{J}_{zcm}}{u_n} \frac{\sinh(\zeta_n c)\sinh(\zeta_{1n} h)}{[\zeta_{1n}\sinh(\zeta_n c)\cosh(\zeta_{1n} h) + \zeta_n \cosh(\zeta_n c)\sinh(\zeta_{1n} h)]} \frac{\cos[u_n(w+s)] - 1}{u_n}\right] \tag{4.19}$$

where I_{TOT}^c is the total z-directed current on the central strip, $\tilde{J}_{zcm}$ and $\tilde{\rho}_{cn}$ are defined as

$$\tilde{J}_{zcm} = \frac{2}{a}\sum_{i=0}^{3}\left(I_{ci}t_{ni} + I_{gi}s_{ni}\right) \tag{4.20a}$$

$$\tilde{\rho}_{cn} = \frac{2}{a}\sum_{i=0}^{3}\left(Q_{ci}t_{ni} + Q_{gi}s_{ni}\right) \tag{4.20b}$$

which can be obtained by the Fourier series expansions for the sources in the original domain as mentioned in Chap. 2, and all of the other quantities in Eq.(4.19) are the same as before.

This completes the determination of the dominant mode charge and relative current amplitudes on both the central strip and the ground planes, the propagation constant, and the characteristic impedance for the enclosed coplanar waveguide with isotropic and anisotropic substrates.

Chapter 5

Coplanar waveguide discontinuities

In this chapter, we extend the dynamic source reversal method to coplanar waveguide open-end discontinuity including anisotropic substrates with the help of the known dispersion characteristics for no discontinuity. In order to treat the problem more efficiently we only use the TP pair for the perturbed source expansion functions.

5.1 Extensions of the dynamic source reversal technique

The dynamic source reversal method used to well-treat microstrip discontinuities can be applied to CPW open end discontinuities, with some techniques modified. For this open-end coplanar waveguide discontinuity, we still assume that the discontinuity is located at z'=0. Then, the dominant mode sources have the same forms as in Eq.(3.1) except that the x' dependence in the equation for the microstrip case must now be replaced by Eq.(4.12). Also, the perturbed sources which are used in this problem are quite similar to Eq.(3.2) with the x' dependence revised accordingly.

Because the discontinuous coplanar waveguide to be characterized contains two ground planes, one on each side of the central strip as shown in Fig. 5.1, the transverse current, at least on these two ground planes when the width of the central strip is small, must be taken into consideration. Therefore, unlike some microstrip discontinuities, we must utilize the vanishing of both tangential components of the electric fields in the x and z directions on the central strip and the ground planes as the boundary conditions that will give the required integral equations.

First considering the condition $E_z = 0$, in which the perturbed sources are included, we obtain

$$
\begin{aligned}
&j\beta\int_{-\infty}^{0}\int_{-w}^{w} G_z J_{pzcr}\,dx'\,dz' + \frac{\partial}{\partial z}\int_{-\infty}^{0}\int_{-w}^{w} G\rho_{pc}\,dx'\,dz' \\
&+j\beta\int_{-\infty}^{0}\int_{g} G_z J_{pzgr}\,dx'\,dz' + \frac{\partial}{\partial z}\int_{-\infty}^{0}\int_{g} G\rho_{pg}\,dx'\,dz' \\
&-j\beta\int_{0}^{\infty}\int_{-w}^{w} G_z jJ_{ozcr}[B_{in}\cos(\beta z') - \sin(\beta z')]dx'\,dz' \\
&-\frac{\partial}{\partial z}\int_{0}^{\infty}\int_{-w}^{w} G\rho_{oc}[B_{in}\sin(\beta z') + \cos(\beta z')]dx'\,dz' \\
&-j\beta\int_{0}^{\infty}\int_{g} G_z jJ_{ozgr}[B_{in}\cos(\beta z') - \sin(\beta z')]dx'\,dz' \\
&-\frac{\partial}{\partial z}\int_{0}^{\infty}\int_{g} G\rho_{og}[B_{in}\sin(\beta z') + \cos(\beta z')]dx'\,dz' = 0
\end{aligned}
\tag{5.1}
$$

Then using the other condition $E_x = 0$ produces

$$
\begin{aligned}
&j\beta\int_{-\infty}^{0}\int_{-w}^{w} G_x J_{pxcr}\,dx'\,dz' + \frac{\partial}{\partial x}\int_{-\infty}^{0}\int_{-w}^{w} G\rho_{pc}\,dx'\,dz' \\
&+j\beta\int_{-\infty}^{0}\int_{g} G_x J_{pxgr}\,dx'\,dz' + \frac{\partial}{\partial x}\int_{-\infty}^{0}\int_{g} G\rho_{pg}\,dx'\,dz' \\
&-j\beta\int_{0}^{\infty}\int_{-w}^{w} G_x jJ_{oxcr}[B_{in}\sin(\beta z') + \cos(\beta z')]dx'\,dz' \\
&-\frac{\partial}{\partial x}\int_{0}^{\infty}\int_{-w}^{w} G\rho_{oc}[B_{in}\sin(\beta z') + \cos(\beta z')]dx'\,dz' \\
&-j\beta\int_{0}^{\infty}\int_{g} G_z jJ_{ozgr}[B_{in}\sin(\beta z') + \cos(\beta z')]dx'\,dz' \\
&-\frac{\partial}{\partial x}\int_{0}^{\infty}\int_{g} G\rho_{og}[B_{in}\sin(\beta z') + \cos(\beta z')]dx'\,dz' = 0
\end{aligned}
\tag{5.2}
$$

After the above integral equations are computed over x' and z' they have the similar forms to Eq.'s (3.9) and (3.20) where just one line is needed for the open end microstrip discontinuity. In order not to repeat too much of the analysis, their final expressions are not listed here explicitly.

Since we found that the TP pair of representations for the perturbed sources in microstrip gap discontinuities resulted in less computational time than the QT pair, we only use the TP pair for the perturbed sources in this problem. The compression techniques used for the microstrip case can be also applied to reduce the number of unknowns. All of the testing results in the z direction for microstrip discontinuities can be used here.

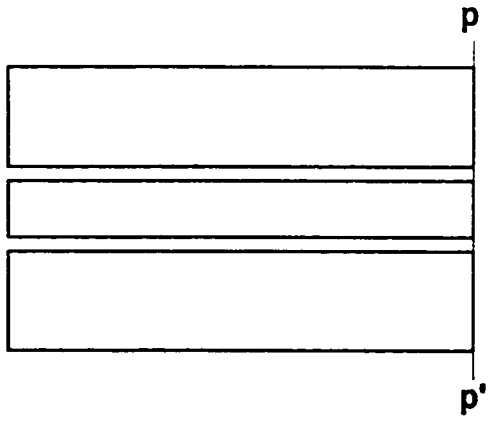

Fig. 5.1 Top view of CPW open end

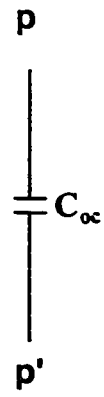

Equivalent circuit

5.2 Calculation of some testing results and the excess capacitance

Applying testing functions in the x and z direction to the above equations, which are already calculated over the source points, a system of linear equations is obtained. Like the microstrip case, the unweighted edge condition for the testing in x is used for this open-end coplanar waveguide discontinuity. For this reason, the resulting integrals which must be made use of are listed below. For testing the central strip,

$$zxt_{ni} = 2\int_0^{\frac{\pi}{2}} \frac{\cos(u_n x_c)\cos(\alpha_j u_c)}{\sqrt{1-k^2\sin^2(\theta)}} d\theta \tag{5.3a}$$

and, for testing the ground planes,

$$zxs_{ni} = 2\int_{\theta_1}^{\frac{\pi}{2}} \frac{\cos(u_n x_g)\cos(\alpha_j u_g)}{\sqrt{1-k^2\sin^2(\theta)}} d\theta \tag{5.3b}$$

where all the symbols have the same definitions as in Chap. 4 and θ_1, x_c, x_g, u_c, and u_g are calculated by

$$\theta_1 = \frac{\pi(w+s)}{2a} \tag{5.4a}$$

$$x_c = \frac{2a}{\pi}\sin^{-1}\left[\sin\left(\frac{\pi w}{2a}\right)\sin(\theta)\right] \tag{5.4b}$$

$$x_g = \frac{2a}{\pi}\sin^{-1}\left\{\sin\left[\frac{\pi(w+s)}{2a}\right]\csc(\theta)\right\} \tag{5.4c}$$

$$u_c = \int_0^{\theta} \frac{d\varphi}{\sqrt{1-k^2\sin^2(\varphi)}} \tag{5.4d}$$

$$u_g = K - \int_{\theta}^{\frac{\pi}{2}} \frac{d\varphi}{\sqrt{1-k^2\sin^2(\varphi)}} \tag{5.4e}$$

Because all of the calculations for this problem are based on numerical methods, the summation approach over n in the Appendix can not be taken

advantage of. Although this is the case, we can still treat these dominant terms very efficiently in the numerical sense as follows

$$f_{ji} = -\int_0^{\frac{\pi}{2}}\int_0^K \ln\left|\tan\left[\frac{\pi(x_c - x_c')}{4a}\right]\tan\left[\frac{\pi(x_c + x_c')}{4a}\right]\right| \frac{\cos(\alpha_i u')\cos(\alpha_j u_c)}{\sqrt{1-k^2\sin^2(\theta)}}du'd\theta \tag{5.5a}$$

$$g_{ji} = -\int_{\theta_1}^{\frac{\pi}{2}}\int_{K_a}^K \ln\left|\tan\left[\frac{\pi(x_g - x_g')}{4a}\right]\tan\left[\frac{\pi(x_g + x_g')}{4a}\right]\right| \frac{\cos(\alpha_i u')\cos(\alpha_j u_g)}{\sqrt{1-k^2\sin^2(\theta)}}du'd\theta \tag{5.5b}$$

$$a_{ji} = \int_0^{\frac{\pi}{2}}\int_{K_a}^K \ln\left|\tan\left[\frac{\pi(x_c - x_g')}{4a}\right]\tan\left[\frac{\pi(x_c + x_g')}{4a}\right]\right| \frac{\cos(\alpha_i u')\cos(\alpha_j u_c)}{\sqrt{1-k^2\sin^2(\theta)}}du'd\theta \tag{5.5c}$$

$$b_{ji} = \int_{\theta_1}^{\frac{\pi}{2}}\int_0^K \ln\left|\tan\left[\frac{\pi(x_g - x_c')}{4a}\right]\tan\left[\frac{\pi(x_g + x_c')}{4a}\right]\right| \frac{\cos(\alpha_i u')\cos(\alpha_j u_g)}{\sqrt{1-k^2\sin^2(\theta)}}du'd\theta \tag{5.5d}$$

Similarly, the same technique as used in Chap. 4 to facilitate the use of the existing testing results for $E_x = 0$ is applied for this problem ; that is, instead of Eq.(4.17), we now utilize Eq.(5.3).

After the matrix formed by the linear equations is inverted, we can find the normalized input susceptance which is simply related to the excess capacitance by the expression

$$C = \frac{B_{in}}{\omega Z_c^e} \tag{5.6}$$

Chapter 6

Simulation results

In this chapter, we show the theoretical results, calculated from the programs written in the C language and run on an HP workstation computer, for the microstrip open-end and gap discontinuities, the coplanar waveguide dispersions, and the coplanar waveguide open-end discontinuity. Anisotropic substrates are included for all the configurations studied. In addition to these results, an accompanying detailed discussion and some comparisons with the existing data for each case of the problems can be found in the corresponding sections.

(6-1)Results for microstrip open-end and gap discontinuities

The unit width, Δ, of the expansion functions in the TP pair is chosen as 0.2h and in the QT pair is chosen as 0.045h. Table I shows the capacitance values for the microstrip open end discontinuity with a sapphire substrate, $\kappa = 9.4$ and $\kappa_y = 11.6$, as a function of microstrip line width. The line width W in the table is equal to 2w. These results obtained using the dynamic source reversal technique are produced by letting $e^{-\gamma\delta}$ and $e^{-\bar{\gamma}\delta}$ be equal to zeros in the programs originally written for the microstrip gap discontinuities.

From the data, we know that there is always a drop in the open end equivalent capacitance values when we include the effects of the transverse current. However, as we can see in the data, only one mode of J_x current needs to be taken into consideration for more accurate results for the equivalent capacitance in microstrip open end discontinuity. Also, the results yielded by using the TP pair as the expansion functions and including no J_x current are in quite good agreement with those by using the QT pair and considering no J_x current.

Since we have to utilize much narrower widths of the expansion functions in the QT pair to obtain the accurate results, the number of unknowns is increased on a large scale, in turn, much increasing the size of the coefficient matrix and the computational time. Therefore, the results generated by the QT pair of the expansion functions are shown only for microstrip open end discontinuity.

In all the data shown for symmetrical and asymmetrical microstrip gap discontinuities, the following relations are used that the line width of the input line W_1 is equal to $2w_1$ and the line width of the output line W_2 is equal to $2w_2$. In addition, all the units for the shunt and coupling capacitances of pi equivalent networks for microstrip gaps are fano Farads.

The results for the capacitances of pi equivalent network modeled for microstrip gap discontinuity with an alumina substrate, $\kappa = 9.7$, are shown in Fig. 6.1.1 and Fig. 6.1.2. They are varied as a function of the line width and the gap spacing all for the symmetrical gap cases. The gap spacing used to obtain the results in the programs is increased every step by 0.2 times the substrate height h.

The lower lines right below the corresponding line with the same marks represent the results with the inclusion of both one mode and two modes for the transverse current. Although they look like one line for each mark, they are actually two lines nearly overlapped. It means that the inclusion of one mode produces almost the same results as those by the consideration of two modes. Therefore, it is suggested that for symmetrical microstrip gap discontinuities, the inclusion of one mode for the transverse current is good enough to obtain accurate results.

From the data shown in these two figures, it is obvious that as the gap spacing increases, the coupling effect decreases. The results for the inclusion

of one mode and two modes for the transverse current are also shown in the figures. For the symmetrical gap cases, consideration of one mode for the transverse current is quite enough for accurate results.

Fig. 6.1.3 shows the shunt capacitances of pi equivalent network modeled for microstrip gap discontinuity with a Epsilam 10 substrate, $\kappa = 13$ and $\kappa_y = 10.3$, and the coupling capacitance of that network is shown in Fig. 6.1.4. The capacitances for both figures are as a function of frequency with 2 GHz as each increment. Accompanied in the figures are the results for an isotropic substrate with $\kappa_{eq} = \sqrt{\kappa\kappa_y}$ and $h_{eq} = \sqrt{\kappa / \kappa_y}h$.

In the low frequencies, the shunt and coupling capacitances for the anisotropic substrate should be reduced to those for the equivalent isotropic substrate as also proved in these figures. To understand it further in the mathematical sense, Eq.(15) in [25] gives us the self-explanation for this problem. Thus, computer programs that solve the open ends and gaps with the corresponding isotropic substrates can, with the equivalent substrate thickness and dielectric constant as input values, give good approximate outcomes for the capacitance(s) of the modeled networks for the same discontinuities with anisotropic substrates.

In the frequency range of interest ; that is, up to 20 GHz, there is less than 1.5% difference between the shunt capacitances for the anisotropic substrate and those for the equivalent isotropic substrate. Also, included in the figures are the outcomes for the consideration of the effects of two modes for the transverse current.

Table II shows the capacitance values of pi equivalent network modeled for microstrip gap discontinuity with a GaAs substrate, $\kappa = 12.9$, including the asymmetrical cases. They are shown as a function of the output line width and the gap spacing. Note that some values of the shunt

capacitances in the capacitive pi network are negative, indicating the equivalent inductances. This phenomenon occurs for the tight coupling and is manifested by the shunt element on the end side of the line with the narrower width.

For the cases of tight coupling, some of the electric field from the narrower line divergently terminate on the wider line or those from the wider line convergently terminate on the narrower line. This effect decreases the capacitance value below that of the capacitance per unit length that is normally associated with a uniform microstrip line and results in negative values for the shunt capacitances on the narrower line side. However, when the gap spacing is increased, the capacitive effects eventually predominate, regardless of the degree of asymmetry between the two lines. This is due to the fact that a lightly coupled gap will behave more like two uncoupled open ends.

Table I

Open end equivalent capacitance C_{oc} as a function of the line width for sapphire, $\kappa = 9.4$ and $\kappa_y = 11.6$. Units are pF/Meter for C_{oc} / W. a=1.0, h=0.1, b=1.1, and f=2 GHz.

	TP pair with no J_x	TP pair with one J_x mode	TP pair with two J_x modes	QT pair with no J_x
W/h	C_{oc} / W	C_{oc} / W	C_{oc} / W	C_{oc} / W
0.5	62.28	58.14	58.08	61.90
1.0	53.61	49.75	49.62	54.46
2.0	48.23	44.53	44.29	49.38

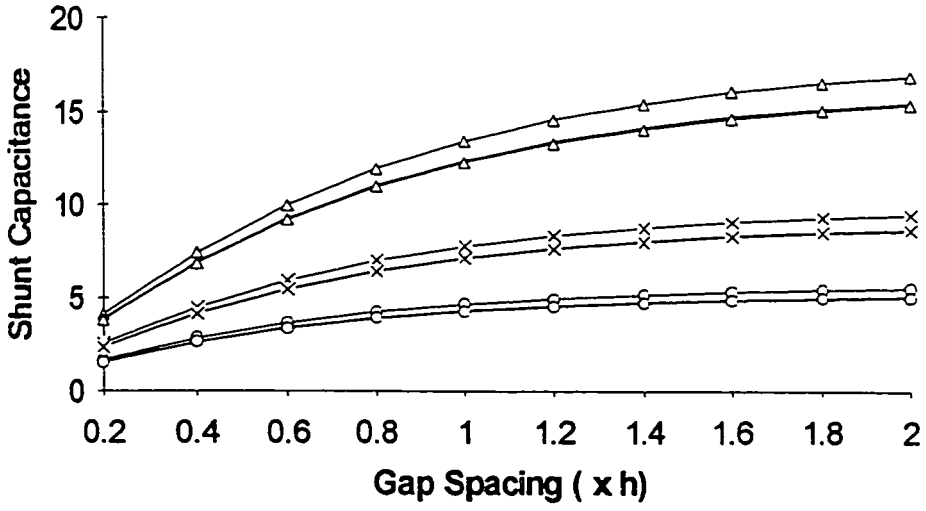

Fig. 6.1.1 Shunt capacitance versus gap spacing for an alumina substrate where h=0.02, a=0.5, c=1.02, $w_1 = w_2$, and f=10 GHz. —o— $W_1 / h = 0.5$, —×— $W_1 / h = 1.0$, and —Δ— $W_1 / h = 2.0$.

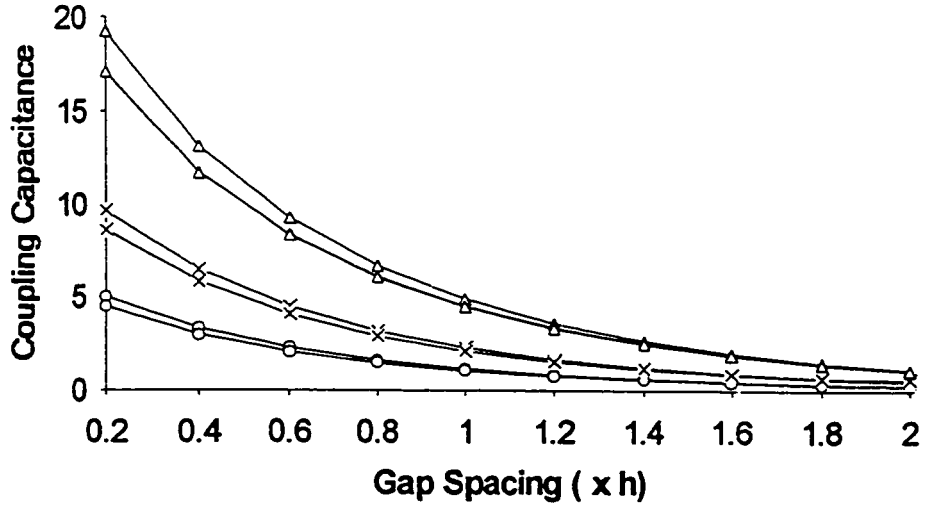

Fig. 6.1.2 Coupling capacitance versus gap spacing for the alumina substrate of Fig. 6.1.1.

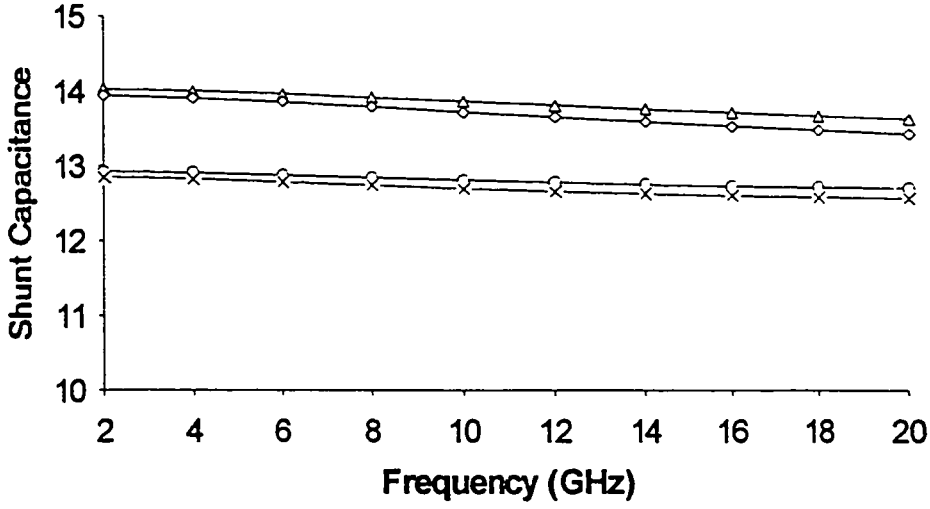

Fig. 6.1.3 Shunt capacitance versus frequency for an Epsilam-10 substrate where h=0.03, a=0.3, b=1.03, $\delta / h = 1.0$, $W_1 / h = 1.0$, and $w_1 = w_2$. —Δ— no mode for J_x, —◊— no mode with κ_{eq} and h_{eq}, —○— two modes, —×— two modes with κ_{eq} and h_{eq}.

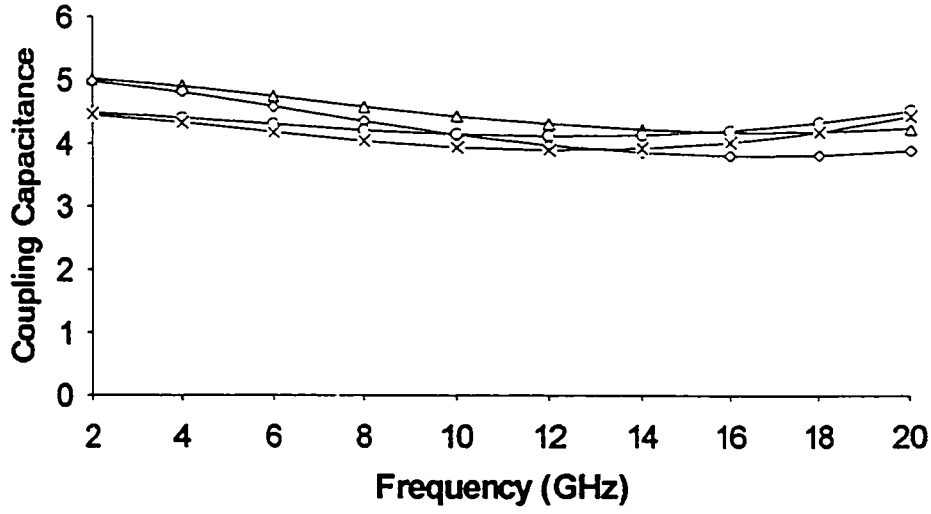

Fig. 6.1.4 Coupling capacitance versus frequency for the Epsilam-10 substrate of Fig. 6.1.3.

Table II

Capacitance values of pi equivalent network as a function of the output line width and the gap spacing for GaAs, $\kappa = 12.9$. Units are fF for C_{s1}, C_g, and C_{s2}. W_1 / h=1.0, a=0.4, h=0.03, b=1.03, and f=14 GHz.

(a) δ / h=0.2

	TP pair with no J_x			TP pair with two J_x modes		
W_2 / h	C_{s1}	C_g	C_{s2}	C_{s1}	C_g	C_{s2}
0.25	11.62	9.47	-1.38	10.98	8.76	-1.20
1.0	5.13	18.18	5.13	4.83	16.88	4.83
4.0	-4.05	27.21	42.93	-2.78	25.37	40.64

(b) δ / h=0.6

	TP pair with no J_x			TP pair with two J_x modes		
W_2 / h	C_{s1}	C_g	C_{s2}	C_{s1}	C_g	C_{s2}
0.25	15.13	4.12	2.93	14.24	3.99	2.66
1.0	11.82	7.85	11.82	11.00	7.62	11.00
4.0	6.64	13.18	50.31	6.12	12.75	47.86

(c) δ / h=1.0

	TP pair with no J_x			TP pair with two J_x modes		
W_2 / h	C_{s1}	C_g	C_{s2}	C_{s1}	C_g	C_{s2}
0.25	17.04	1.87	4.98	15.98	1.97	4.52
1.0	15.39	3.61	15.39	14.27	3.77	14.27
4.0	12.56	6.52	55.35	11.32	6.79	52.48

(6-2)Results for coplanar waveguide dispersion characteristics

Many ways are used to verify the validity of our method. First of all, our results obtained in the transformed domain from the general expressions for the sources are checked against those from the Fourier series expansions in the original spatial domain for the sources. The results in both cases are obtained for the propagation characteristics of microstrip line (MS) including anisotropic substrates. Although the method using Eq.(2.35) to find the dispersions of MS with a top cover is also developed and included in the dissertation, it produces, if the cover is far enough away from the substrate, almost the same data as those in [25] which discussed and compared with a lot of the results shown by many other authors.

We compute the microstrip line dispersion data shown in Fig. 6.2.1 and 6.2.2 for an alumina substrate whose typical dielectric constant is quoted as 9.7. Fig. 6.2.3 and 6.2.4 give the microstrip line dispersion data for a sapphire substrate with $\kappa = 9.4$ and $\kappa_y = 11.6$. All the lines in these four figures with diamond marks are our results by the method using Eq.(2.31) for the source expressions and solving the problem in the original domain. The other lines with triangular marks are our results by the method using Eq.(4.13) for the source expressions and solving the problem in the transformed domain.

In addition, we examine the results produced by this method for coplanar waveguide dispersions against those that were given by the quasi-static approximation equation in [28]. This equation was derived by assuming that the semi-infinite ground planes on each side of the central strip which, as mentioned above, contradicts the real structures usually encountered.

Also, we find that the finite widths of the ground planes do influence the dispersions to some extent and this fact was not taken into consideration in the quasi-static equation. Because this kind of the structures of coplanar

waveguides can support a perturbed TE_{10} rectangular waveguide mode, this phenomenon results in a limitation for the width of the dielectric-loaded waveguide ; namely, the value of a.

The CPW dispersion data for a GaAs substrate using the dielectric constant $\kappa = 12.9$ are shown in Fig. 6.2.5 and 6.2.6. The lines with circle marks are our results and the other lines with cross marks are those by the quasi-static equation. We use an Epsilam-10 substrate as an example to obtain the CPW dispersion data, with anisotropic substrates, as shown in Fig. 6.2.7 and 6.2.8. The substrate has anisotropic dielectric constant with $\kappa = 13$ and $\kappa_y = 10.3$.

In all four figures for coplanar waveguide propagation characteristics, our results with both isotropic and anisotropic substrates show a slight increase for effective dielectric constants with frequency and a very slight decrease for characteristic impedances against frequency.

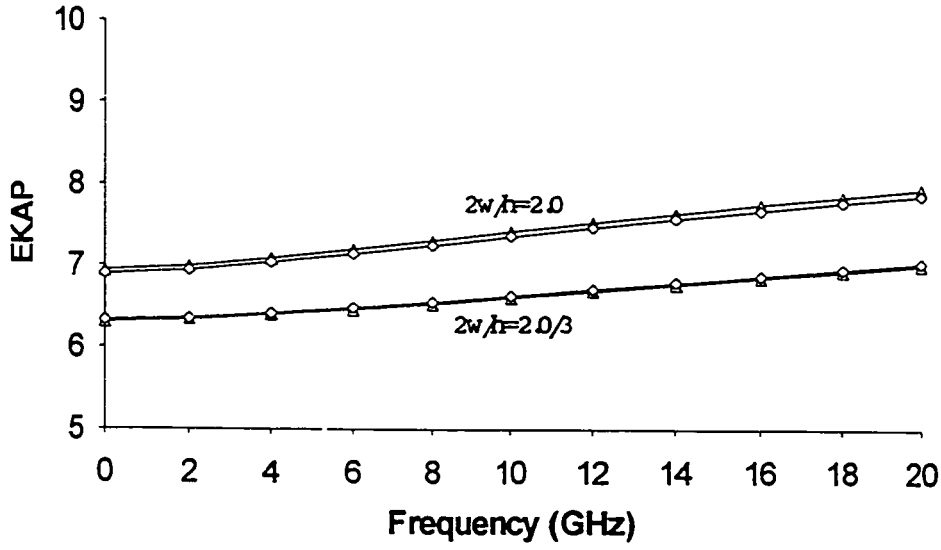

Fig. 6.2.1 MS effective dielectric constant for an alumina substrate where h=0.0635, a=1.0, and c=1.0365 for both cases. —Δ— the method in Chap. 2, —◊— the method in Chap. 4.

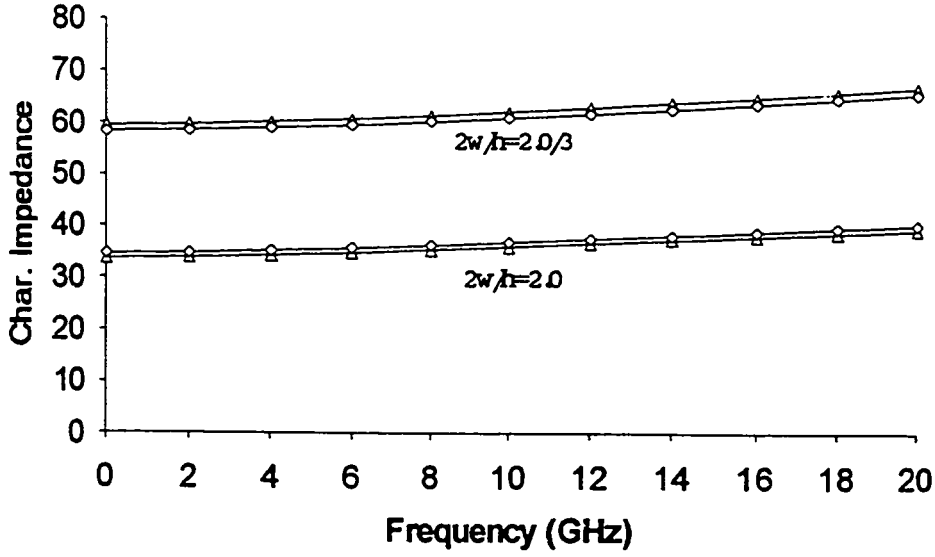

Fig. 6.2.2 Characteristic impedance for the MS of Fig. 6.2.1.

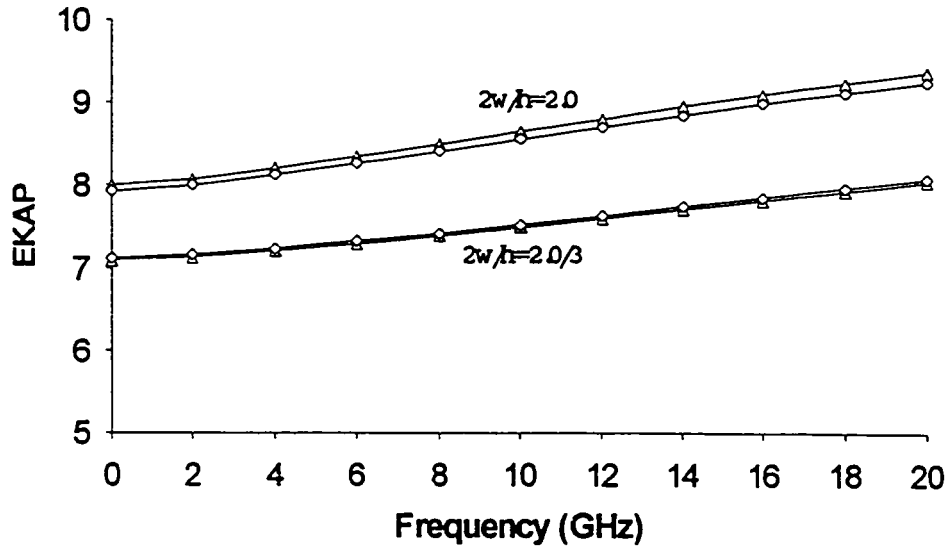

Fig. 6.2.3 MS effective dielectric constant for a sapphire substrate where h=0.0635, a=1.0, and c=1.0365 for both cases. —Δ— the method in Chap. 2, —◊— the method in Chap. 4.

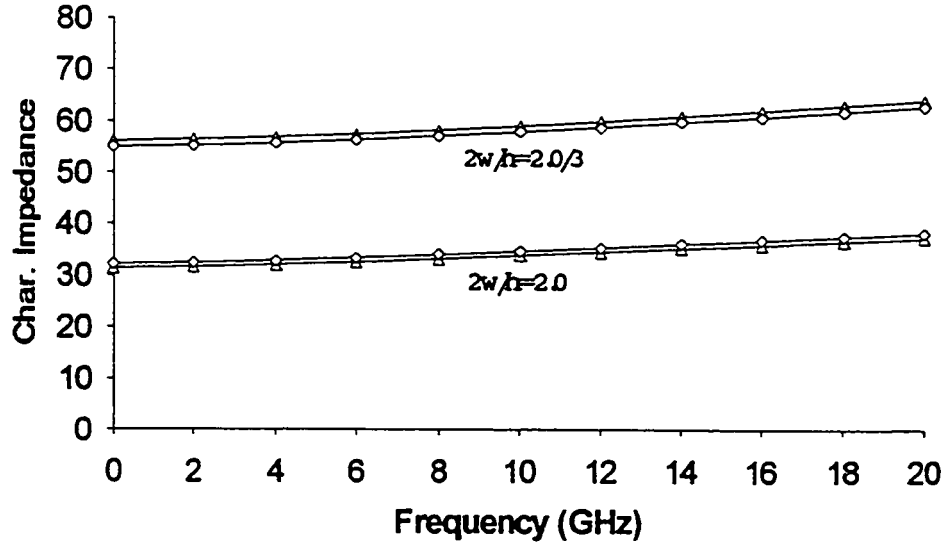

Fig. 6.2.4 Characteristic impedance for the MS of Fig. 6.2.3.

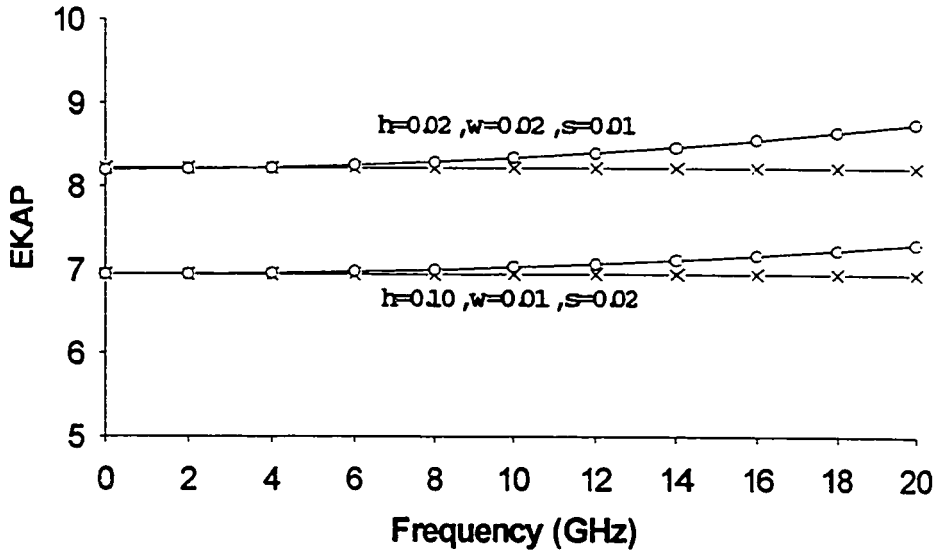

Fig. 6.2.5 CPW effective dielectric constant for a GaAs substrate where a=0.1 and c=0.1 for both cases. —×— [28], —o— this dissertation.

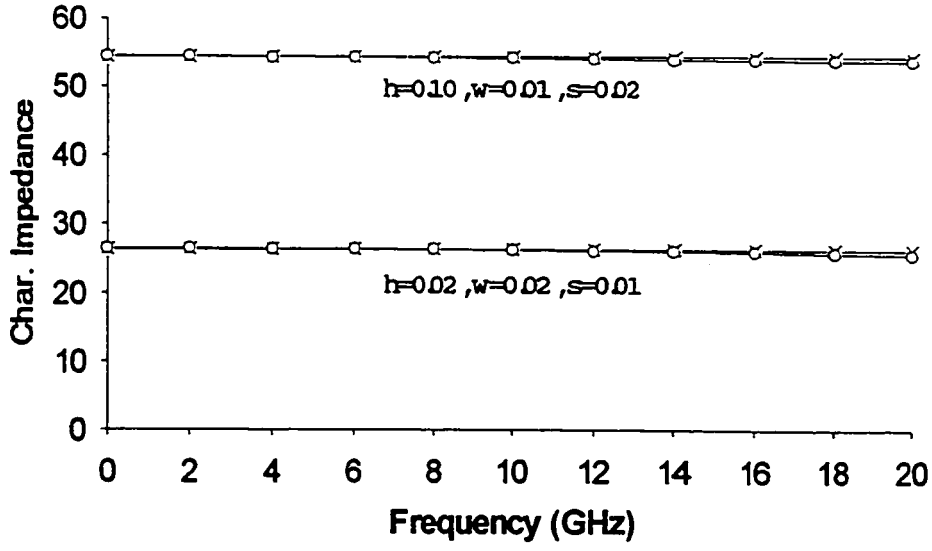

Fig. 6.2.6 Characteristic impedance for the CPW of Fig. 6.2.5.

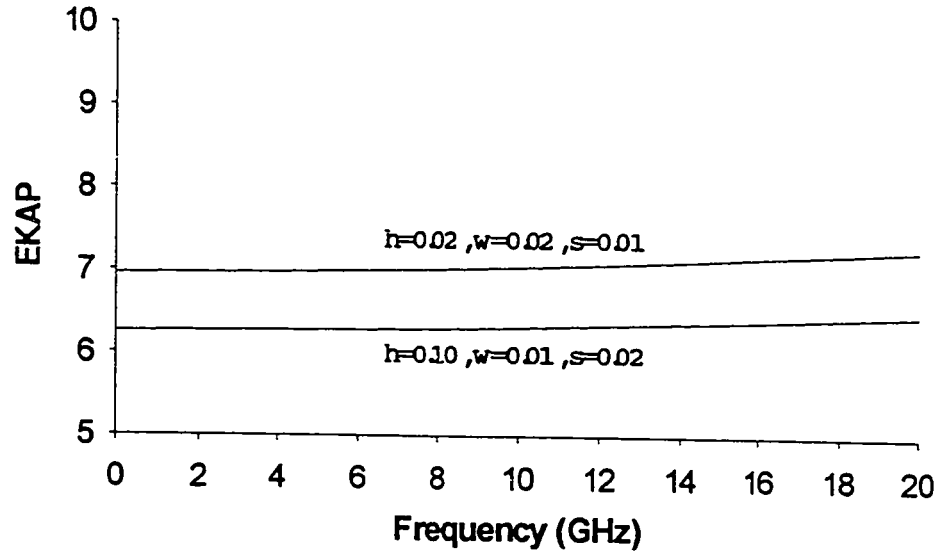

Fig. 6.2.7 CPW effective dielectric constant for an Epsilam-10 substrate where a=0.1 and c=0.1 for both cases.

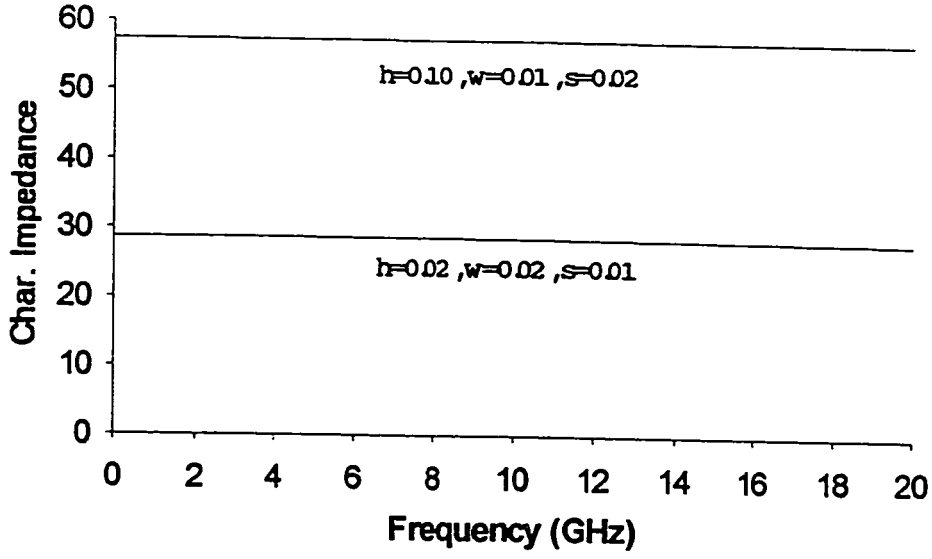

Fig. 6.2.8 Characteristic impedance for the CPW of Fig. 6.2.7.

(6-3)Results for coplanar waveguide open-end discontinuities

First of all, we check our result against the result shown in [33] on the same condition that the structure parameters for a GaAs substrate are chosen as h=0.01, w=0.01, s=0.01 except that a=0.5 and c=0.1 are used for our shielded configuration. In this case, ours is 11.75 fF obtained for 1 GHz and that in [33] is 12.56 fF calculated by a static three-dimensional finite difference method with no consideration of the effects of the currents, let alone, the transverse current which must especially be taken into account for the ground planes of coplanar waveguides.

Like the similar phenomenon to that mentioned in the previous section, we find that the finite widths of the ground planes actually influence the equivalent capacitance to some extent and this fact was not considered for the structure studied by the static method in [33]. This kind of the structures of coplanar waveguides which can support a perturbed TE_{10} rectangular waveguide mode results in a limitation for the width of the dielectric-loaded waveguide.

We compute the equivalent shunt capacitance, right at the end side of the coplanar waveguide open end discontinuities, shown in Fig. 6.3.1 for an alumina substrate, $\kappa = 9.7$. For the two lines shown in the figure we maintain all the other structure parameters and change the slot spacing. From the data, it shows that this does not influence the capacitances much. For the frequency range of interest, the sample values by 2 GHz for each increment show very few differences. The maximum and the minimum capacitances for each line in this figure deviate from each other by less than 1%.

Fig. 6.3.2 gives the capacitance data of CPW open end discontinuity for a sapphire substrate with $\kappa = 9.4$ and $\kappa_y = 11.6$. For these two lines in the figure the width of the central strip line is varied, and so is the slot spacing.

Obviously, the wider the central strip is, the larger the capacitance for the coplanar waveguide open end is.

The CPW open end capacitance data for a GaAs substrate using the dielectric constant $\kappa = 12.9$ is shown in Fig. 6.3.3. The same indication of the outcomes as that for an alumina substrate is observed for this substrate. We use an Epsilam-10 substrate as another example for anisotropic substrates to obtain the CPW open end equivalent capacitance as shown in Fig. 6.3.4. The substrate has anisotropic dielectric constant with $\kappa = 13$ and $\kappa_y = 10.3$. Also, the increase of the open end capacitances with the width of the central strip is seen for this anisotropic substrate.

In all four figures for coplanar waveguide open end capacitances, our results for both isotropic and anisotropic substrates indicate a very slight change against frequency. The maximum and the minimum capacitances for each line in the four figures vary from each other by at most around 1% for frequencies up to 20 GHz.

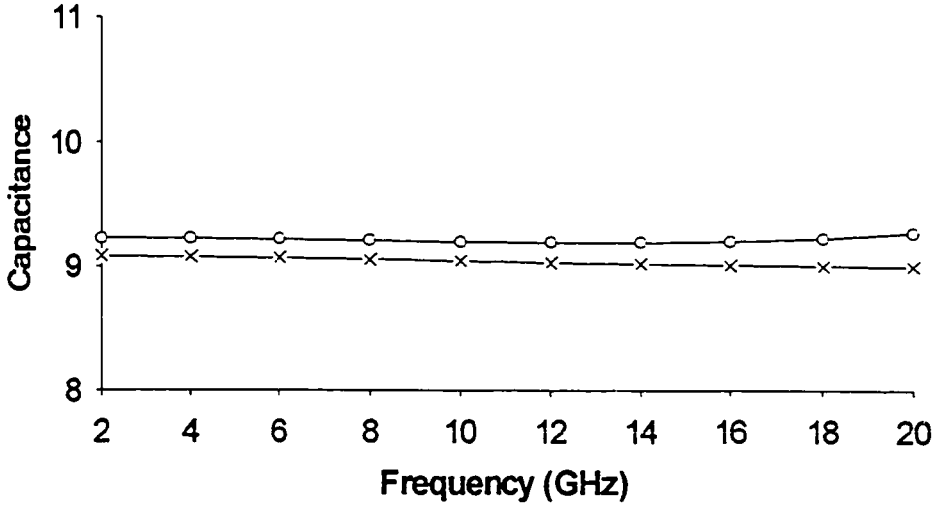

Fig. 6.3.1 Equivalent capacitance for the CPW open end discontinuities with an alumina substrate where h=0.01, w=0.01, a=0.11, and c=0.1 for both cases ; i.e. , —x— s=0.01 and —o— s=0.02.

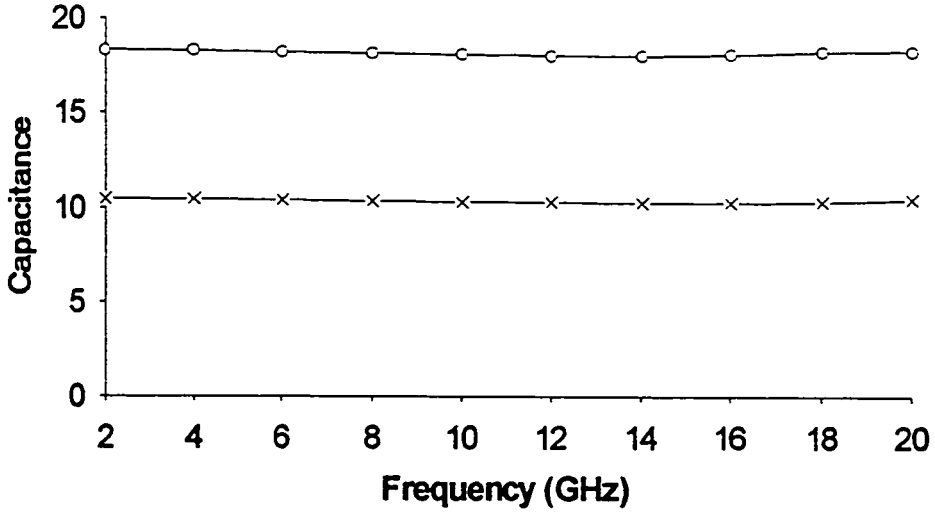

Fig. 6.3.2 Equivalent capacitance for the CPW open end discontinuities with a sapphire substrate where h=0.02, a=0.1, and c=0.1 for both cases ; i.e. , —x— w=0.01, s=0.02 and —o— w=0.02, s=0.01.

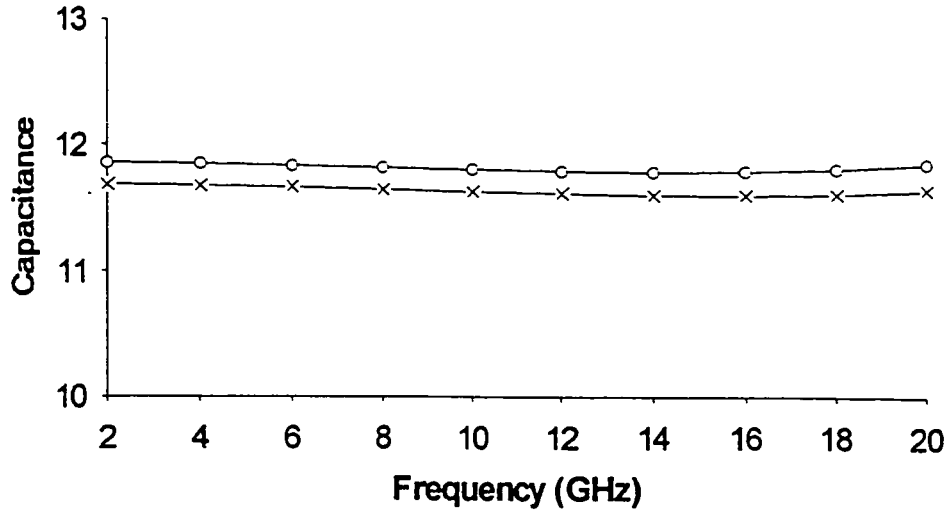

Fig. 6.3.3 Equivalent capacitance for the CPW open end discontinuities with a GaAs substrate where h=0.01, w=0.01, a=0.09, and c=0.1 for both cases ; i.e. , —×— s=0.01 and —o— s=0.02.

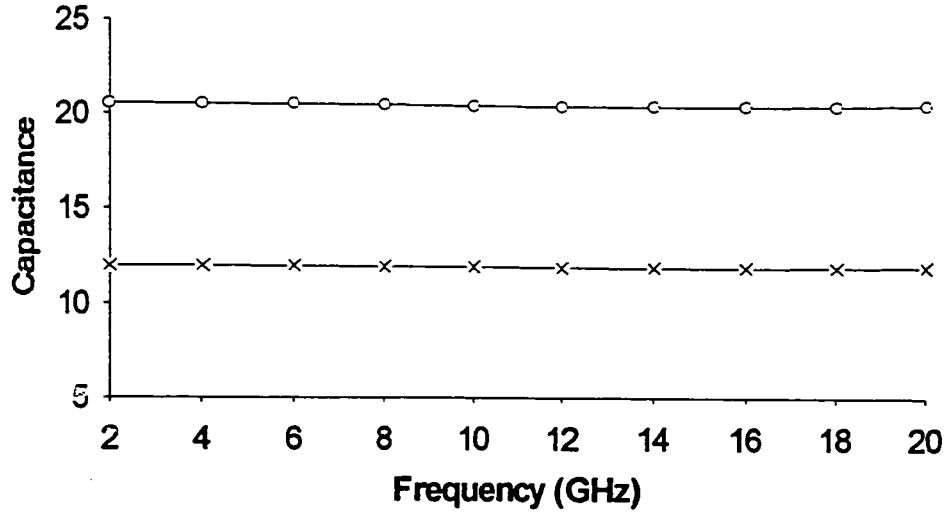

Fig. 6.3.4 Equivalent capacitance for the CPW open end discontinuities with an Epsilam-10 substrate where h=0.02, a=0.09, and c=0.1 for both cases ; i.e. , —×— w=0.01, s=0.02 and —o— w=0.02, s=0.01.

Chapter 7

Conclusion

There are three main topics contained in this dissertation. First of all, we develop the dynamic source reversal method, based on potential theory, to characterize microstrip discontinuities including anisotropic substrates. In microstrip open-end and symmetrical gap problems, only one mode for the transverse current needs to be included to obtain accurate results. However, for asymmetrical gap problems two modes for the transverse current are needed.

In treating these microstrip discontinuities, we use two pairs of expansion functions for the perturbed current and charge. From the data produced by using the shifted and unshifted unipolar testing functions for each pair respectively, we find that QT pair is not so efficient as TP pair. It is suggested that the efficiency of QT pair might be much improved by utilizing the bipolar testing functions.

For microstrip open ends and gaps with anisotropic substrates, the assumption of an equivalent isotropic substrate is found to be a useful technique to obtain the equivalent capacitance(s) of the modeled network.

In the second place, we develop an efficient method to solve coplanar waveguide propagation characteristics in the transform domain. The use of the sources on coplanar waveguides as obtained by conformal mapping allows a very effective iteration method to be implemented to find the dispersions containing anisotropic substrates. Owing to these new general expressions for the sources, it is proved that this method can also be reduced to work out the problems of microstrip dispersions containing anisotropic substrates.

Finally, we apply the dynamic source reversal method to characterize coplanar waveguide open end discontinuity with the help of the efficient method used to find the dispersions of coplanar waveguides. In all the above results for these three topics, very good accuracy and excellent efficiency has been observed.

It is believed that the dynamic source reversal method can be applied to treat a few more microstrip discontinuities such as steps, some more discontinuous configurations of coplanar waveguides, and a lot of finline discontinuities. In addition, the efficient method used to solve coplanar waveguide dispersions can be modified further to treat the propagation characteristics of finlines.

Appendix 1 Summing results of some series expressions over m and n

In the development of our method there are a few sets of double sums, over the index n and m, which do not have the exponential decay associated with them. Since their convergence is very slow, these terms must be first summed over m by a mathematical method. As proved in [1], we can use the residue theory to accomplish this. Only the results are shown here, but the readers who have interest in the details of the derivation can refer to [1].

With the help of the residue theory applied to the chosen functions of spatial frequency, we obtain

$$\sum_m \frac{F_m}{\gamma_{nm}^2+\beta^2} = \frac{1}{2}\frac{\sinh(\zeta_n c)\sinh(\zeta_{1n} h)}{\left[\zeta_{1n}\sinh(\zeta_n c)\cosh(\zeta_{1n} h)+\zeta_n\cosh(\zeta_n c)\sinh(\zeta_{1n} h)\right]} = TF(n) \tag{a.1.1}$$

and

$$\sum_m \left[\frac{H_m}{\gamma_{nm}^2+\beta^2}+\frac{\bar{H}_m}{\bar{\gamma}_{nm}^2+\beta^2}\right] = \frac{\sinh(\zeta_n c)}{2(u_n^2+\beta^2)}\left[\frac{k_0^2\sinh(\zeta_{1n} h)}{D_{vn1}}+\frac{\zeta_n\zeta_{2n}\sinh(\zeta_{2n} h)}{D_{vn2}}\right] = TG(n) \tag{a.1.2}$$

where $D_{vn1}=\left[\zeta_{1n}\sinh(\zeta_n c)\cosh(\zeta_{1n} h)+\zeta_n\cosh(\zeta_n c)\sinh(\zeta_{1n} h)\right]$ and $D_{vn2}=\left[\kappa\zeta_n\sinh(\zeta_n c)\cosh(\zeta_{2n} h)+\zeta_{2n}\cosh(\zeta_n c)\sinh(\zeta_{2n} h)\right]$.

As n approaches to infinity we have the approximations for the above two equations as follows

$$\lim_{n\to\infty} TF(n) = \frac{1}{4u_n} = AF(n) \quad \text{and} \quad \lim_{n\to\infty} TG(n) = \frac{\kappa_r}{2u_n} = AG(n) \tag{a.1.3}$$

where $\kappa_r = \dfrac{(\kappa/\kappa_y)^{\frac{1}{2}}}{[\kappa+(\kappa/\kappa_y)^{\frac{1}{2}}]}$.

With these we can rewrite the expressions including double testing results as

$$\sum_n \sum_m \frac{F_m}{\gamma_{nm}^2+\beta^2} p_{ni} p_{nj} = \sum_n [TF(n) - AF(n)] p_{ni} p_{nj} + \frac{a}{2\pi} \sum_n \frac{1}{n} p_{ni} p_{nj} \tag{a.1.4a}$$

and

$$\sum_n \sum_m \left[\frac{H_m}{\gamma_{nm}^2+\beta^2} + \frac{\overline{H}_m}{\overline{\gamma}_{nm}^2+\beta^2} \right] p_{ni} p_{nj} = \sum_n [TG(n) - AG(n)] p_{ni} p_{nj} + \frac{a}{\pi} \kappa_r \sum_n \frac{1}{n} p_{ni} p_{nj} \tag{a.1.4b}$$

In these equations let us consider

$$\sum_{n=1,3}^{\infty} \frac{1}{n} p_{ni} p_{nj}$$

$$4 \int_0^{\frac{\pi}{2}} \int_0^{\frac{\pi}{2}} \sum_{n=1,3}^{\infty} \frac{1}{n} \cos\left[\frac{n\pi w}{2a} \sin(\theta)\right] \cos\left[\frac{n\pi w}{2a} \sin(\theta')\right] \cos(2i\theta) \cos(2j\theta') \, d\theta \, d\theta' \tag{a.1.5}$$

where $x = \sin(\theta)$ is used. Note that we can extract the summation item in the double integrals first and simplify it as follows

$$\sum_{n=1,3}^{\infty} \frac{1}{n} \cos(u_n x) \cos(u_n x') = \sum_{n=1,3}^{\infty} \frac{1}{n} \cos\left[\frac{n\pi w}{2a} \sin(\theta)\right] \cos\left[\frac{n\pi w}{2a} \sin(\theta')\right] = -\ln\left|\tan\left[\frac{\pi(x-x')}{4a}\right] \tan\left[\frac{\pi(x+x')}{4a}\right]\right|$$

$$= -\frac{1}{4}\ln\left(\frac{\pi w}{4a}\right)^2 - \frac{1}{4}\ln\left|\sin^2(\theta) - \sin^2(\theta')\right|$$

$$= \frac{1}{4}\ln\left(\frac{8a}{\pi w}\right)^2 + \sum_{n=1}^{\infty}\frac{\cos(2n\theta)\cos(2n\theta')}{2n} \tag{a.1.6}$$

Therefore we obtain, after substituting Eq.(a.1.6) into (a.1.5),

$$\sum_{n=1,3}^{\infty}\frac{1}{n}p_{ni}p_{nj} =$$

$$\int_0^{\frac{\pi}{2}}\int_0^{\frac{\pi}{2}}\left[\sum_{n=1,3}^{\infty}\ln\left(\frac{8a}{\pi w}\right)^2 + \sum_{n=1}^{\infty}\frac{2\cos(2n\theta)\cos(2n\theta')}{n}\right]\cos(2i\theta)\cos(2j\theta')d\theta\, d\theta' \tag{a.1.7}$$

where the orthogonal property can now be applied to yield the final results as shown below

$$\sum_{n=1,3}^{\infty}\frac{1}{n}p_{ni}p_{nj} = \begin{cases} \dfrac{\pi^2}{4}\ln\left(\dfrac{8a}{\pi w}\right)^2 & i=j=0 \\ \dfrac{\pi^2}{8} & i=j=1 \\ \dfrac{\pi^2}{16} & i=j=2 \end{cases} \tag{a.1.8}$$

Similarly we can calculate the other summation over n. For the case of testing that does not emphasize the field at the edge we get

$$\sum_{n=1,3}^{\infty}\frac{1}{n}p_{ni}zp_{nj} = \begin{cases} \dfrac{\pi}{2}\dfrac{(-1)^{j+1}}{(2j)^2-1}\ln\left(\dfrac{8a}{\pi w}\right)^2 & i=0 \\ \dfrac{\pi}{4}(-1)^{j+1}\left[\dfrac{3}{3^2-(2j)^2} - \dfrac{1}{1^2-(2j)^2}\right] & i=1 \\ \dfrac{\pi}{4}\dfrac{(-1)^{j+2}}{2}\left[\dfrac{5}{5^2-(2j)^2} - \dfrac{3}{3^2-(2j)^2}\right] & i=2 \end{cases} \tag{a.1.9}$$

REFERENCES

(1) S. Toncich, "Characterization of microstrip discontinuities by a dynamic source reversal technique using potential theory", Ph.D. Thesis, CWRU, OH, 1990.

(2) P. Silvester and P. Benedek, "Equivalent capacitance of microstrip open circuits", IEEE Trans. on MTT, vol. MTT-20, pp. 511-516, 1972.

(3) A. Farrar and A. T. Adams, "Matrix methods for microstrip three dimensional problems", IEEE Trans. on MTT, vol. MTT-20, pp. 497-504, 1972.

(4) M. Maeda, "An analysis of gap in microstrip lines", IEEE Trans. on MTT, vol. MTT-20, pp. 390-396, 1972.

(5) Y. Rahmat Samii, T. Itoh, and R. Mittra, "A spectral domain analysis for solving microstrip discontinuity problems", IEEE Trans. on MTT, vol. MTT-22, pp. 372-378, 1974.

(6) P. Silvester and P. Benedeck, "Equivalent capacitance for microstrip gaps and steps", IEEE Trans. on MTT, vol. MTT-20, pp. 729-733, 1972.

(7) P. Benedeck and P. Silvester, "Microstrip discontinuity capacitances for right angle bends, T-junctions, and crossings", IEEE Trans. on MTT, vol. MTT-21, pp. 341-346, 1973.

(8) A. Thompson and G. Gopinath, "Calculation of microstrip discontinuity inductances", IEEE Trans. on MTT, vol. MTT-23, pp. 648-655, 1975.

(9) P. Silvester and P. Benedeck, "Electrostatics of the microstrip revisited", IEEE Trans. on MTT, vol. MTT-20, pp. 756-758, 1972.

(10) M. Kobayashiu, "Longitudinal and transverse current distributions on microstrip lines and their closed form expressions", IEEE Trans. on MTT, vol. MTT-33, pp. 784-739, 1985.

(11) B. Easter, "The equivalent circuit of swome microstrip discontinuities", IEEE Trans. on MTT, vol. MTT-23, pp. 655-660, 1975.

(12) C. Gupta, B. Easter, and A. Gopinath. "Some results on the end effects of microstriplines", IEEE trans. on MTT, vol. MTT-26, pp. 649-652, 1978.

(13) T. Itoh, "Analysis of microstrip resonators", IEEE Trans. on MTT, vol. MTT-22, pp. 946-952, 1974.

(14) I. Wolff, G. Kompa, and R. Mehran, "Calculation method for microstrip discontinuities and T-junctions", Electron lett., vol. 8, pp. 177-179, 1972.

(15) W. Getsinger, "Microstrip dispersion model", IEEE Trans. on MTT, Vol. MTT-21, pp. 34-39, 1973.

(16) N. H. L. Koster and R. H. Jansen, "The equivalent circuit of the asymmetrical series gap in microstrip and suspended substrate lines", IEEE Trans. on MTT-30, pp. 1273-1279, 1982.

(17) N. H. L. Koster and R. H. Jansen, "The microstrip step discontinuity: A revised description", IEEE Trans. on MTT, vol. MTT-34, pp. 213-223, 1986.

(18) R. E. Collin, "Field theory of guided waves", IEEE Press, New York, Second edition, Chapter 5, 1991.

(19) P. B. Katehi and N. G. Alexopoulos, "Frequency dependent characteristics of microstrip discontinuities in millimeter wave integrated circuits", IEEE Trans. on MTT, vol. MTT-33, pp. 1029-1035, 1985.

(20) L. P. Dunleavy and P. B. Katehi, "A generalized method for analyzing shielded thin microstrip discontinuities", IEEE Trans. on MTT, vol. MTT-36, pp. 1758-1766, 1988.

(21) X. Zhang and K. K. Mei, "Time domain finite difference approach to the calculation of frequency dependent characteristics of microstrip discontinuities", IEEE Trans. on MTT, vol. MTT-36, pp. 1775-1787, 1988.

(22) N. K. Uzunoglu et. al., "Frequency dependent analysis of a shielded microstrip step discontinuity using an efficient mode matching technique", IEEE Trans. on MTT, vol. MTT-36, pp. 976-985, 1988.

(23) R. W. Jackson and D. M. Pozar, "Full wave analysis of microstrip open end and gap discontinuities", IEEE Trans. on MTT, vol. MTT-33, pp. 1030-1042, 1983.

(24) R. W. Jackson, "Full wave, finite element analysis of irregular microstrip discontinuities", IEEE Trans. on MTT, vol. MTT-37, pp. 81-89, 1989.

(25) B. E. Kretch and R. E. Collin, "Microstrip dispersion including anisotropic substrates", IEEE Trans. on MTT, vol. MTT-35, pp. 710-718, 1987.

(13) T. Itoh, "Analysis of microstrip resonators", IEEE Trans. on MTT, vol. MTT-22, pp. 946-952, 1974.

(14) I. Wolff, G. Kompa, and R. Mehran, "Calculation method for microstrip discontinuities and T-junctions", Electron lett., vol. 8, pp. 177-179, 1972.

(15) W. Getsinger, "Microstrip dispersion model", IEEE Trans. on MTT, Vol. MTT-21, pp. 34-39, 1973.

(16) N. H. L. Koster and R. H. Jansen, "The equivalent circuit of the asymmetrical series gap in microstrip and suspended substrate lines", IEEE Trans. on MTT-30, pp. 1273-1279, 1982.

(17) N. H. L. Koster and R. H. Jansen, "The microstrip step discontinuity: A revised description", IEEE Trans. on MTT, vol. MTT-34, pp. 213-223, 1986.

(18) R. E. Collin, "Field theory of guided waves", IEEE Press, New York, Second edition, Chapter 5, 1991.

(19) P. B. Katehi and N. G. Alexopoulos, "Frequency dependent characteristics of microstrip discontinuities in millimeter wave integrated circuits", IEEE Trans. on MTT, vol. MTT-33, pp. 1029-1035, 1985.

(20) L. P. Dunleavy and P. B. Katehi, "A generalized method for analyzing shielded thin microstrip discontinuities", IEEE Trans. on MTT, vol. MTT-36, pp. 1758-1766, 1988.

(21) X. Zhang and K. K. Mei, "Time domain finite difference approach to the calculation of frequency dependent characteristics of microstrip discontinuities", IEEE Trans. on MTT, vol. MTT-36, pp. 1775-1787, 1988.

(22) N. K. Uzunoglu et. al., "Frequency dependent analysis of a shielded microstrip step discontinuity using an efficient mode matching technique", IEEE Trans. on MTT, vol. MTT-36, pp. 976-985, 1988.

(23) R. W. Jackson and D. M. Pozar, "Full wave analysis of microstrip open end and gap discontinuities", IEEE Trans. on MTT, vol. MTT-33, pp. 1030-1042, 1983.

(24) R. W. Jackson, "Full wave, finite element analysis of irregular microstrip discontinuities", IEEE Trans. on MTT, vol. MTT-37, pp. 81-89, 1989.

(25) B. E. Kretch and R. E. Collin, "Microstrip dispersion including anisotropic substrates", IEEE Trans. on MTT, vol. MTT-35, pp. 710-718, 1987.

(37) T. Becks and I. Wolff, "Full-wave analysis of various coplanar bends and T-junctions with respect to different types of air-bridges", IEEE MTT-S Digest, pp. 697-700, 1993.

(38) S. Visan, O. Picon, V. F. Hanna, "3 D characterization of air bridges and via holes in conductor-backed coplanar waveguides for MMIC applications", IEEE MTT-S Digest, pp. 709-712, 1993.

(39) R. N. Simons and G. E. Ponachak, "Modeling of some coplanar waveguide discontinuities", IEEE Trans. on MTT, vol. MTT-36, pp. 1796-1803, 1988.

(40) A. W. Glisson and D. R. Wilton, "Simple and efficient numerical methods for problems of electromagnetic radiation and scattering from surfaces", IEEE Trans. on A, vol. AP-28, pp. 593-603, 1980.